

UC Berkeley

UC Berkeley Previously Published Works

Title

Emerging Multiferroic Memories

Permalink

<https://escholarship.org/uc/item/5nn0m3jx>

ISBN

9781489975362

Authors

Martin, Lane W

Chu, Ying-Hao

Ramesh, R

Publication Date

2014

DOI

10.1007/978-1-4899-7537-9_3

Peer reviewed

Chapter 3

Emerging Multiferroic Memories

Lane W. Martin, Ying-Hao Chu, and R. Ramesh

3.1 Introduction

Thus far in this book, we have focused on ferroelectric and magnetic spin torque transfer memories. In this chapter, we describe the recent discoveries in the emerging field of multiferroic-based memories. In the last decade, considerable attention has been focused on the search for and characterization of new multiferroic materials as scientists and researchers have been driven by the promise of exotic materials functionality (especially electric field control of ferromagnetism). In this chapter we develop a holistic picture of multiferroic materials, including details on the nature

L.W. Martin (✉)

Department of Materials Science and Engineering, University of California,
210 Hearst Mining Building, Berkeley, CA 94720, USA

Materials Science Division, Lawrence Berkeley National Laboratory,
Berkeley, CA 94720, USA
e-mail: lwmartin@illinois.edu

Y.-H. Chu

Department of Materials Science and Engineering, National Chiao Tung University,
HsinChu, Taiwan 30010

R. Ramesh

Department of Materials Science and Engineering, University of California,
210 Hearst Mining Building, Berkeley, CA 94720, USA

Department of Physics, University of California, Berkeley, CA 94720, USA

Materials Science Division, Lawrence Berkeley National Laboratory,
Berkeley, CA 94720, USA

of order parameters and coupling in these materials, the scarcity of such materials, routes to create and control the properties in these materials, and prospects for these materials in next generation devices—with special attention given to memory applications.

Complex oxides represent a vast class of materials encompassing a wide range of crystal structures and functionalities. Amongst these interesting properties, the study of magnetic, ferroelectric, and, more recently, multiferroic properties has driven considerable research. Specifically, in the last few years there has been a flurry of research focused on multiferroic and magnetoelectric materials [1–3]. From the investigation of bulk single crystals to novel characterization techniques that probe order parameters, coupling, spin dynamics, and more this is truly a diverse field, rich with experimental and theoretical complexity. By definition, a single-phase multiferroic [4] is a material that simultaneously possesses two or more of the so-called ferroic order parameters—ferroelectricity, ferromagnetism, and ferroelasticity. Magnetoelectric coupling typically refers to the linear magnetoelectric effect or the induction of magnetization by an electric field or polarization by a magnetic field [5]. The promise of coupling between magnetic and electronic order parameters and the potential to manipulate one through the other has captured the imagination of researchers worldwide. The ultimate goal for device functionality would be a single-phase multiferroic with strong coupling between ferroelectric and ferromagnetic order parameters making for simple control over the magnetic nature of the material with an applied electric field at room temperature.

Driven by advances in the synthesis of both bulk and thin-film versions of these materials (see, for example, [6, 7], respectively), there has been a renewed interest in these materials for a number of applications. As part of this chapter we will discuss a number of different classes of multiferroic materials, coupling between order parameters in these materials, a number of model multiferroic thin film systems that are candidate materials for memory applications, as well as the state-of-the-art work on multiferroics based devices, before finally developing a picture of the advances, both in terms of basic materials and device architectures, needed to see multiferroic-based memories significantly impact the technology landscape.

3.2 Multiferroic Materials

Multiferroism describes materials in which two or all three of the properties ferroelectricity (spontaneous polarization that is both stable and can be switched by application of an electric field), ferromagnetism (spontaneous magnetization that is stable and can be switched by application of a magnetic field), and ferroelasticity (spontaneous deformation that is stable and can be switched by application of an electric field) occur in the same phase. The overlap required of ferroic materials to be classified as *multiferroic* is shown schematically in Fig. 3.1a. Only a small subgroup of all magnetically and electrically polarizable materials are either ferromagnetic or ferroelectric and fewer still simultaneously exhibit both order parameters.

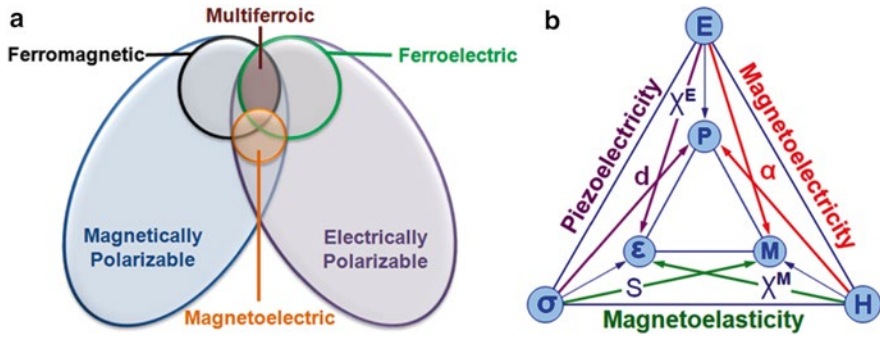


Fig. 3.1 (a) Relationship between multiferroic and magnetoelectric materials. Illustrates the requirements to achieve both in a material (adapted from [7]). (b) Schematic illustrating different types of coupling present in materials. Much attention has been given to materials where electric and magnetic order is coupled. These materials are known as magnetoelectric materials (adapted from [8])

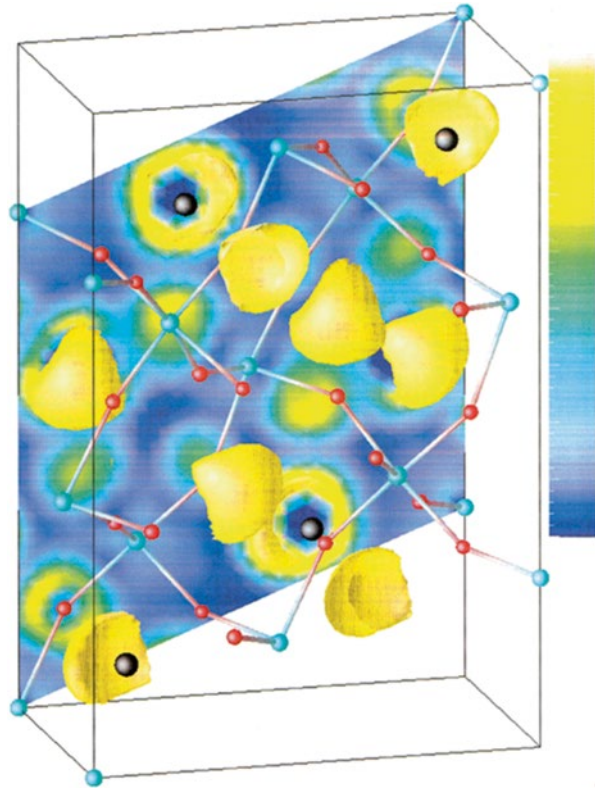
In these select materials, however, there is the possibility that electric fields cannot only reorient the polarization but also control magnetization; similarly, a magnetic field can change electric polarization. This functionality offers an extra degree of freedom and we refer to such materials as *magnetoelectrics* (Fig. 3.1b). Magnetoelectricity is an independent phenomenon that can arise in any material with both magnetic and electronic polarizability, regardless of whether it is multiferroic or not. By the original definition a magnetoelectric multiferroic must be simultaneously both ferromagnetic and ferroelectric [4], but it should be noted that the current trend is to extend the definition of multiferroics to include materials possessing two or more of any of the ferroic or corresponding antiferroic properties such as antiferroelectricity (possessing ordered dipole moments that are aligned antiparallel and therefore cancel each other completely across the sample) and antiferromagnetism (possessing ordered magnetic moments that are aligned antiparallel and therefore cancel each other completely across the sample). More recently it has also been extended to include the so-called ferrotoroidic order (a spontaneous order parameter that is taken to be the curl of a magnetization or polarization) [8]. This said, it should be abundantly obvious why there has been considerable renewed interest in these materials over the last decade. The prospects for these materials in applications are wide ranging and have driven a spectrum of both fundamental and applied studies. Multiferroics have been proposed for use in applications ranging from next generation logic and memory to sensing to tunable RF and much more. Although we will only explicitly explore the implications for memory applications, it is important to recognize the versatile possibilities for these materials.

With this as a background, the single largest limiting factor that has kept multiferroics from making substantial in-roads into current technology is the scarcity of multiferroics. This scarcity has been recently reviewed by Khomskii [9]. Taking as an example the perovskite (ABO_3) compounds, one can obtain a detailed list of

magnetic perovskites in the tables compiled by Goodenough and Longo [10] and further investigation will reveal similar tables of ferroelectric perovskites compiled by Mitsui et al. [11]. What becomes apparent after investigating these tables is that there is essentially no overlap between these lists—magnetism and ferroelectricity in materials are seemingly incompatible. Key insights into this scarcity of multiferroic phases can be understood by investigating a number of factors including symmetry, electronic properties, and chemistry [12, 13]. To begin, it should be noted that there are only 13 point groups that can give rise to multiferroic behavior. Strong magnetism in itinerant ferromagnets requires the presence of conduction electrons in partially filled inner shells (*d*- or *f*-shells); even in double exchange ferromagnets such as the manganites, magnetism is mediated by incompletely filled *3d* shells. The situation in ferroelectrics, however, is somewhat more complicated as many different mechanisms for ferroelectric ordering and a number of different types of ferroelectrics exist. Generally it is observed, however, that ferroelectrics (which are by definition insulators) typically possess (for instance, in transition metal oxides) cations that have a formal d^0 electronic state. This d^0 state is thought to be required to drive the formation of strong covalency with the surrounding oxygen, thereby, shifting the transition metal ion from the center of the unit cell and inducing a spontaneous polarization (this is the so-called second-order Jahn–Teller effect) [14]. The second-order Jahn–Teller effect describes the structural changes resulting from a non-degenerate ground-state interacting with a low-lying excited state and it occurs when the energy gap between the highest occupied (HOMO) and lowest unoccupied (LUMO) molecular orbital is small and there is a symmetry allowed distortion permitting the mixing of the HOMO and LUMO states. Mathematically, the second-order Jahn–Teller effect can be understood through the use of second-order perturbation group theory, but this is beyond the scope of this chapter [15]. Thus, in the end, it becomes clear that there exists a seeming contradiction between the conventional mechanism of off-centering in a ferroelectric and the formation of magnetic order which helps explain the scarcity of ferromagnetic–ferroelectric multiferroics. The focus of many researchers, therefore, has been on designing and indentifying new mechanisms that lead to magnetoelectric coupling and multiferroic behavior. In the following section we will investigate a number of these pathways.

An investigation of these various pathways to multiferroism is aided by separation of all multiferroic materials into one of two types [16]. Type I multiferroics are materials in which ferroelectricity and magnetism have different sources and appear largely independent of one another. One can create a Type I multiferroic, for instance, by engineering the functionality on a site-by-site basis in model systems such as the perovskites (ABO_3) where one can make use of the stereochemical activity of an *A*-site cation with a lone pair (i.e., $6s$ electrons in Bi or Pb) to induce a structural distortion and ferroelectricity while inducing magnetism with the *B*-site cation. This is the case in the multiferroics BiFeO_3 [17], BiMnO_3 [18, 19], and PbVO_3 [20–23]. From the microscopic view, it can be understood that the orientation of the lone-pairs in the materials can give rise to local dipoles that can order thereby creating a

Fig. 3.2 Electron localization function representation of the isosurface of the valence electrons in BiMnO_3 projected within a unit cell. Dark colors correspond to a lack of electron localization and light to complete localization (adapted from [24])



net polarization as has been demonstrated with *ab initio* models (Fig. 3.2) [24]. Much like the polarization observed in the classic ferroelectrics (i.e., BaTiO_3), materials such as BiFeO_3 and BiMnO_3 are referred to as *proper* ferroelectrics. In a proper ferroelectric structural instability towards a polar state, associated with the electronic pairing, is the main driving force for the transition. If, on the other hand, polarization is only a part of a more complex lattice distortion or if it appears as an accidental by-product of some other ordering, the ferroelectricity is called *improper* [25]. One pathway by which one can obtain an improper ferroelectric, Type I multiferroic is through geometrically driven effects where long-range dipole–dipole interactions and anion rotations drive the system towards a stable ferroelectric state. This is thought to drive multiferroism in materials such as the hexagonal manganites (i.e., YMnO_3) (Fig. 3.3) [26, 27]. Again, in these materials ferroelectricity is achieved despite violating the requirement of having a d^0 electron configuration on the *B*-site cation. Despite this fact, the resulting ferroelectric transition temperatures for these hexagonal manganites are typically quite high (~ 900 – $1,000$ K)—suggesting a robustness to the order parameter. Recent results also suggest that the off-center shift of the Mn^{3+} ions (which, it should be noted, are not Jahn–Teller ions) from the center

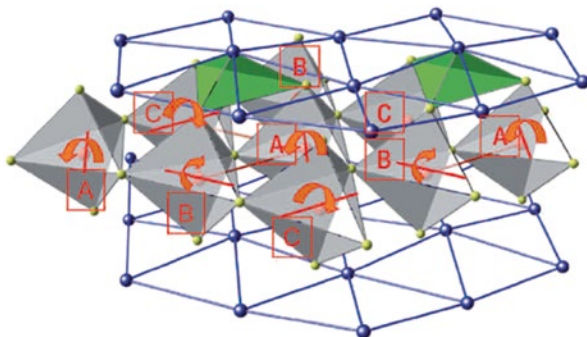


Fig. 3.3 Schematic illustration of the cooperative rotation of bipyramids in YMnO_3 that give rise to ferroelectric polarization. The resulting rotations are shown with the *arrows* (adapted from [26])

of the O_5 trigonal bipyramid are quite small and are, in turn, not the major mechanism for ferroelectric order in the system. Instead it is thought that the main dipole moments are formed (for instance, in YMnO_3) by the Y–O pairs—thus suggesting that the mechanism of ferroelectricity in these materials is distinctly different from that observed in classic ferroelectric materials such as BaTiO_3 [27].

Still another pathway by which one can achieve improper ferroelectricity in a Type I multiferroic is via charge ordering where non-centrosymmetric charge ordering arrangements result in ferroelectricity in magnetic materials as is found, for instance, in LuFe_2O_4 [28]. It has long been known that in many narrow band metals with strong electronic correlations, charge carriers become localized at low temperatures and form periodic superstructures. The most famous example is magnetite (Fe_3O_4), which undergoes a metal–insulator transition at ~ 125 K (the Verwey transition) with a rather complex pattern of ordered charges of iron ions [29, 30]. This charge ordering (which occurs in a non-symmetric manner) induces an electric polarization. More recently it has been suggested that the coexistence of bond-centered and site-centered charge ordering in $\text{Pr}_{1-x}\text{Ca}_x\text{MnO}_3$ leads to a non-centrosymmetric charge distribution and a net electric polarization (Fig. 3.4a) [31]. In the case of LuFe_2O_4 , the charge ordering results in a bilayer structure and appears to induce electric polarization. The average valence of Fe ions in LuFe_2O_4 is $2.5+$, and in each layer these ions form a triangular lattice. Below ~ 350 K, it is thought that alternating layers with $\text{Fe}^{2+}:\text{Fe}^{3+}$ ratios of 2:1 and 1:2 are produced, which result in a net polarization (Fig. 3.4b) [28].

So far we have investigated Type I multiferroics, where magnetism and ferroelectricity result from two unrelated mechanisms. In these systems because the ordering results from very different mechanisms, one would not, a priori, expect there to be strong magnetoelectric coupling in these materials. On the other hand, Type II multiferroics are materials in which magnetism causes ferroelectricity—implying a strong coupling between the two order parameters. The prototypical examples of this sort of behavior are TbMnO_3 [32] and TbMn_2O_5 [33] where ferroelectricity

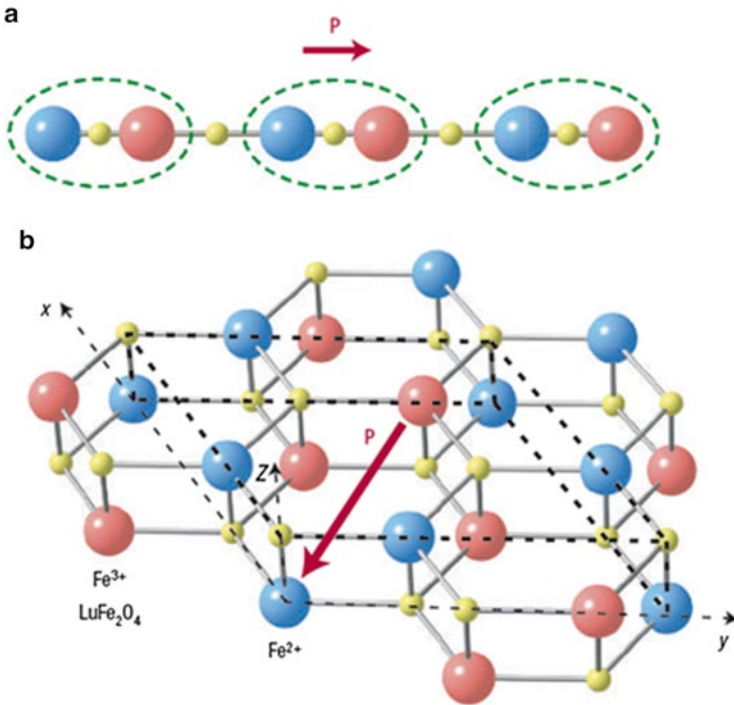


Fig. 3.4 (a) Illustration describing how ferroelectric order can be achieved in charge-ordered systems. The *spheres* correspond to cations with more/less charge and ferroelectricity is induced by the presence of simultaneous site-centered and bond-centered charge ordering. Dimers are marked by the *dashed lines*. (b) Charge ordering in LuFe₂O₄ with a triangular lattice of Fe-ions in each layer—charge transfer from the top to bottom layer gives rise to a net electric polarization (adapted from [2])

is induced by the formation of a symmetry-lowering magnetic ground state that lacks inversion symmetry. For instance, in TbMnO₃, the onset of ferroelectricity is directly correlated with the onset of spiral magnetic order at ~28 K [34]. The intimate connection between magnetic and ferroelectric order results in extraordinary coupling—including the ability to change the direction of electric polarization with an applied magnetic field in TbMnO₃ [32] and switching from positive to negative polarization in TbMn₂O₅ with a magnetic field [33]. The true nature of the mechanism for ferroelectric ordering in these materials is still under debate. Current theories have noted that for most of these materials the ferroelectric state is observed only when there is a spiral or helicoidal magnetic structure. The idea is that via some mechanism, for instance the Dzyaloshinskii–Moriya antisymmetric exchange interaction [35, 36] which is a relativistic correction to the usual superexchange with strength proportional to the spin–orbit coupling constant, the magnetic spiral can exert an influence on the charge and lattice subsystems, thereby creating ferroelectric order. Similar effects have also been observed in Ni₃V₂O₈ [37].

3.3 Principles of Magnetoelectricity in Multiferroics

From an applications standpoint, the real interest in multiferroic materials lies in the possibility of strong magnetoelectric coupling and the possibility to create new functionalities in materials. The magnetoelectric effect was proposed as early as 1894 by Curie [38], but experimental confirmation of the effect remained elusive until work on Cr_2O_3 in the 1960s [39–42]. As early as the 1970s a wide range of devices, including devices for the modulation of amplitudes, polarizations, and phases of optical waves, magnetoelectric data storage and switching, optical diodes, spin-wave generation, amplification, and frequency conversion had been proposed that would take advantage of magnetoelectric materials [43]. The magnetoelectric effect in its most general definition delineates the coupling between electric and magnetic fields in matter. Magnetoelectric coupling may exist regardless of the nature of the magnetic and electrical order parameters and can arise from direct coupling between two order parameters or indirectly via the lattice or strain. A better understanding of magnetoelectric coupling arises from expansion of the free energy of a material, i.e.

$$F(\vec{E}, \vec{H}) = F_0 - P_i^S E_i - M_i^S H_i - \frac{1}{2} \epsilon_0 \epsilon_{ij} E_i E_j - \frac{1}{2} \mu_0 \mu_{ij} H_i H_j - \frac{1}{2} \beta_{ijk} E_i H_j H_k - \frac{1}{2} \gamma_{ijk} H_i E_j E_k - \dots \quad (3.1)$$

with \vec{E} and \vec{H} as the electric field and magnetic field, respectively. Differentiation leads to the constitutive order parameters polarization

$$P_i(\vec{E}, \vec{H}) = -\frac{\partial F}{\partial E_i} = P_i^S + \epsilon_0 \epsilon_{ij} E_j + \alpha_{ij} H_j + \frac{1}{2} \beta_{ijk} H_j H_k + \gamma_{ijk} H_i E_j + \dots \quad (3.2)$$

and magnetization

$$M_i(\vec{E}, \vec{H}) = -\frac{\partial F}{\partial H_i} = M_i^S + \mu_0 \mu_{ij} H_j + \alpha_{ij} E_i + \beta_{ijk} E_i H_j + \frac{1}{2} \gamma_{ijk} E_j E_k + \dots \quad (3.3)$$

where ϵ and μ are the electric and magnetic susceptibilities, respectively, and α represents the induction of polarization by a magnetic field or magnetization by electric field and is designated the linear magnetoelectric effect. It should be noted that higher order magnetoelectric effects like β and γ are possible, however, they are often much smaller in magnitude than the lowest order terms. Furthermore, it can be shown that the magnetoelectric response is limited by the relation $\alpha_{ij}^2 < \epsilon_{ii} \mu_{jj}$ or more rigorously $\alpha_{ij}^2 < \chi_{ii}^e \chi_{jj}^m$ where χ^e and χ^m are the electric and magnetic susceptibilities. This means that the magnetoelectric effect can only be large in ferroelectric and/or ferromagnetic materials. To date the largest magnetoelectric responses have

been identified in composite materials where the magnetoelectric effect is the product property of a magnetostrictive and a piezoelectric material and in multiferroic materials [5].

Symmetry also has a key role to play in magnetoelectricity. In fact, Curie's early work had already pointed to the fact that symmetry was a key issue in the search for magnetoelectric materials, but it was not until much later that researchers realized magnetoelectric responses could only occur in time-asymmetric materials [44]. Detailed symmetry analyses [45–47] have produced lists of magnetoelectric point groups and tensor elements. By definition the magnetoelectric effect involves both magnetic and electric fields, thereby ruling out materials with either time reversal or inversion symmetry. In the end there are only 58 magnetic point groups that allow the magnetoelectric effect. These symmetry concerns have led to a strict set of criteria that must be met for a material to exhibit magnetoelectric behavior.

3.4 Multiferroic Materials for Memory Applications

Multiferroics have a storied history dating back to the 1950s. At that time, Soviet scientists attempted to replace partially diamagnetic ions with paramagnetic ones on the *B*-site of octahedral perovskites [48, 49] making the phases $\text{Pb}(\text{Fe}_{1/2}\text{Nb}_{1/2})\text{O}_3$ and $\text{Pb}(\text{Fe}_{1/2}\text{Ta}_{1/2})\text{O}_3$ which were found to be both ferroelectric and antiferromagnetic. This sparked the birth of the field of multiferroics. Following this initial period of interest throughout the 1960s and 1970s, these materials were relegated to the realms of physics novelty as the complex nature of these materials made it quite difficult to produce high quality materials that possessed the desired combination of properties. The so-called renaissance of magnetoelectric multiferroics [50] came in the early 2000s as combined advances in the production of high-quality thin films and bulk single crystals were augmented by significant advances in materials characterization (especially scanning probe, optical, neutron, and synchrotron-based techniques) made it, for the first time, possible to synthesize high-quality samples and characterize multiple order parameters in these materials.

Today there are roughly four major classes of multiferroic materials (1) materials with the perovskite structure, (2) materials with hexagonal structure, (3) boracites, and (4) BaMF_4 compounds. Briefly we will investigate each of these classes of multiferroics before proceeding to focus on one major example. Let us begin at the end of the list by investigating multiferroics with BaMF_4 ($M = \text{Mg, Mn, Fe, Co, Ni, and Zn}$) structure. These materials have been studied since the late 1960s and are typically defined by their orthorhombic structure and $2mm$ point group symmetry [51, 52]. Often their extrapolated Curie temperatures are very high (in excess of the melting point) and at low temperatures (<100 K) the ferroelastic, ferroelectric structure exhibits antiferromagnetic or weakly ferromagnetic order [53]. Moving on to some of the other common multiferroic structures, the boracites, with general chemical formula $M_3\text{B}_7\text{O}_{13}\text{X}$ ($M = \text{Cr, Mn, Fe, Co, Cu, Ni}$; $\text{X} = \text{Cl, Br}$), are typically ferroelastic ferroelectric, antiferromagnets (and occasionally weakly ferromagnetic).

In some cases the ferroelectric Curie temperature can exceed room temperature, but (again) the magnetic ordering temperatures are generally less than 100 K [53]. The materials undergo a classic transition from a high-temperature cubic phase ($-43m$ symmetry) [54] at high temperatures to an orthorhombic structure ($mm2$ symmetry). Note that some phases also possess subsequent phase transitions to m and $3m$ symmetry at lower temperatures [55, 56]. The third common class of multiferroic materials are those possessing hexagonal structure and general chemical formula ABO_3 or $A_2B'B''O_6$. Of these materials, the best known and studied are the hexagonal ferroelectric, antiferromagnetic manganites ($RMnO_3$, $R = \text{Sc, Y, In, Ho, Er, Tm, Yb, Lu}$) which were first discovered in the late 1950s [57, 58]. These materials are defined by $6mm$ symmetry and up to four long-range ordered subsystems, including the ferroelectric lattice with Curie temperatures typically between 570 and 990 K [53, 58], the antiferromagnetic Mn^{3+} lattice with Néel temperatures typically between 70 and 130 K [59], and two rare-earth sublattices with magnetic order temperatures below ~ 5 K [60]. This brings us to the oldest and best known class of multiferroic materials that are based on the perovskite structure with general chemical formula ABO_3 , $A_2B'B''O_6$, or a large variety of doped or chemically substituted phases. Generally multiferroic perovskites do not possess ideal cubic symmetry ($m3m$), but have some slight deformation (i.e., a rhombohedral distortion as is the case in BiFeO_3 which has $3m$ symmetry). There are a large number of multiferroic perovskites (for a nice listing see [53]), but by far the most widely studied material has been BiFeO_3 . Bismuth ferrite or BiFeO_3 is a ferroelastic ferroelectric, antiferromagnet with high ordering temperatures and can be chemically alloyed to tune the properties. Because of the versatility of this material, the high ordering temperatures, and the robust order parameters, it has attracted unprecedented attention since the first half of the 2000s.

The re-emergence of interest in multiferroics has been driven, in part, by the development of thin film growth techniques that allow for the production of non-equilibrium phases of materials and strain engineering of existing materials [61]. Thin films offer a pathway to the discovery and stabilization of a number of new multiferroics in conjunction with the availability of high-quality materials that can be produced in larger lateral sizes than single crystal samples. Much of the recent success in strain engineering of multiferroics has arisen from the development of new oxide substrate materials. Techniques and materials developed during the intense study of high-temperature superconductors in the 1980s and 1990s have led to a wide variety of oxide substrates. Many of the current technologically relevant multiferroics materials possess perovskite or perovskite-derived structures and thus chemically and structurally compatible perovskite substrates are needed [62]. These substrates include YAlO_3 , LaSrAlO_4 , LaAlO_3 , LaSrGaO_4 , NdGaO_3 , $(\text{LaAlO}_3)_{0.29}(\text{Sr}_{0.5}\text{Al}_{0.5}\text{TaO}_3)_{0.71}$ (LSAT), LaGaO_3 , SrTiO_3 , DyScO_3 , GdScO_3 , SmScO_3 , KTaO_3 , and NdScO_3 that give quality starting materials with lattice parameters from as low as ~ 3.70 Å to ~ 4.0 Å. Using such substrates, multiferroic thin films and nanostructures have been produced using a wide variety of growth techniques including sputtering, spin coating, pulsed laser deposition, sol-gel processes, metal-organic chemical vapor deposition, molecular beam epitaxy, and more.

Despite the fact that there are a number of algorithms with which one can create multiferroism in materials, to date only a limited number of single-phase multiferroics produced as thin films include the hexagonal manganites and Bi- and Pb-based perovskites. In this section we will investigate these single-phase thin film multiferroics in more detail.

3.4.1 Manganite Thin Films

The rare-earth manganites ($RE\text{MnO}_3$) are an intriguing materials system and depending on the size of the RE ion the structure takes on an equilibrium orthorhombic ($RE=\text{La-Dy}$) or hexagonal ($RE=\text{Ho-Lu}$, as well as Y) structure [63]. All of the hexagonal rare-earth manganites are known to show multiferroic behavior with relatively high ferroelectric ordering temperatures (typically in excess of 590 K) and relatively low magnetic ordering temperatures (typically between 70 and 120 K) [64]. In these hexagonal phases, the ferroelectric ordering is related to the tilting of the rigid MnO_5 trigonal bipyramid [27]. On the other hand, only the orthorhombic phases with $RE=\text{Dy, Tb, and Gd}$ are multiferroic in nature and have very low ($\sim 20\text{--}30$ K) ferroelectric ordering temperatures [32, 65]. In these materials the ferroelectricity arises from magnetic ordering induced lattice modulations.

One of the earliest thin-film multiferroic manganites to be produced was the hexagonal manganite YMnO_3 (Fig. 3.5a) [67]. Work on YMnO_3 in the 1960s suggested that it was both a ferroelectric [63] and an A-type antiferromagnet [59]; however, it was not until sometime later that the true nature of ferroelectricity in this material was understood to arise from long-range dipole-dipole interactions and oxygen rotations working together to drive the system towards a stable ferroelectric state [27]. The first films [67] were grown via radio-frequency magnetron sputtering and obtained epitaxial (0001) films on MgO (111) and ZnO (0001)/sapphire (0001)

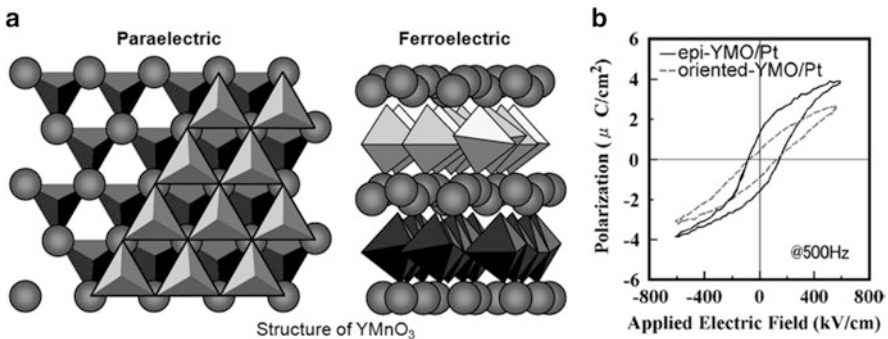


Fig. 3.5 YMnO_3 . (a) The crystal structure of YMnO_3 in the paraelectric and ferroelectric phases. The trigonal bipyramids depict MnO_5 polyhedra and the spheres represent Y ions. (Adapted from [27]) (b) P - E hysteresis of the epitaxial-YMO/Pt and the oriented-YMO/Pt. (Adapted from [66])

and polycrystalline films on Pt (111)/MgO (111). It was soon shown that using the epitaxial strain intrinsic to such thin films, one could drive the hexagonal phase of YMnO_3 to a metastable, non-ferroelectric orthorhombic perovskite phase by growth on the appropriate oxide substrates including SrTiO_3 (001) and NdGaO_3 (101) [68]. This work was of great interest because it was the first evidence for a competition between hexagonal and orthorhombic YMnO_3 phases and how epitaxial thin film strain could be used to influence the structure of this material. This is a perfect example of the power of epitaxial thin film growth and how it can give researchers access to high pressure and temperature phases that are not easily accessible by traditional bulk synthesis techniques. Since this time YMnO_3 has been grown on a number of other substrates including Si (001) [67, 69], $\text{Pt/TiO}_2/\text{SiO}_2/\text{Si}$ (001) [70], Y-stabilized ZrO_2 (111) [71], and GaN/sapphire (0001) [72, 73] and with a wide range of deposition techniques including sputtering [69, 72], spin coating [70], sol-gel processes [74], pulsed laser deposition [75, 76], metal-organic chemical vapor deposition [77], and molecular beam epitaxy [72].

Although thin films of YMnO_3 typically exhibit a reduction in the ferroelectric polarization as compared to bulk single crystals [67], high quality epitaxial films of YMnO_3 have also been shown to possess better ferroelectric properties than oriented-polycrystalline films (Fig. 3.5b) [66]. Polarization–electric field (P – E) hysteresis loops for YMnO_3 films have revealed that the saturation polarization in YMnO_3 is rather small (just a few $\mu\text{C}/\text{cm}^2$) and that films can have a retention time of 10^4 s at ± 15 V applied voltages. Such results have led some to suggest that YMnO_3 films could be a suitable material for ferroelectric gate field-effect transistors [66], but the high growth temperatures (800 °C [66, 78]–850 °C [79]) make it impractical for integration into current applications. Work has also shown that doping the A -site with more than 5 %-Bi can decrease the deposition temperatures to under 700 °C without detrimentally affecting the electric properties of the material [79]. Like many other manganites, however, A -site doping can also have strong effects on the properties of YMnO_3 [80]. A -site doping with Zr has been shown to decrease leakage currents, while doping with Li and Mg has been found to lead to increases in leakage currents, and finally Li-doping can also drive the antiferromagnetic YMnO_3 to become a weak ferromagnet [78]. The weak ferromagnetic moment is thought to have arisen from a small canting of the Mn spins. The hope that by controlling the carrier concentration researchers could make the normally antiferromagnetic YMnO_3 a robust ferromagnet has not been realized. Additionally, doping on the B -site has been shown to enhance the magnetoelectric coupling in the form of changes in the magnetocapacitance by two orders of magnitude [81].

Over the last few years thin films of a wide range of hexagonal- REMnO_3 materials have been grown. This includes studies of films with $RE = \text{Nd, Ho, Tm, Lu}$ [82], Yb [83], and more recently Tb [84], Dy, Gd, and Sm [85]. Despite all of this focus, researchers have yet to find a REMnO_3 compound that exhibits both room temperature ferroelectricity and magnetism, but hexagonal manganites remain a diverse system with intriguing scientific implications for multiferroic materials. An increasing amount of work has been reported on thin films of TbMnO_3 , including the first report of in early 2005 [86]. Soon after, Lee et al. [84] showed that a hexagonal thin

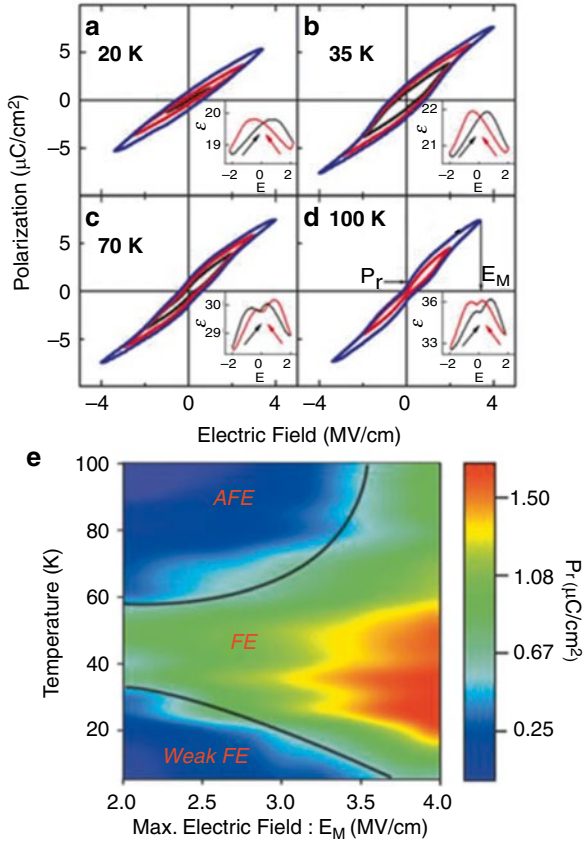


Fig. 3.6 TbMnO_3 . Ferroelectric properties of hexagonal TbMnO_3 as a function of the electric field at selected temperatures. Polarization versus electric field hysteresis loops measured at 2 kHz at (a) 20 K, (b) 35 K, (c) 70 K, and (d) 100 K. Insets show the hysteresis loops of the dielectric constant versus the electric field at 100 kHz. (e) A phase diagram showing the ferroelectric and antiferroelectric regions as a function of temperature and electric field. The maximum remnant polarization value is also plotted. (Adapted from [84])

film form of TbMnO_3 can be stabilized that shows 20 times larger remnant polarization and an increase in the ferroelectric ordering temperature to near 60 K (Fig. 3.6). More recently, studies have also demonstrated the ability to create ferromagnetic interactions (below an ordering temperature of ~ 40 K) in partially strained TbMnO_3 films on SrTiO_3 substrates [87, 88] and possible connection between the domain structure of these films and the enhanced magnetization [89]. What has become apparent is that these hexagonal/orthorhombic manganites serve as a model system in the study of the power of thin film epitaxy to engineer new phases and properties—and the role of epitaxial strain in stabilizing the hexagonal- REMnO_3 phases is paramount in creating high quality samples of these materials for further study. Additionally, more recently the $\text{RE}\text{Mn}_2\text{O}_5$ ($\text{RE}=\text{rare earth, Y, and Bi}$) family of

materials has been studied extensively and has been shown to possess intriguing fundamental physics including coinciding transition temperatures for magnetism and ferroelectricity as well as strong coupling between these order parameters [33]. Prior to 2010, most studies focused on these materials were centered on bulk or single crystal samples and only recently have thin films for these materials been created [90].

3.4.2 *BiMnO₃ Thin Films*

Conventional growth of bulk samples of the ferromagnetic, ferroelectric [18] BiMnO_3 required high temperatures and pressures [91] because the phase is not normally stable at atmospheric pressure. Such phases lend themselves well to thin film growth where epitaxial strain stabilization of metastable phases can be achieved. The first growth of BiMnO_3 thin films was on SrTiO_3 (001) single crystal substrates using pulsed laser deposition [92] and was quickly confirmed in other studies [93]. Films of BiMnO_3 have been found to be ferroelectric below ~ 450 K and undergo an unusual orbital ordering leading to ferromagnetism at ~ 105 K (Fig. 3.7a) [19].

Temperature-dependent magnetic measurements have also shown that the ferromagnetic transition temperature varies depending on the substrate and can be as low as 50 K on LaAlO_3 [94]. This depression in Curie temperature has been attributed to concepts as varied as stoichiometry issues, strain, and size effects. The ferromagnetic nature of BiMnO_3 has led some to study it as a potential barrier layer in magnetically and electrically controlled tunnel junctions [95] and eventually led to the production of a four-state memory concept based on La-doped BiMnO_3 multiferroics [96]. Gajek et al. reported La-doped BiMnO_3 films that retained their multiferroic character down to thicknesses less than 2 nm and proved that multiferroic materials could be used to create new memories by demonstrating the possibility of spin-dependent tunneling using multiferroic barrier layers in magnetic tunnel junctions.

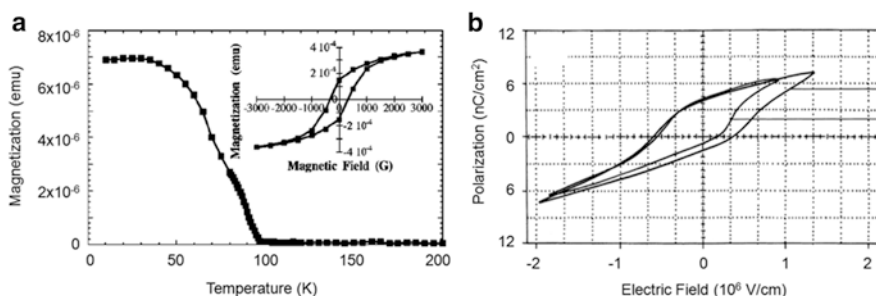


Fig. 3.7 BiMnO_3 . (a) Magnetization curve of a BiMnO_3 film cooled under no applied magnetic field. The *inset* shows the ferromagnetic hysteresis loop at 5 K. (Adapted from [92]) (b) P - E hysteresis loop of a thin film of BiMnO_3 on Si (100) above and below the ferromagnetic T_C . (Adapted from [18])

More recently, significantly La-doped BiMnO_3 films have been shown to exhibit a 70-fold increase in the magnetodielectric effect compared to pure BiMnO_3 [97]. Unfortunately, it coincides with a decrease in the ferroelectric Curie temperature to ~ 150 K and is observed only at applied magnetic fields of $9T$. Additionally, optical second-harmonic measurements with applied electric fields [93], as well as Kelvin force microscopy techniques [94], have been used to confirm the presence of ferroelectric polarization in BiMnO_3 films. High levels of leakage, however, have limited direct P - E hysteresis loop measurements (Fig. 3.7b) on thin film samples and recently the reanalysis of diffraction data [98] and first-principles calculations [99] have called into question the ferroelectricity in BiMnO_3 . Some calculations have predicted a small polar canting of an otherwise antiferroelectric structure (weak ferroelectricity) that could be used to explain the experimental findings [100]. Regardless, recent studies of dielectric properties of BiMnO_3 thin films done using impedance spectroscopy between 55 and 155 K reveal that there is a large peak in the dielectric permittivity in thin films at the paramagnetic–ferromagnetic transition that could point to indirect coupling effects via the lattice in this material [101].

3.4.3 BiFeO_3 Thin Films

No other single-phase multiferroic has experienced the same level of attention as BiFeO_3 in the last 7 years and because of this we will discuss the evolution of this material in more length. The perovskite BiFeO_3 was first produced in the late 1950s [102] and many of the early studies were focused on the same concepts important today—the potential for magnetoelectric coupling [103]. Throughout the 1960s and 1970s much controversy surrounded the true physical and structural properties of BiFeO_3 , but as early as the 1960s BiFeO_3 was suspected to be an antiferromagnetic, ferroelectric multiferroic [104, 105]. The true ferroelectric nature of BiFeO_3 , however, remained somewhat in question until ferroelectric measurements made at 77 K in 1970 [105] revealed a spontaneous polarization of $\sim 6.1 \mu\text{C}/\text{cm}^2$ along the 111-direction which were found to be consistent with the rhombohedral polar space group $R3c$ determined from single crystal X-ray diffraction [106] and neutron diffraction studies [107]. These findings were at last confirmed by detailed structural characterization of ferroelectric/ferroelastic monodomain single crystal samples of BiFeO_3 in the late 1980s [103]. Chemical etching experiments on ferroelastic single domains later proved without a doubt that the BiFeO_3 was indeed polar, putting to rest the hypothesis that BiFeO_3 might be antiferroelectric, and proved that the ferroelectric/ferroelastic phase was stable from 4 K to $\sim 1,103$ K [108]. The structure of BiFeO_3 can be characterized by two distorted perovskite blocks connected along their body diagonal or the pseudocubic $\langle 111 \rangle$, to build a rhombohedral unit cell (Fig. 3.8a). In this structure the two oxygen octahedra of the cells connected along the $\langle 111 \rangle$ are rotated clockwise and counterclockwise around the $\langle 111 \rangle$ by $\pm 13.8(3)^\circ$ and the Fe-ion is shifted by 0.135 \AA along the same axis away from the oxygen octahedron center position. The ferroelectric state is realized by a large displacement of the Bi-ions relative to the FeO_6 octahedra (Fig. 3.8a–c) [103, 111].

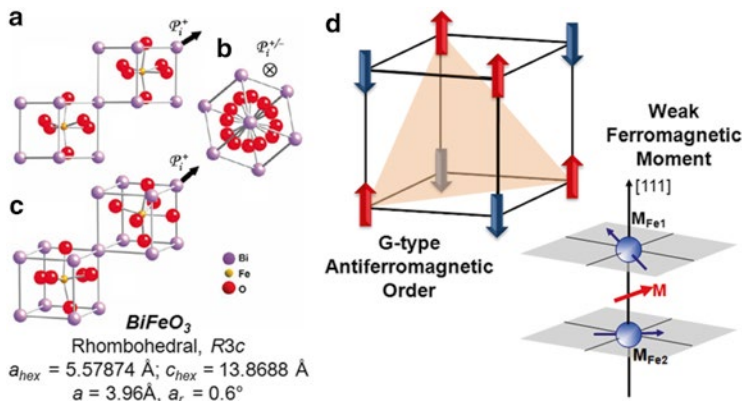


Fig. 3.8 BiFeO_3 . (a) Structure of BiFeO_3 shown looking (a) down the pseudocubic- $[109]$, (b) down the pseudocubic- $[110]$ polarization direction, and (c) a general three-dimensional view of the structure. (d) The magnetic structure of BiFeO_3 is shown including G-type antiferromagnetic ordering and the formation of the weak ferromagnetic moment. (Adapted from [7])

During the 1980s, the magnetic nature of BiFeO_3 was studied in detail. Early studies indicated that BiFeO_3 was a G-type antiferromagnet (G-type antiferromagnetic order is shown schematically in Fig. 3.8d) with a Néel temperature of $\sim 673 \text{ K}$ [112] and possessed a cycloidal spin structure with a period of $\sim 620 \text{ \AA}$ [113]. This spin structure was found to be incommensurate with the structural lattice and was superimposed on the antiferromagnetic order. It was also noted that if the moments were oriented perpendicular to the $\langle 111 \rangle$ -polarization direction the symmetry also permits a small canting of the moments in the structure resulting in a weak ferromagnetic moment of the Dzyaloshinskii–Moriya type (Fig. 3.8d) [35, 36].

In 2003 a paper focusing on the growth and properties of thin films of BiFeO_3 spawned a hailstorm of research into thin films of BiFeO_3 that continues to the present day. The paper reported enhancements of polarization and related properties in heteroepitaxially constrained thin films of BiFeO_3 [17]. Structural analysis of the films suggested differences between films (with a monoclinic structure) and bulk single crystals (with a rhombohedral structure) as well as enhancement of the polarization up to $\sim 90 \mu\text{C}/\text{cm}^2$ at room temperature and enhanced thickness-dependent magnetism compared to bulk samples. In reality, the high values of polarization observed actually represented the intrinsic polarization of BiFeO_3 . Limitations in the quality of bulk crystals had kept researchers from observing such high polarization values until much later in bulk samples [109]. More importantly this report indicated a magnetoelectric coupling coefficient as high as $3 \text{ V}/\text{cm Oe}$ at zero applied field [17]. A series of detailed first-principles calculations utilizing the local spin-density approximation (LSDA) and LSDA+U methods helped shed light on the findings in this paper. Calculations of the spontaneous polarization in BiFeO_3 suggested a value between 90 and $100 \mu\text{C}/\text{cm}^2$ (consistent with those measured in 2003) [110] which have since been confirmed by many other experimental reports (an example is shown in Fig. 3.9) [114].

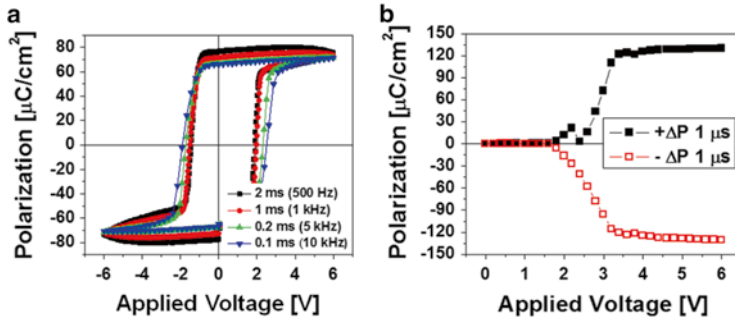


Fig. 3.9 (a) Ferroelectric polarization—electric field hysteresis loop of epitaxial BiFeO_3 thin film measured at various frequencies and (b) PUND measurement for varying voltages at 1 μs voltage pulses. (Adapted from [114])

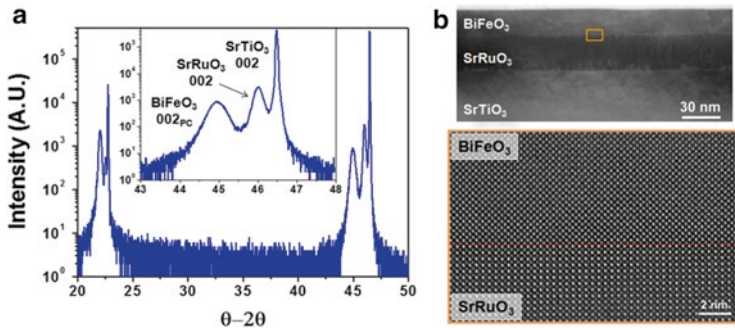


Fig. 3.10 (a) X-ray diffraction results from a fully epitaxial, single-phase $\text{BiFeO}_3/\text{SrRuO}_3/\text{SrTiO}_3$ (001) heterostructure. (b) Low- and high-resolution transmission electron microscopy images of this same heterostructure (adapted from [7])

Today, much progress has been made in understanding the structure, properties, and growth of thin films of BiFeO_3 . High quality epitaxial BiFeO_3 films have been grown via molecular beam epitaxy [115, 116], pulsed laser deposition [17, 117], radio-frequency (RF) sputtering [118, 119], metal-organic chemical vapor deposition (MOCVD) [120, 121], and chemical solution deposition (CSD) [122] on a wide range of substrates including traditional oxide substrates as well as Si [117, 123] and GaN [124]. This work has shown that high quality films, like those shown in Fig. 3.10 can be produced. Typical XRD $\theta-2\theta$ measurements (Fig. 3.10a) show the ability of researchers to produce high quality, fully epitaxial, single-phase films of BiFeO_3 (data here is for a $\text{BiFeO}_3/\text{SrRuO}_3/\text{SrTiO}_3$ (001) heterostructure). Detailed XRD analysis has shown that films possess a monoclinic distortion of the bulk rhombohedral structure over a wide range of thicknesses, but the true structure of very thin films (<15 nm) remains unclear [125]. The quality of such heterostructures as produced by pulsed laser deposition can be probed further by transmission electron microscopy (TEM) (Fig. 3.10b). TEM imaging reveals films that are uniform

over large areas and with the use of high-resolution TEM we can examine the atomically abrupt, smooth, and coherent interface between BiFeO_3 and a commonly used bottom electrode material SrRuO_3 .

3.4.3.1 Controlling Domain Structures in BiFeO_3

Today, aided by such thin film synthesis techniques, significant advances have been made in controlling domain structures in thin films of BiFeO_3 . This work, in turn, has enabled significant progress in the understanding of this complex multiferroic material. In addition to being of great interest for photonic devices, nanolithography, and more, fine control of the domain structures and the ability to create extremely high quality thin films of these materials make it possible to probe a number of important questions related to this material. To begin this discussion, it is essential that we first understand what kinds of domain patterns can be obtained in rhombohedral ferroelectrics. Several theoretical studies have been published that provide equilibrium domain patterns of rhombohedral ferroelectrics such as BiFeO_3 . On the $(001)_c$ perovskite surface, there are eight possible ferroelectric polarization directions corresponding to four structural variants of the rhombohedral ferroelectric. Early work published by Streiffer et al. [126] found that domain patterns can develop with either $\{100\}_c$ or $\{101\}_c$ boundaries for $(001)_c$ oriented rhombohedral films. In both cases, the individual domains in the patterns are energetically degenerate and thus equal width stripe patterns are theoretically predicted. Zhang et al. [127] have gone on to use phase field simulations to understand how strain state can affect the polarization variants and to predict the domain structures in epitaxial BiFeO_3 thin films with different orientations. In these models, long-range elastic and electrostatic interactions were taken into account as were the effects of various types of substrate constraints on the domain patterns. These findings suggest that the domain structure of BiFeO_3 thin films can be controlled by selecting proper film orientations and strain constraints. Moreover, these phenomenological analyses reveal that both the depolarization energy and the elastic energy play a key role in determining the equilibrium domain structures. For instance, in the case of an asymmetrical electrostatic boundary condition (i.e., the presence of a bottom electrode) the dominant domain scaling mechanism changes from electrostatic-driven to elastic-driven. Therefore, the domain size scaling law in epitaxial BiFeO_3 films is predicted to show a different behavior from the conventional elastic domains: the 101-type or the so-called 71° domains are expected to be much wider than the 100-type or the so-called 109° domains despite the fact that these $\{100\}$ boundaries possess a larger domain wall energy.

Experimental demonstration of similar ideas has progressed in recent years. In 2006, Chu et al. [128] demonstrated an approach to create one-dimensional nanoscale arrays of domain walls in epitaxial BiFeO_3 films. Focusing on $\text{BiFeO}_3/\text{SrRuO}_3/\text{DyScO}_3$ (110) heterostructures, the authors took advantage of the close lattice matching between BiFeO_3 , SrRuO_3 , and DyScO_3 (110) and the anisotropic in-plane lattice parameters of DyScO_3 ($a_1=3.951 \text{ \AA}$ and $a_2=3.946 \text{ \AA}$) to pin the

structure of the SrRuO_3 layer and, in turn, the ferroelectric domain structure of BiFeO_3 . This anisotropic in-plane strain condition leads to the exclusion of two of the possible structural variants. Phase field modeling of the ferroelectric domain structure in such heterostructures predicted stripe-like ferroelectric domain structures which were confirmed in the final BiFeO_3 films. The growth mechanism of the underlying SRO layer was found to be important in determining the final ferroelectric domain structure of the BiFeO_3 films. SRO layers grown via step-bunching and step-flow growth mechanisms resulted in ferroelectric domain structures with 4-polarization variants and 2-polarization variants, respectively. These films have been shown to exhibit excellent ferroelectric properties with room temperature $2P_r = 120\text{--}130 \mu\text{C}/\text{cm}^2$ and strong intrinsic ferroelectric properties [114].

In 2007, Chu et al. [129] further demonstrated the ability to create different domain structures in epitaxial BiFeO_3 films on (001), (110), and (111) SrTiO_3 substrates that were consistent with phase field models. Such a result made a connection between the theoretical predictions and experiments and offered one pathway for researchers to simplify the complex domain structure of the BiFeO_3 films. What was discovered was that one must induce a break in the symmetry of the various ferroelectric variants. One avenue to accomplish this is through the use of vicinal SrTiO_3 substrates. Beginning with a (001) oriented substrate, one can progressively tilt the crystal along different directions to end up with different orientations. For instance, by tilting 45° along the 010-direction one can obtain a (110) oriented substrate, while tilting by another 45° along the 110-direction gives rise to a (111) oriented substrate. Through the use of carefully controlled, vicinally cut (001) SrTiO_3 substrates researchers were able to demonstrate fine control of the ferroelectric domain structure in BiFeO_3 . This includes evolving the domain structure from possessing 4-variants, 2-variants, and 1-variant. Added control comes from the use of asymmetric boundary conditions including the use of SrRuO_3 bottom electrodes that drives the out-of-plane component of polarization to be preferentially downward pointing. Other reports have also demonstrated similar findings in films grown on highly miscut SrTiO_3 (001) substrates [119]. These films represent an important step forward in that they provide a set of model thin films that can be used to further explore the magnetoelectric properties of this system as well as its interactions with other layers. Additionally, multiferroic materials with electrically controllable periodic domain structures such as these could be of great interest for applications in photonic devices.

Finally, in 2009, Chu et al. [130], through the careful control of electrostatic boundary conditions, such as the thickness of the underlying SrRuO_3 bottom electrode, were able to demonstrate the creation of ordered arrays of the prototypical domain structures as predicted by Streiffer et al. nearly 10 years earlier [126] (Fig. 3.11a, b). Figure 3.11a represents a series of 71° domain walls located on 101-type planes and Fig. 3.11b represents a series of 109° domain walls located on 100-type planes. When the bottom electrode layer is thick (typically >10 nm and thus a good metal) the presence of an asymmetric boundary condition results in the formation of a film that is fully out-of-plane polarized downward towards the SrRuO_3 layer and elastic energy is the dominant energy in the system. On the other

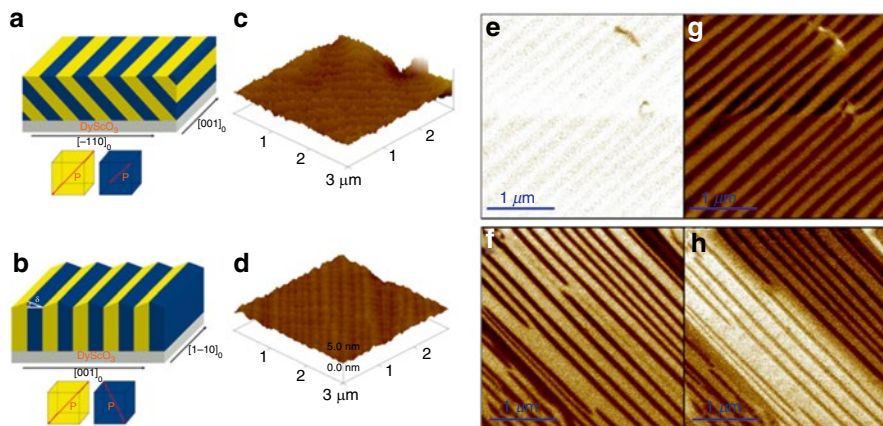


Fig. 3.11 Ordered arrays of ferroelectric domains and domain walls. (a) and (b) Schematics of equilibrium structure of an ordered array of 71° and 109° domain walls, respectively. (c) and (d) Surface topography as measured by AFM of 71° and 109° domain walls samples, respectively. Out-of-plane (e) and (f) as well as in-plane (g) and (h) PFM images for samples possessing ordered arrays of 71° and 109° domain walls. (Adapted from [130])

hand, when the SrRuO₃ layer is very thin, electrostatic energy becomes the dominant energy and drives the film to have domains alternatively pointing up and down. The surface morphology of the resulting films with 71° (Fig. 3.11c) and 109° (Fig. 3.11d) is consistent with the theoretically predicted structure. The corresponding out-of-plane (Fig. 3.11e, f) and in-plane (Fig. 3.11g, h) PFM images confirm the presence of the periodic, equilibrium domain structures. Similarly, studies focused on BiFeO₃ films grown on the new substrate TbScO₃ (which has <-0.3 % lattice mismatch with BiFeO₃) resulted in BiFeO₃ films possessing ordered arrays of (010) domain walls [131].

In addition to epitaxial growth control of ferroelectric domain structures, recent advances in scanning probe-based manipulation of ferroelectric domain structures have opened up the next level of control. Zavaliche et al. [111] have developed a standard procedure to use PFM to characterize and understand the domain structure of such ferroelectric materials. These studies have identified locally three possible polarization switching mechanisms namely 71°, 109°, and 180° rotations of the polarization direction. 180° polarization reversals appear to be the most favorable switching mechanism in epitaxial films under an applied bias along [001]. A combination of phase field modeling and scanning force microscopy of carefully controlled, epitaxial [109] BiFeO₃ films with a simplified domain structure revealed that the polarization state can be switched by all three primary switching events by selecting the direction and magnitude of the applied voltage [132]. Moreover, the instability of certain ferroelastic switching processes and domains can be dramatically altered through a judicious selection of neighboring domain walls. The symmetry breaking of the rotationally invariant tip field by tip motion enables deter-

ministic control of non-180° switching in rhombohedral ferroelectrics. The authors also demonstrated the controlled creation of a ferrotoroidal order parameter. The ability to control local elastic, magnetic and toroidal order parameters with an electric field will make it possible to probe local strain and magnetic ordering, and engineer various magnetoelectric, domain-wall-based and strain-coupled devices.

For eventual device applications, the use of a coplanar epitaxial electrode geometry has been proposed to aid in controlling multiferroic switching in BiFeO₃ [133]. PFM has been used to detect and manipulate the striped ferroelectric domain structure of a BiFeO₃ thin film grown on DyScO₃ (110) substrates. Time-resolved imaging revealed ferroelastic switching of domains in a needle-like region that grew from one electrode toward the other. Purely ferroelectric switching was suppressed by the geometry of the electrodes. Such results demonstrate the capability to control the ferroelectric order parameter and domain structures in device architectures.

3.4.3.2 Evolution of Magnetism and Domain Wall Functionality in BiFeO₃

The ability to control domain structures has also been demonstrated to have serious implications for the evolution of magnetism in thin films (i.e., variations from the bulk picture and the mechanism of enhanced magnetism in thin films) and has suggested the strong role of domain walls in determining macroscopic properties. In this section we investigate the evolution of magnetic properties in BiFeO₃.

Early theoretical treatments attempted to understand the nature of magnetism and coupling between order parameters in BiFeO₃. Such calculations confirmed the possibility of weak ferromagnetism arising from a canting of the antiferromagnetic moments in BiFeO₃. The canting angle was calculated to be $\sim 1^\circ$ and would result in a small, but measurable, magnetization of ~ 8 emu/cm³ or $\sim 0.05 \mu_B$ per unit cell [134]. It was also found that the magnetization should be confined to an energetically degenerate easy {111} perpendicular to the polarization direction in BiFeO₃. These same calculations further discussed the connection of the weak ferromagnetism and the structure (and therefore ferroelectric nature) of BiFeO₃. This allowed the authors to extract three conditions necessary to achieve electric-field-induced magnetization reversal (1) the rotational and polar distortions must be coupled; (2) the degeneracy between different configurations of polarization and magnetization alignment must be broken; (3) there must be only one easy magnetization axis in the (111) which could be easily achieved by straining the material [134].

This work coincided with considerable experimental work reporting on the nature of magnetism in thin film BiFeO₃. This subject, although contentious for some time, appears to be nearly fully understood. The original work of Wang et al. presented an anomalously large value of magnetic moment (of the order of 70 emu/cm³) [17], which is significantly higher than the expected canted moment of ~ 8 emu/cm³. There have been several studies aimed at clarifying the origins of this anomalous magnetism. Eerenstein et al. [135] proposed that the excess magnetism was associated with magnetic second phases (such as γ -Fe₂O₃); this was supported by

the studies of Béa et al. [136] who showed that BiFeO₃ films, when grown under reducing conditions (for example, under oxygen pressures lower than 1×10^{-3} Torr) showed enhanced magnetism as a consequence of the formation of magnetic second phases. It is, however, important to note that low oxygen pressure during growth is not the cause for the enhanced moment in the 2003 report by Wang et al. where films were grown in oxygen pressures between 100 and 200 mTorr and cooled in 760 Torr rendering formation of such secondary magnetic phases thermodynamically unlikely and there was no evidence (despite extensive study of samples with X-ray diffraction and transmission electron microscopy techniques) for such second phases. Furthermore, subsequent X-ray magnetic circular dichroism studies supported the assertion that this magnetism is *not* from a magnetic γ -Fe₂O₃ impurity phase [137]. To date, additional mixed reports—including reports of enhanced magnetism in nanoparticles of BiFeO₃ [138] as well as the observation of samples exhibiting no such enhancement—have been presented.

What has emerged, however, is that the synthesis process can have considerable effect on the overall magnetic properties of this complex material—especially in the study of epitaxially strained thin films. For instance, Ederer and Spaldin found that only one easy magnetization axis in the energetically degenerate 111-plane of BiFeO₃ might be selected when one was to strain the material appropriately [134]. Until recently this scientifically and technologically important question of how magnetic order in multiferroics such as BiFeO₃ develops with strain and size effects had remained unanswered. In early 2010, using angle and temperature-dependent dichroic measurements and photoemission spectromicroscopy (Fig. 3.12), Holcomb et al. [139] discovered that the antiferromagnetic order in BiFeO₃ did indeed evolve and change systematically as a function of thickness and strain. Lattice mismatch induced strain was found to break the easy-plane magnetic symmetry of the bulk and leads to an easy axis of magnetization that can be controlled via the sign of the strain—110-type for tensile strain and 112-type for compressive strain. This understanding of the evolution of magnetic structure and the ability to manipulate the magnetism in this model multiferroic has significant implications for eventual utilization of such magnetoelectric materials in applications.

Also during the last few years, a number of exciting findings have come to light that are poised to definitively answer the questions surrounding the wide array of magnetic properties observed in BiFeO₃ thin films. There is now a growing consensus that epitaxial films (with a thickness less than ~ 100 nm) are highly strained and thus the crystal structure is more akin to a monoclinic phase rather than the bulk rhombohedral structure. Furthermore, a systematic dependence of the ferroelectric domain structure in films as a function of the growth rate has been observed [140]. Films grown very slowly (for example by MBE, laser-MBE, or off-axis sputtering) exhibit a classical stripe-like domain structure that is similar to ferroelastic domains in tetragonal Pb(Zr_xTi_{1-x})O₃ films. Due to symmetry considerations, two sets of such twins are observed. These twins are made up of 71° ferroelastic walls, that form on the {101}-type planes (which is a symmetry plane). In contrast, if the films are grown rapidly (as was done in the original work of Wang et al. [17]) the domain structure is dramatically different. It now resembles a mosaic-like ensemble that

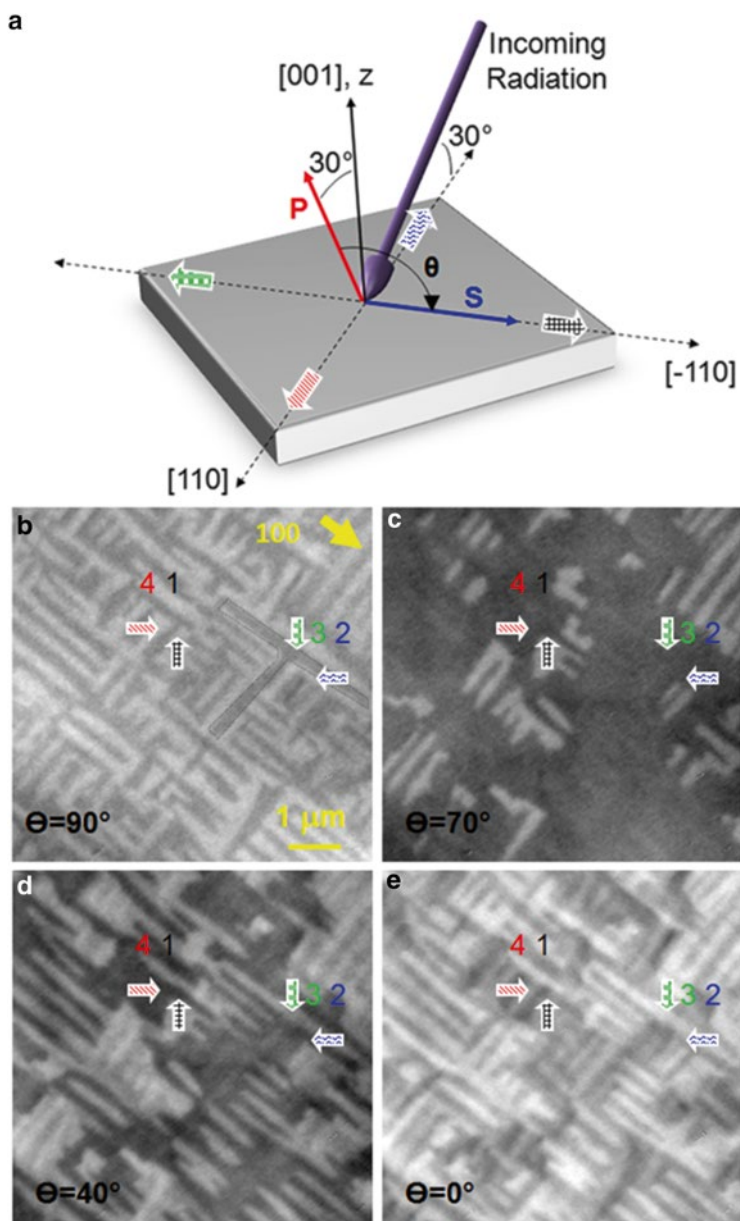


Fig. 3.12 (a) Schematic illustrating the experimental geometries used to probe the angle dependent linear dichroism in BiFeO₃. Photoemission electron microscopy images of BiFeO₃ at several angles of the electric vector of incident linear polarization α . The outlined arrows show the in-plane projection of the four ferroelectric directions. Images of domain structures taken at (b) $\theta=90^\circ$, (c) $\theta=70^\circ$, (d) $\theta=40^\circ$, and (e) $\theta=0^\circ$ (adapted from [139])

consists of a dense distribution of 71° , 109° , and 180° domain walls. It should be noted that 109° domain walls form on $\{001\}$ -type planes (which is not a symmetry plane for this structure). Preliminary measurements reveal a systematic difference in magnetic moment between samples possessing different types and distributions of domain walls. The work of Martin et al. [140] suggests that such domain walls could play a key role in the many observations of enhanced magnetic moment in BiFeO_3 thin films.

This suggestion builds off of the work of Přívratká and Janovec [141, 142], where detailed symmetry analyses were used to conclude that magnetoelectric coupling could lead to the appearance of a net magnetization in the middle of antiferromagnetic domain walls. Specifically, they showed that this effect is allowed for materials with the $R3c$ space group (i.e., that observed for BiFeO_3). Although such analysis raises the possibility of such an effect, the group-symmetry arguments do not allow for any quantitative estimate of that moment. The idea that novel properties could occur at domain walls in materials presented by Přívratká and Janovec is part of a larger field of study of the morphology and properties of domains and their walls that has taken place over the last 50 years with increasing recent attention given to the study novel functionality at domain walls [143–145]. For instance, recent work has demonstrated that spin rotations across ferromagnetic domain walls in insulating ferromagnets can induce a local polarization in the walls of otherwise non-polar materials [2, 145], preferential doping along domain walls has been reported to induce 2D superconductivity in WO_{3-x} [146] and enhanced resistivity in phosphates [147], while in paraelectric (non-polar) SrTiO_3 the ferroelastic domain walls appear to be ferroelectrically polarized [148]. Taking this idea one step further, Daraktchiev et al. [149, 150] have proposed a thermodynamic (Landau-type) model with the aim of quantitatively estimating whether the walls of BiFeO_3 can be magnetic and, if so, to what extent they might contribute to the observed enhancement of magnetization in ultrathin films. One can develop a simple thermodynamic potential incorporating two order parameters expanded up to P^6 and M^6 terms (the transitions in BiFeO_3 are found experimentally to be first order, and the low-symmetry $(\pm P_0, 0)$ phase is described here) with biquadratic coupling between the two order parameters (biquadratic coupling is always allowed by symmetry, and therefore always present in any system with two order parameters). Because biquadratic free energy terms such as P^2M^2 are scalars in any symmetry group, this potential can be written thusly:

$$\begin{aligned}
 G_{\text{MP}} &= G_0 + \frac{\kappa}{2}(\nabla P)^2 + \frac{\lambda}{2}(\nabla M)^2 + L_{\text{MP}}(P, M) \\
 &= G_0 + \frac{\kappa}{2}(\nabla P)^2 + \frac{\lambda}{2}(\nabla M)^2 + \frac{\alpha}{2}P^2 + \frac{\beta}{4}P^4 + \frac{\eta}{6}P^6 \\
 &\quad + \frac{a}{2}M^2 + \frac{b}{4}M^4 + \frac{n}{6}M^6 + \frac{\gamma}{2}P^2M^2
 \end{aligned} \tag{3.4}$$

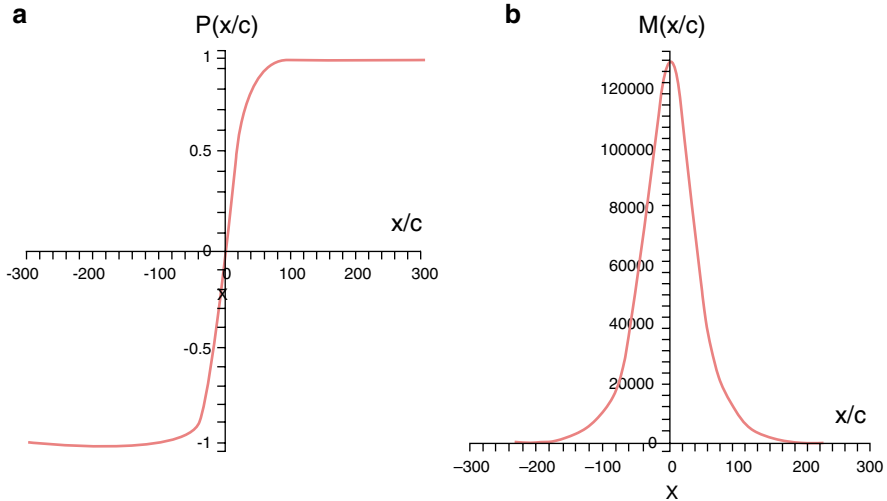


Fig. 3.13 Shape of (a) ferroelectric polarization and (b) magnetism across a domain wall in BiFeO₃ (adapted from [149, 150])

When one goes from $+P$ to $-P$, it is energetically more favorable for the domain wall energy trajectory not to go through the center of the landscape ($P=0, M=0$), but to take a diversion through the saddle points at $M_0 \neq 0$, thus giving rise to a finite magnetization (Fig. 3.13). The absolute values of the magnetic moment at the domain wall will depend on the values of the Landau coefficients as well as the boundary conditions imposed on the system, namely whether the material is magnetically ordered or not. Analysis of the phase space of this thermodynamic potential shows that it is possible for net magnetization to appear in the middle of ferroelectric walls even when the domains themselves are not ferromagnetic (Fig. 3.13b). The authors of this model note, however, that it is presently only a *toy model* which does not take into account the exact symmetry of BiFeO₃, so it cannot yet quantitatively estimate how much domain walls can contribute to the magnetization. The exact theory of magnetoelectric coupling at the domain walls of BiFeO₃ also remains to be formulated.

Recently, a holistic picture of the connection between processing, structure, and properties has brought to light the role of magnetism at ferroelectric domain walls in determining the magnetic properties in BiFeO₃ thin films. By controlling domain structures through epitaxial growth constraints and probing these domain walls with a range of techniques (including detailed magnetotransport studies) He et al. [151] have demonstrated that the formation of certain types of ferroelectric domain walls (i.e., 109° walls) can lead to enhanced magnetic moments in BiFeO₃. Building off of the work of Martin et al. [140], the authors of this study were able to demonstrate that samples possessing 109° domain walls show significant magnetoresistance (up

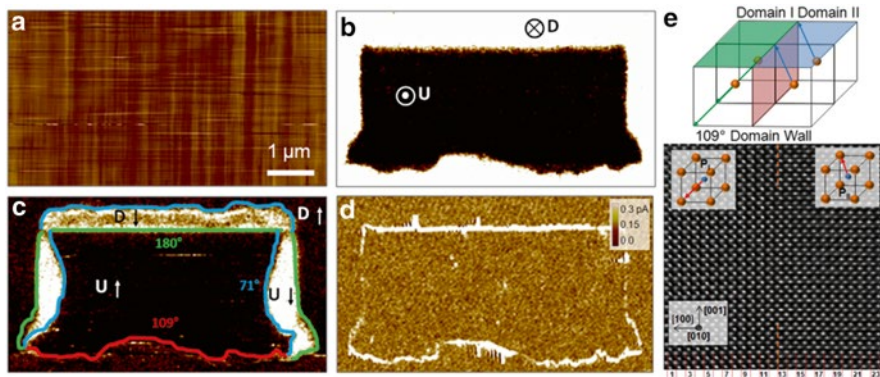


Fig. 3.14 Conduction at domain walls in BiFeO_3 . **(a)** Topographic image of the surface of a model $\text{BiFeO}_3/\text{SrRuO}_3/\text{SrTiO}_3$ (110) sample. Corresponding **(b)** out-of-plane and **(c)** in-plane piezoresponse force microscopy image of an electrically poled region of this film. **(d)** Conducting-atomic force microscopy image reveals that 109° and 180° domain walls are conducting. **(e)** Schematic illustration of a 109° domain wall and a corresponding high-resolution transmission electron microscopy image of a 109° domain wall (adapted from [152])

to 60 %). In summary, it appears certain domain walls can give rise to enhanced magnetic behavior in BiFeO_3 thin films.

It is also important to note that Seidel et al. [152], motivated by the desire to understand similar magnetic properties at domain walls in BiFeO_3 , undertook a detailed scanning probe-based study of these materials and discovered a new and previously unanticipated finding: the observation of room temperature electronic conductivity at certain ferroelectric domain walls. The origin of the observed conductivity was explored using high-resolution transmission electron microscopy and first-principles density functional computations. The results showed that domain walls in a multiferroic ferroelectric such as BiFeO_3 can exhibit unusual electronic transport behavior on a local scale that is quite different from that in the bulk of the material. Using a model (110)-oriented $\text{BiFeO}_3/\text{SrRuO}_3/\text{SrTiO}_3$ heterostructure with a smooth surface (Fig. 3.14a), the researchers were able to switch the BiFeO_3 material in such a way that enabled them to create all the different types of domain walls possible in BiFeO_3 (i.e., 71° , 109° , and 180° domain walls) in a local region (Fig. 3.14b, c). Conducting-atomic force microscopy (c-AFM) measurements (Fig. 3.14d) revealed conduction at 109° and 180° domain walls. Detailed high-resolution transmission electron microscopy studies (Fig. 3.14e) revealed this conductivity was, in part, structurally induced and can be activated and controlled on the scale of the domain wall width—about 2 nm in BiFeO_3 . From the combined study of conductivity measurements, electron microscopy analysis, and density functional theory calculations, two possible mechanisms for the observed conductivity at the domain walls have been suggested: (1) an increased carrier density as a consequence of the formation of an electrostatic potential step at the wall; and/or (2)

a decrease in the band gap within the wall and corresponding reduction in band offset with the *c*-AFM tip. It was noted that both possibilities are the result of structural changes at the wall and both may, in principle, be acting simultaneously, since they are not mutually exclusive.

It is important to step back and recognize the importance of these discoveries and the implications for this work on memory applications. For some time now, domain walls in ferromagnets have been explored for logic and storage applications (see, for example, [153]). Since 2000 there has been increasing effort to probe domain walls in materials for functional devices—including the pioneering work of Allwood et al. [154] who identified possible circuit manifestations for AND and NOR gates using magnetic domain walls. More recently, domain walls in other systems—especially ferroelectric and multiferroic systems—have joined the fray. The observation of conducting domain walls provides an exciting opportunity to create yet another pathway by which it might be possible to store information. This would be particularly facilitated if the conduction at the walls were to be made significantly larger. Research in this direction, however, is still in its infancy, but this topic appears to be an attractive topic for future research. An insulator–metal transition would be a highly desirable pathway to accomplish such large changes in conduction, that are controllable with electric fields. Finally, E. Salje recently summarized the status and promise of twin boundaries in ferroelectrics, as well as curved interfaces between crystalline and amorphous materials, for future device applications [155]. In the end, interface engineering has experienced a great increase in attention of the last decade and the development of new phenomena at interfaces is poised to enable new devices and applications in the future.

3.4.3.3 Magnetoelectric Coupling in BiFeO₃

Although many researchers anticipated strong magnetoelectric coupling in BiFeO₃, until the first evidence for this coupling in 2003 there was no definitive proof. Two years after this first evidence, a detailed report was published in which researchers observed the first visual evidence for electrical control of antiferromagnetic domain structures in a single-phase multiferroic at room temperature. By combining X-ray photoemission electron microscopy (PEEM) imaging of antiferromagnetic domains (Fig. 3.15a, b) and piezoresponse force microscopy (PFM) imaging of ferroelectric domains (Fig. 3.15c, d) the researchers were able to observe direct changes in the nature of the antiferromagnetic domain structure in BiFeO₃ with application of an applied electric field (Fig. 3.15e) [156]. This research showed that the ferroelastic switching events (i.e., 71° and 109°) resulted in a corresponding rotation of the magnetization plane in BiFeO₃ (Fig. 3.15f) and has paved the way for further study of this material in attempts to gain room temperature control of ferromagnetism (to be discussed in detail later). This work has since been confirmed by neutron diffraction experiments in single crystal BiFeO₃ as well [157, 158].

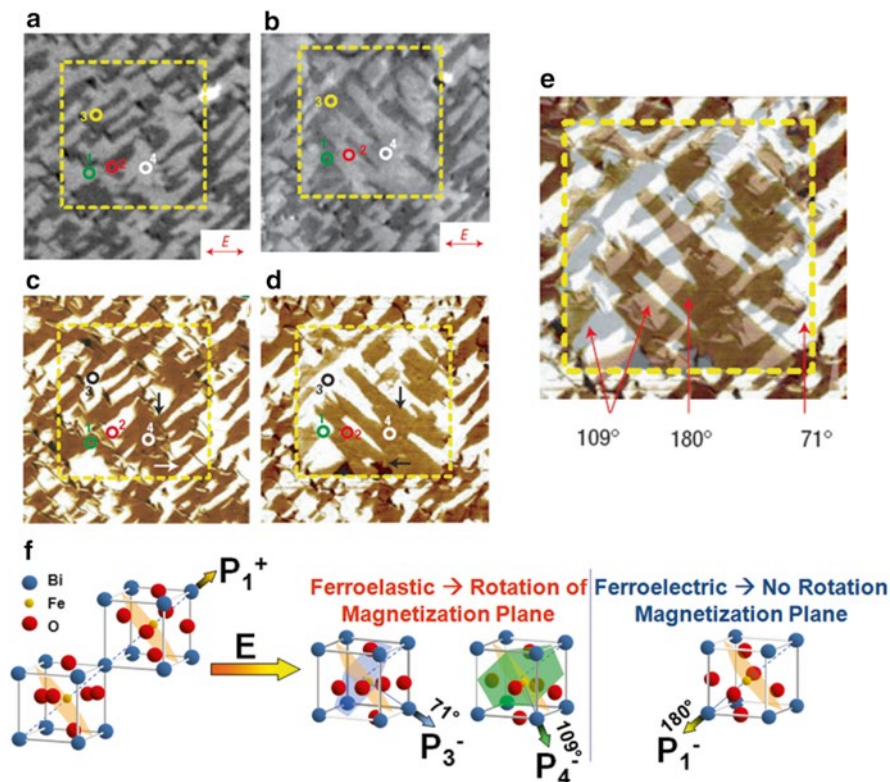


Fig. 3.15 Determination of strong magnetoelastic coupling in BiFeO₃. Photoemission electron microscopy (PEEM) images before (a) and after (b) electric field poling. The arrows show the X-ray polarization direction during the measurements. In-plane piezoresponse force microscopy images before (c) and after (d) electric field poling. The arrows show the direction of the in-plane component of ferroelectric polarization. Regions 1 and 2 (marked with green and red circles, respectively) correspond to 109° ferroelectric switching, whereas 3 (black and yellow circles) and 4 (white circles) correspond to 71° and 180° switching, respectively. In regions 1 and 2 the PEEM contrast reverses after electrical poling. (e) A superposition of in-plane PFM scans shown in (c) and (d) used to identify the different switching mechanisms that appear with different colors and are labeled in the figure (adapted from [156]). (f) Schematic illustration of coupling between ferroelectricity and antiferromagnetism in BiFeO₃. Upon electrically switching BiFeO₃ by the appropriate ferroelastic switching events (i.e., 71° and 109° changes in polarization) a corresponding change in the nature of antiferromagnetism is observed

3.4.3.4 Routes to Enhance Properties in BiFeO₃

One considerable challenge to the full acceptance of BiFeO₃ into modern technology has been the traditionally leaky nature of this material. Unlike more traditional ferroelectric materials—which are robust electronic insulators—multiferroic materials such as BiFeO₃ are asked to perform multiple tasks (i.e., magnetism and ferroelectricity) and thus the electronic structure is highly susceptible to defects which

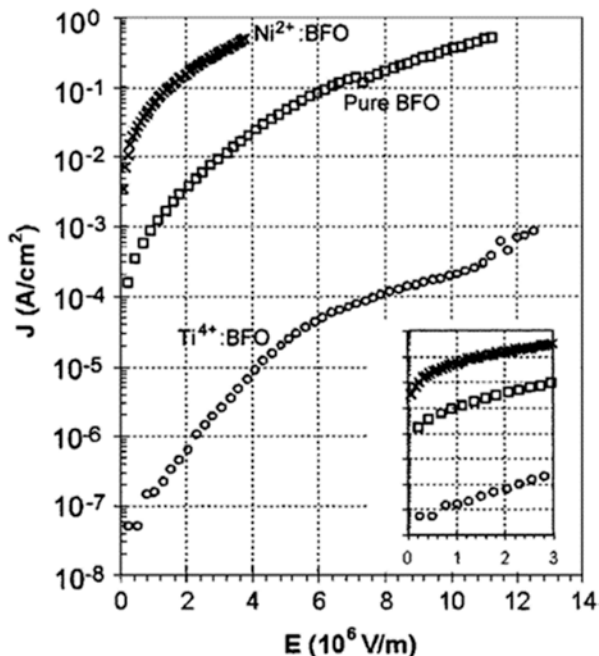
can reduce the resistance of the material. In turn, researchers have attempted to take head-on the common challenges that have traditionally limited the widespread usage of such materials in devices—high leakage currents, small remnant polarizations, high coercive fields, ferroelectric reliability, and inhomogeneous magnetic spin structures [159]. The most common practice in this spirit is to study doped or alloyed (here used interchangeably) BiFeO_3 thin films (both *A*-site and *B*-site doping) in an attempt to improve these various areas of concern. In this section we will describe the work done to date on chemical routes to control properties in BiFeO_3 .

Following the rejuvenation of interest in BiFeO_3 in the early 2000s, a number of studies came forth aimed at understanding how to enhance properties in this exciting material. One of the earliest studies looked at alloying the *B*-site of BiFeO_3 with the transition metal ions Ti^{4+} and Ni^{2+} which are similar in size to the Fe^{3+} ion [160]. The idea was that the addition of 4+ ions into the BiFeO_3 would require charge compensation which would be achieved either by filling of oxygen vacancies, decreasing the valence of the Fe-ions, or creation of cation vacancies. On the other hand, addition of 2+ ions would likely create anion vacancies or change the Fe-ion valence. In the end the hope was that Ti^{4+} alloying would help to eliminate oxygen vacancies and Ni^{2+} alloying would introduce more oxygen vacancies. This study, in turn, showed that alloying with Ti^{4+} led to an increase in film resistivity by over three orders of magnitude while doping with Ni^{2+} resulted in a decrease in resistivity by over two orders of magnitude (Fig. 3.16). Additionally, the study suggested that the current–voltage behavior was affected by the alloying and that increased densities of oxygen vacancies lead to higher levels of free carriers and higher conductivity. Over the next few years numerous other reports of the effect of alloying on the properties of BiFeO_3 were published. Other studies also focused on *B*-site alloying, including alloying with Nd which helped to enhance piezoelectricity in the films and improve electric properties [161, 162], doping with Cr which was shown to greatly reduce leakage currents in BiFeO_3 films [163], and others.

Although there are a number of studies on *B*-site alloyed BiFeO_3 , greater attention has been given to *A*-site alloyed phases. The most widely studied dopants are materials from the Lanthanide series—especially La, Dy, Gd, etc. As early as 1991 work on these materials was undertaken [164], but again it was not until after 2003 that the number of studies on these alloyed systems really took off. Early studies probe the effect of La-alloying on the magnetic structure of BiFeO_3 and showed that the spin-modulated structure disappeared in single crystals with only 20 % addition of La [165]. Soon after studies on La-alloyed thin films showed that the structure of the films was greatly affected and that the ferroelectric fatigue life was seemingly enhanced [159, 166]. Later studies showed that careful control of La-doping could be used to control domain structures, switching, and produce robust ferroelectric properties in films on Si substrates [167]. Other studies have also investigated Ba- [168], Sr-, Ca-, and Pb-doping [169], and many others. It should be noted that there are numerous studies of *A*-site alloying, too many to be covered thoroughly here.

Another exciting discovery occurred when researcher doped rare-earth elements into BiFeO_3 . Upon doping BiFeO_3 with Sm (at ~14 % Sm), a lead-free morphotropic phase boundary was discovered [170]. The researchers found a rhombohedral

Fig. 3.16 Leakage current density as a function of applied electric field for pure and doped BiFeO_3 thin films. Ti -doped BiFeO_3 is shown to have significantly reduced leakage currents. *Inset* shows a zoom in of the low voltage region of the data (adapted from [160])



to pseudo-orthorhombic structural transition (and an associated ferroelectric to anti-ferroelectric transition) that produced an out-of-plane piezoelectric coefficient comparable to $\text{PbZr}_x\text{Ti}_{1-x}\text{O}_3$ materials near the chemically derived morphotropic phase boundary in that material. Further investigations of this morphotropic phase boundary have investigated the effects of Sm doping and have shown that the Sm^{3+} first creates antiparallel cation displacements in local pockets and, with additional Sm , a series of phase transitions and superstructural phases are formed [171, 172]. This work has recently culminated in the observation of a universal behavior in such rare-earth substituted versions of BiFeO_3 [173]. By combining careful experimental and first-principles approaches to the study of complex phase development in this system, researchers have discovered that the structural transition between a rhombohedral ferroelectric phase and an orthorhombic phase with a double-polarization hysteresis loop and significantly enhanced electromechanical response is found to occur independent of the rare-earth dopant species as long as the average ionic radius of the A-site cation is controlled. Despite the somewhat complicated phase space related to such doped versions of BiFeO_3 , researchers have been able to identify and manipulate dopants to greatly enhance the properties of this material. The work in alloyed BiFeO_3 materials was undertaken with the expectation that this would present an exciting pathway to unprecedented control and properties in this material. The findings, although useful and insight full, had failed to produce a ground breaking discovery until very recently. In 2009, Yang et al. [174], building off of the prior observation of the development of interesting materials phenomena such as high- T_C superconductivity in the cuprates and colossal magnetoresistance in the manganites

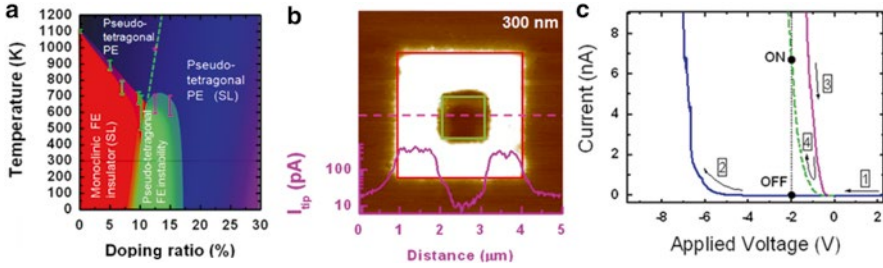


Fig. 3.17 (a) Pseudo-phase diagram of the evolution of structures and properties in Ca-doped BiFeO_3 . (b) Conducting-atomic force microscopy image of an electrically poled and re-poled area of a doped BiFeO_3 film. The as-grown state (*outside the outer box*) is insulating in nature, the electrically poled area (*inside the outer box and outside the inner box*) has become conducting, and the area that has been electrically poled twice (*inside inner box*) is insulating again. (c) Illustration of the process to create a multi-state memory from such physical properties (adapted from [174])

arise out of a doping-driven competition between energetically similar ground states, investigated doped multiferroics as a new example of this generic concept of phase competition. The results were the observation of an electronic conductor–insulator transition by control of band-filling in Ca-doped BiFeO_3 . Application of electric field enables us to control and manipulate this electronic transition to the extent that a p – n junction can be created, erased, and inverted in this material. A ‘dome-like’ feature in the doping dependence of the ferroelectric transition is observed around a Ca concentration of 1/8, where a new pseudo-tetragonal phase appears and the electric modulation of conduction is optimized (Fig. 3.17a). c-AFM images (Fig. 3.17b) reveal that upon application of an electric field the material becomes conducting and that subsequent application of electric fields can reversibly turn the effect on and off. It has been proposed that this observation could open the door to merging magnetoelectrics and magnetoelectronics at room temperature by combining electronic conduction with electric and magnetic degrees of freedom already present in the multiferroic BiFeO_3 . Figure 3.17c shows the quasi-non-volatile and reversible modulation of electric conduction accompanied by the modulation of the ferroelectric state. The mechanism of this modulation in Ca-doped BiFeO_3 is based on electronic conduction as a consequence of the naturally produced oxygen vacancies that act as donor impurities to compensate Ca acceptors and maintain a highly stable Fe^{3+} valence state.

As we have noted, epitaxy presents a powerful pathway to control the phase stability and electronic properties in thin-film systems [175]. The BiFeO_3 system presents a fascinatingly complex strain-driven structural evolution. Although the structure of BiFeO_3 had been studied for many years [103, 107, 176], in 2005 the structural stability of the parent phase had come into question [177, 178]. This was followed, in turn, by a number of thin-film studies reporting that a tetragonally distorted phase (derived from a structure with $P4mm$ symmetry, $a \sim 3.665 \text{ \AA}$, and $c \sim 4.655 \text{ \AA}$) with a large spontaneous polarization may be possible [177, 179, 180]. In 2009, the so-called mixed-phase thin films possessing tetragonal- and

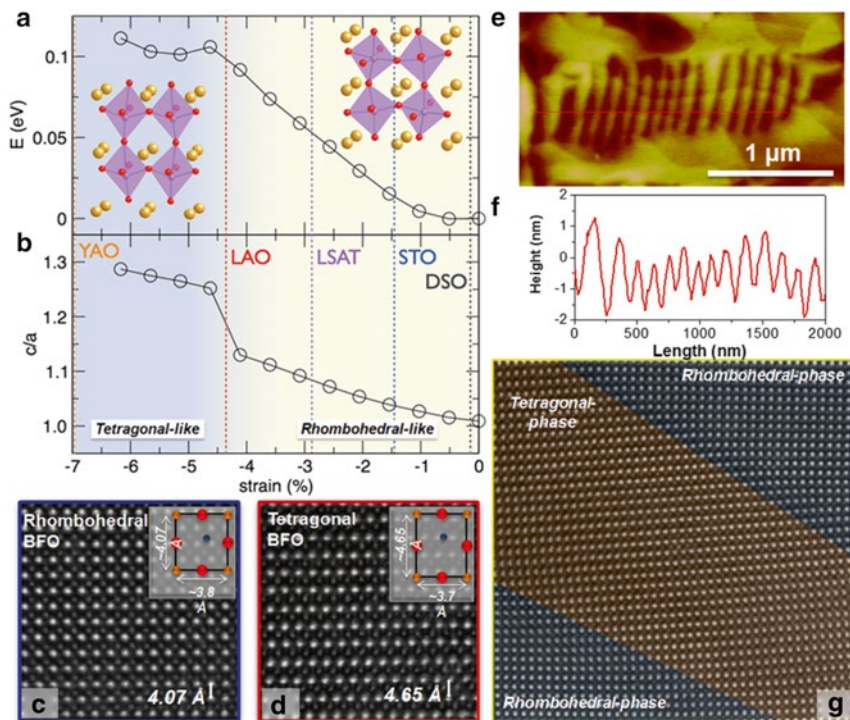


Fig. 3.18 Strain-induced phase complexity in BiFeO₃. First-principle calculations provide information on the strain evolution of (a) the overall energy of the system and (b) the c/a lattice parameter ratio. High-resolution transmission electron microscopy (HRTEM) reveals the presence of two phase (c) a monoclinic version of the bulk rhombohedral phase and a (d) high-distorted monoclinic version of a tetragonal structure. These complex phase boundaries manifest themselves on the surface of the sample as imaged via (e) atomic force microscopy and these features correspond to dramatic surface height changes as shown from (f) the line trace. (g) HRTEM imaging of boundaries shows a smooth transition between phases. (Adapted from [181])

rhombohedral-like phases in complex stripe-like structures (and large electromechanical responses) [181] dramatically changed the study of structures in BiFeO₃. It was found that the rhombohedral bulk crystal structure of the parent phase can be progressively distorted into a variety of unit cell structures through epitaxial strain. Ab initio calculations of the role of epitaxial strain clearly demonstrate how it can be used to drive a strain-induced structural change in BiFeO₃ (Fig. 3.18a, b). These calculations suggest that at a certain value of epitaxial strain, in the absence of misfit accommodation through dislocation formation, the structure of BiFeO₃ morphs from the distorted rhombohedral parent phase to a tetragonal-like (actually monoclinic) structure that is characterized by a large c/a ratio of ~ 1.26 . Direct atomic resolution images of the two phases (Fig. 3.18c, d) clearly show the difference in the crystal structures.

Much recent attention has been given to what happens when films are grown at intermediate strain levels (e.g., $\sim 4.5\%$ compressive strain, corresponding to growth on LaAlO_3 substrates). It has been observed that the result is a nanoscale mixed-phase structure (Fig. 3.18e, f). Figure 3.18g is an atomic resolution TEM image of the interface between these two phases and reveals one of the most provocative aspects of these structures. Although there is a large “formal” lattice mismatch between the two phases, the interface appears to be coherent, i.e., it shows no indication for the formation of interphase dislocations. Indeed, this mismatch appears to be accommodated by the gradual deformation of the structure between different phases.

Considerable detail has emerged concerning the symmetry of these phases including the fact that the so-called tetragonal-like phase is actually monoclinically distorted (possessing *Cc*, *Cm*, *Pm*, or *Pc* symmetry) [182–185]. Other techniques such as second harmonic generation have been used to probe these different structures as well [186]. Recent reports [187] have also investigated the driving force for the formation of these so-called mixed-phase structures and have revealed a complex temperature- and thickness-dependent evolution of phases in the $\text{BiFeO}_3/\text{LaAlO}_3$ system. A thickness-dependent transformation from the monoclinically distorted tetragonal-like phase to a complex mixed-phase structure likely occurs as the consequence of a strain-induced spinodal instability. Additionally, a breakdown of this strain-stabilized metastable mixed-phase structure to non-epitaxial microcrystals of the parent rhombohedral structure of BiFeO_3 is observed to occur at a critical thickness of ~ 300 nm. Other reports have demonstrated routes to stabilize these structures [188]. At the same time, electric field-dependent studies to these mixed-phase structures have also revealed the capacity for large electromechanical responses (as large as $4\text{--}5\%$). In situ TEM studies coupled with nanoscale electrical and mechanical probing suggest that these large strains result from the motion of boundaries between different phases [189]. Despite this work, a thorough understanding of the complex structure of these phase boundaries in BiFeO_3 remained incomplete until 2011.

A perspective by Scott [190] discussed the symmetry and thermodynamics of the phase transition between these two phases as well as a number of other model isosymmetric phase transitions in other crystal systems. Soon after, a very detailed thermodynamic and elastic domain theory analysis of the mixed-phase structure was completed by Ouyang et al [191]. In that treatment, a balance of interdomain elastic, electrostatic, and interface energies was analyzed and compared to provide an anticipated low-energy structural configuration. Subsequent studies by Damodaran et al. [192] helped uniquely identify and examine the numerous phases present at these phase boundaries and resulted in the discovery of an intermediate monoclinic phase in addition to the previously observed rhombohedral- and tetragonal-like phases. Further analysis determined that the so-called mixed-phase regions of these films were not mixtures of the parent rhombohedral- and tetragonal-like phases, but were mixtures of highly distorted monoclinic phases with no evidence for the presence of the rhombohedral-like parent phase. This work helped confirm the mechanism for the enhanced electromechanical response and provide a

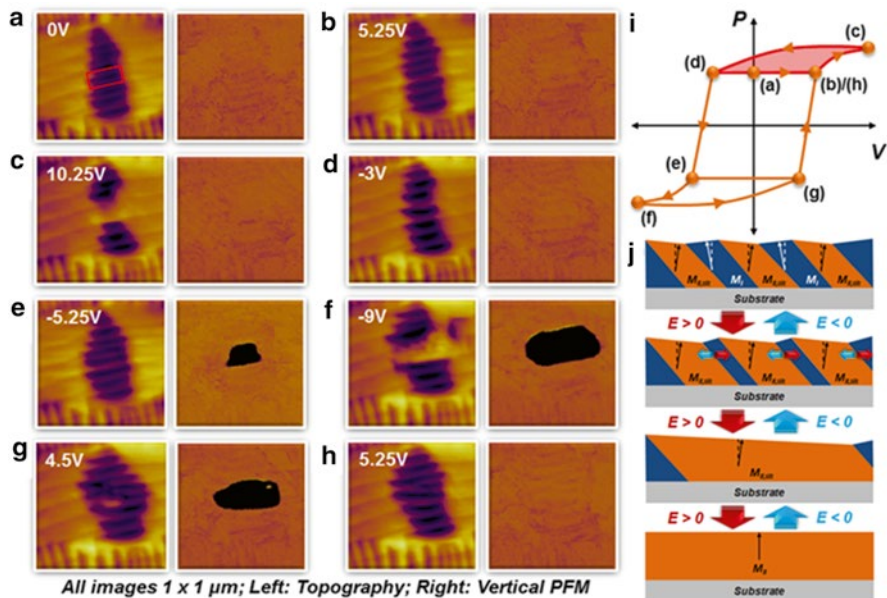


Fig. 3.19 AFM image (*left*) and vertical PFM image (*right*) of 100 nm BiFeO₃/La_{0.5}Sr_{0.5}CoO₃/LaAlO₃ (001) in the (a) as-grown state and after being poled in the box at (b) 5.25 V, (c) 10.25 V, (d) -3 V, (e) -5.25 V, (f) -9 V, (g) 4.5 V, and (h) 5.25 V. (All images are 1 × 1 μm). (i) A schematic hysteresis loop with letters corresponding to the images in (a–h) shows the multiple pathways to enhanced electromechanical response. (j) Illustration of the proposed mechanism for the large electromechanical response without the need for ferroelectric switching. (Adapted from [192])

model for how these phases interact at the nanoscale to produce large surface strains (Fig. 3.19). By undertaken local electric field switching studies and navigating the hysteretic nature of electric field response in this material, a number of important features were revealed: (1) the large surface strains (4–5 %) occur any time the material transforms from a mixed-phase structure to the highly distorted monoclinic phase, (2) transformations between these two states are reversible, and (3) there are numerous pathways to achieve large electromechanical responses in these materials—including ones that do not need ferroelectric switching. The key appears to be the ability to transform between the different phases through a diffusion-less phase transition (akin to a martensitic phase). Similar discussions of the nature of the electric field driven phase transformation have also been reported [193]. This report additionally included single-point spectroscopic studies that suggest that the tetragonal-like to rhombohedral-like transition is activated at a lower voltage compared to a ferroelectric switching of the tetragonal-like phase and the formation of complex rosette domain structures that have implications for future devices.

A number of additional studies on these strain-induced phases have been reported in recent months. This includes considerable discussion on magnetic and magneto-electric properties of these materials. Researchers have investigated the emergence of

an enhanced spontaneous magnetization in the so-called mixed-phase structures [194]. Using X-ray magnetic circular dichroism-based photoemission electron microscopy coupled with macroscopic magnetic measurements, the researchers found that the spontaneous magnetization of the new intermediate monoclinic phase is significantly enhanced above the expected moment of the parent phase as a consequence of a piezomagnetic coupling to the adjacent tetragonal-like phase. Soon after this report, researchers suggested that the magnetic Néel temperature of the strained BiFeO_3 is suppressed to around room temperature and that the ferroelectric state undergoes a first-order transition to another ferroelectric state simultaneously with the magnetic transition [195]. This has strong implications for room temperature magnetoelectric applications. This observation builds off of a detailed neutron scattering study of a nearly phase-pure film of the highly distorted tetragonal-like phase which confirms antiferromagnetism with largely G-type character and a $T_N=324$ K, a minority magnetic phase with C-type character, and suggests that the coexistence of the two magnetic phases and the difference in ordering temperatures from the bulk phase can be explained through simple Fe–O–Fe bond distance considerations [196]. At the same time, other reports suggest the possibility of a reversible temperature-induced phase transition at about 373 K in the highly distorted tetragonal-like phase as studied by temperature-dependent Raman measurements [197]. Similar results have been reported from temperature-dependent X-ray diffraction studies that reveal a structural phase transition at ~ 373 K between two monoclinic structures [198]. Finally there are reports of a concomitant structural and ferroelectric transformation around 360 K based on temperature-dependent Raman studies. This work suggests that the low-energy phonon modes related to the FeO_6 octahedron tilting show anomalous behavior upon cooling through this temperature—including an increase of intensity by one order of magnitude and the appearance of a dozen new modes [199]. Truly this is an exciting and fast-moving field of study today. Such electric field and temperature-induced changes of the phase admixture is also reminiscent of the CMR manganites or the relaxor ferroelectrics and is accompanied by large electromechanical strains, but there appears to be much more to these mixed-phase structures. Such structural softness in regular magnetoelectric multiferroics—i.e., tuning the materials to make their structure strongly reactive to applied fields—makes it possible to obtain very large magnetoelectric effects [200].

All of these observations of exotic phenomena have implications for memories and future devices. For instance, the recent observation of large piezoelectric responses in mixed-phase, strained BiFeO_3 thin films could provide a possible pathway to enable probe based data storage elements [201]. Such materials require considerable development before they can be utilized in devices and a number of key questions must be answered in this regard. Among the most important for this application is what is the smallest length scale of coexistence of these two phases? This question is motivated by the desire to create the mixed phases responsible for the large electromechanical effects on the same length scales as relaxor ferroelectrics (i.e., just a few nm). Likewise, the possibility of converting an insulating, ferroelectric state in doped BiFeO_3 (such as in the example shown above of Ca-doped BiFeO_3) into a relatively conducting state could be used for information storage

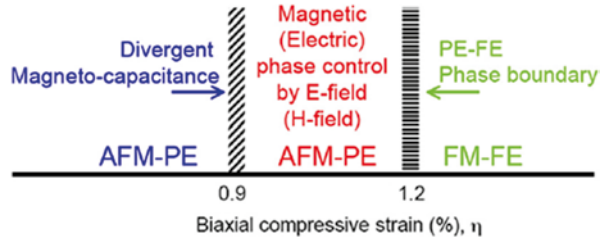
purposes. However, the exact physical mechanisms behind such changes in conductivity are still unclear. An ideal scenario would be one in which the insulating, ferroelectric state is converted into a conducting state via a true phase transition that is triggered by an electric field. Such a sophisticated mechanism is still not available.

3.4.4 Other Single-Phase Multiferroics

Finally, we note that a number of other candidate multiferroic materials with lone-pair active *A*-sites and magnetic transition metal *B*-sites have been produced in the last few years. As early as 2002, Hill et al. [202] had predicted BiCrO₃ to be antiferromagnetic and antiferroelectric, but not until 2006 were thin films of this material produced. Thin films of BiCrO₃ were grown on LaAlO₃ (001), SrTiO₃ (001), and NdGaO₃ (110) substrates and were shown to be antiferromagnetic, displaying weak ferromagnetism, with an ordering temperature of ~120–140 K. Early reports suggested that these films showed piezoelectric response and a tunable dielectric constant at room temperature [203] while others suggested that the films were antiferroelectric as predicted in theory [204]. Other phases of interest include BiCoO₃. Bulk work on BiCoO₃ [205] and theoretical predictions of giant electronic polarization of more than 150 μC/cm² [206] have driven researchers to attempt creating this phase as a thin film as well. To date only solid solutions of BiFeO₃–BiCoO₃ have been grown via MOCVD [207]. Another phase similar to BiCoO₃ that has been produced as a thin film is PbVO₃ [22], PbVO₃ films were grown on LaAlO₃, SrTiO₃, (La_{0.18}Sr_{0.82})(Al_{0.59}Ta_{0.41})O₃, NdGaO₃, and LaAlO₃/Si substrates and were found to be a highly tetragonal perovskite phase with a *c/a* lattice parameter ratio of 1.32. Further analysis of this material using second harmonic generation and X-ray dichroism measurements revealed that PbVO₃ is both a polar, piezoelectric and likely an antiferromagnet below ~130 K [23]. There has also been attention given to double-perovskite structures such as Bi₂NiMnO₆ which have been shown to be both ferromagnetic (*T*_C ~ 100 K) and ferroelectric with spontaneous polarization of ~5 μC/cm² [208].

It is also important to note the power of first-principles investigations and the strong predictive power of modern computational approaches and the role they have played in the discovery and study of multiferroics (for complete review of first-principles approaches to multiferroics see [209–211]). For instance, in 2006 Fennie and Rabe predicted a design strategy by which one could induce multiferroicity in materials such as EuTiO₃ (Fig. 3.20) [212]. By applying tensile strain to the material, normally a paraelectric antiferromagnet, it was suggested that a ferromagnetic and ferroelectric phase could be produced. Recent results suggest that indeed this should be possible. Soon after similar predictions suggested multiferroic behavior might be possible in phases such as FeTiO₃ [213]. This prediction has also been confirmed experimentally [214]. At high pressures (or strains) FeTiO₃ takes on a LiNbO₃-like structure, a combination of piezoresponse force microscopy, optical second harmonic generation, and magnetometry has since revealed that this phase is

Fig. 3.20 Schematic phase diagram describing the strain-driven changes in EuTiO_3 —candidate material for strain-driven multiferroism (adapted from [212])



both ferroelectric and displays a weak ferromagnetic response. More recently, new calculations have suggested the material SrMnO_3 could also exhibit strain-driven multiferroicity [215]. Although these are but a few of the many examples of the close interaction between computation and experimental work, they are illustrative of the power of modern approaches to modeling and predicting materials properties. It is clear that such approaches will continue to play an essential role in the future development of this field.

3.4.5 Horizontal Multilayer Structures

Beyond single-phase multiferroics, great strides have been made in the area of composite magnetoelectric systems. These systems operate by coupling the magnetic and electric properties between two materials, generally a ferroelectric material and a ferrimagnetic material, via strain. An applied electric field creates a piezoelectric strain in the ferroelectric, which produces a corresponding strain in the ferrimagnetic material and a subsequent piezomagnetic change in magnetization or the magnetic anisotropy. Work started in the field several decades ago using bulk composites, although experimental magnetoelectric voltage coefficients were far below those calculated theoretically [216]. In the 1990s theoretical calculations showed possible strong magnetoelectric coupling in a multilayer (2-2) configuration; an ideal structure to be examine by the burgeoning field of complex oxide thin-film growth [217]. In this spirit, researchers experimentally tested a number of materials in a laminate thick-film geometry, including ferroelectrics such as $\text{Pb}(\text{Zr}_x\text{Ti}_{1-x})\text{O}_3$ [218–223], $\text{Pb}(\text{Mg}_{0.33}\text{Nb}_{0.67})\text{O}_3$ - PbTiO_3 (PMN-PT) [224], and ferromagnets such as TbDyFe_2 (Terfenol-D) [218], NiFe_2O_4 [219, 221], CoFe_2O_4 [223], $\text{Ni}_{0.8}\text{Zn}_{0.2}\text{Fe}_2\text{O}_4$ [220], $\text{La}_{0.7}\text{Sr}_{0.3}\text{MnO}_3$ [222], $\text{La}_{0.7}\text{Ca}_{0.3}\text{MnO}_3$ [222], and others. These experiments showed great promise and magnetoelectric voltage coefficients up to $\Delta E/\Delta H = 4,680$ mV/cm Oe have been observed. Work also continued investigating thin-film heterostructures by combining such ferroelectrics as $\text{Ba}_{0.6}\text{Sr}_{0.4}\text{TiO}_3$, BaTiO_3 [225], and PMN-PT [226] with ferromagnets such as $\text{Pr}_{0.85}\text{Ca}_{0.15}\text{MnO}_3$ [225] and Tb-Fe/Fe-Co multilayers [226]; however, these attempts were unable to produce magnetoelectric voltage coefficients above a few tens of mV/cm Oe. Current theories suggest that the in-plane magnetoelectric interface is limiting the magnitude of this coefficient due to the clamping effect of the substrate on the ferroelectric phase [227]. Since the

amount of strain that can be imparted by the ferroelectric phase is limited via this in-plane interfacial geometry, the magnetoelectric voltage coefficient can be reduced by up to a factor of five. A set of excellent reviews of this film can be found in [228–231].

3.4.6 Vertical Nanostructures

A seminal paper by Zheng et al. [232] showed that magnetoelectric materials could also be fabricated in a nanostructured columnar fashion (Fig. 3.21a). By selecting materials that spontaneously separate due to immiscibility, such as spinel and perovskite phases [216], one can create nanostructured phases made of pillars of one material embedded in a matrix of another. In this initial paper, researchers reported structures consisting of CoFe_2O_4 pillars embedded in a BaTiO_3 matrix. The large difference in lattice parameter between these phases leads to the formation of pillars with dimensions on the order of tens of nanometers, which ensures a high interface-to-volume ratio, an important parameter when attempting to couple the two materials via strain. Such structures were shown to exhibit strong magnetoelectric coupling (Fig. 3.21b) via changes in magnetization occurring at the

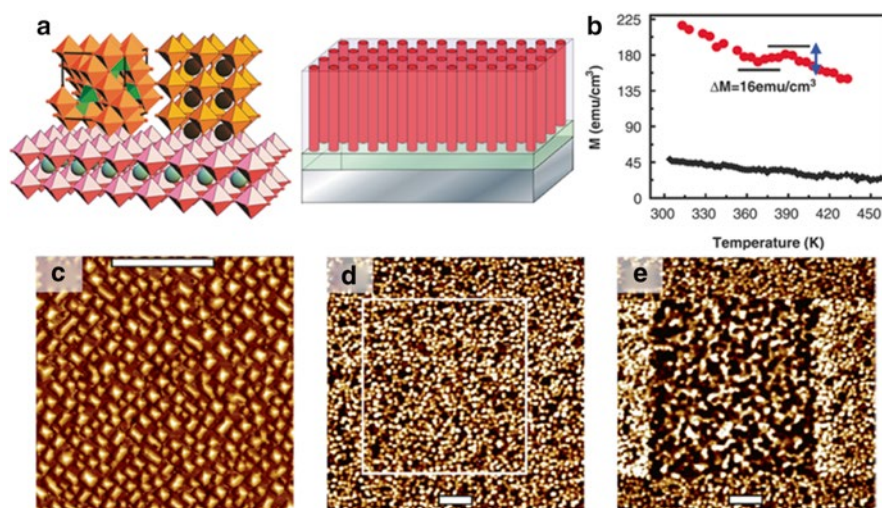


Fig. 3.21 Multiferroic Nanostructures. (a) Schematic illustrations of vertical nanostructure of spinel pillars embedded in a perovskite matrix grown on a perovskite substrate. (b) Magnetization versus temperature curve measured at 100 Oe showing a distinct drop in magnetization at the ferroelectric Curie temperature—proof of strong magnetoelectric coupling. (c) Surface topography of a $\text{CoFe}_2\text{O}_4/\text{BiFeO}_3$ nanostructure as imaged by atomic force microscopy. Magnetic force microscopy scans taken in the same area before (d) and after electrical poling at -16 V (e) (Scale bars are $1 \mu\text{m}$). (Adapted from [232, 233])

ferroelectric Curie temperature of the matrix material. These nanostructures, in which the interface is perpendicular to the substrate, remove the effect of substrate clamping and allow for better strain-induced coupling between the two phases. An explosion of research into alternate material systems followed as the design algorithm proved to be widely applicable to many perovskite-spinel systems. Nanostructured composites with combinations of a number of perovskite (BaTiO_3 [234], PbTiO_3 [235], $\text{Pb}(\text{Zr}_x\text{Ti}_{1-x})\text{O}_3$ [236, 237], and BiFeO_3 [238, 239]) and spinel (CoFe_2O_4 [236, 237], NiFe_2O_4 [235, 238], and $\gamma\text{-Fe}_2\text{O}_3$ [239]) or corundum ($\alpha\text{-Fe}_2\text{O}_3$ [239]) structures have been investigated. The magnetic properties of such systems are generally well-behaved, but the ferroelectric properties are highly dependent on the synthesis technique. When satisfactory ferroelectric properties can be produced, more substantial magnetoelectric voltage coefficients are generally achieved. Pulsed laser deposition has proven to be a successful growth technique for achieving satisfactory properties in these nanostructured films [234, 240, 241].

Zavaliche et al. [242] showed $\Delta E/\Delta H = 100$ V/cm Oe at room temperature in a system comprised of CoFe_2O_4 pillars embedded in a BiFeO_3 matrix. These films were analyzed with scanning probe techniques that utilized both magnetized and conducting tips. Typical surface morphology for such samples is shown in Fig. 3.21c. Magnetic measurements show the preference of such structures to maintain magnetization along the length of the nanopillars. Magnetic force microscopy scans both before (Fig. 3.21d) and after electric field poling (Fig. 3.21e) show a significant number of CoFe_2O_4 pillars switch their magnetic state from a downward direction to an upward direction upon application of an electric field [233]. This work further showed that the magnetization-switching event was non-deterministic and could be improved by applying a small magnetic field (700 Oe) to the sample. This field is essential to break time reversal symmetry and overcome the degeneracy between the up and down magnetization states. Nonetheless, these structures have been shown to be very versatile and offer an excellent opportunity for electrically controlled magnetic storage.

We also note that other interesting nanoscale composite geometries have been investigated. Using anodized aluminum oxide templates, Liu et al. [243] successfully synthesized nanowires of NiFe_2O_4 surrounded by a shell of PZT. However, successful magnetoelectric coupling has been not yet shown in such a system. Overall, it has been shown that nanostructured composite multiferroics have shown significantly enhanced magnetoelectric properties over traditional multilayer heterostructures and are excellent candidates for a wide range of devices that would take advantage of the strong magnetoelectric coupling that can be achieved in these structures.

3.5 Design of Multiferroic-Based Memories

One of the major questions in the study of multiferroics today is how and when will multiferroics make their way into a room temperature device and what will these devices look like? Device manifestation of multiferroics and magnetoelectrics can be broadly classified into a number of areas, including (1) information storage elements

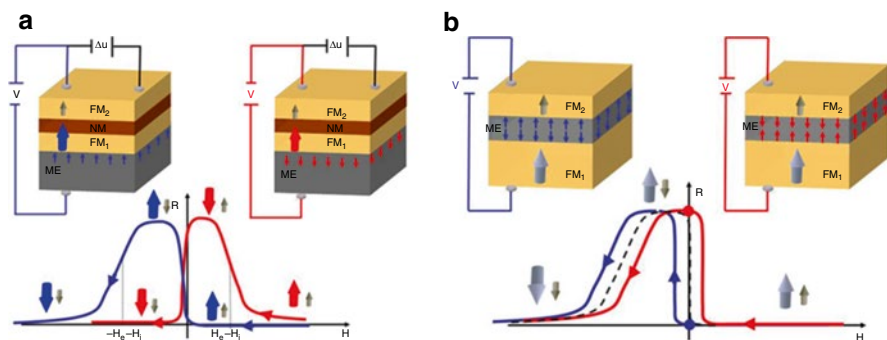


Fig. 3.22 Multiferroic-based Magnetoelectronics. **(a)** Schematic of the magnetoresistance curve of a GMR device involving a magnetoelectric, multiferroic film as a pinning layer. Half-hysteresis curves are shown, after saturation at positive field values. The change of polarity of the magnetoelectric, multiferroic layer upon application of an electric field changes the direction of the net magnetization of the pinning field. The pinned layer (FM1) switches first at large positive field, or second at large negative field. The low field magnetic configuration is therefore either antiparallel or parallel, controlled by the magnetoelectric, multiferroic. **(b)** Schematic of the magnetoresistance curve of a TMR device involving a magnetoelectric, multiferroic film as a tunnel barrier. Half-hysteresis curves are shown, after saturation at positive field values. The arrows denote the magnetization directions, with the bottom layer FM1 being harder (or pinned) than the top one FM2. The *dashed curve* is the expected TMR behavior. The change of voltage polarity changes the direction of the net magnetization of the magnetoelectric, multiferroic layer, adding an exchange bias magnetic field to the resistance curve. The *two curves* indicate shifting of half-hysteresis curves towards positive or negative fields, depending on the polarity of the applied voltage. At zero magnetic field, the change of voltage polarity changes the resistance value of the device (*dashed*). (Adapted from [244])

(i.e., memories), (2) information processing elements (i.e., logic elements), (3) sensors, (4) high-frequency RF elements, and more. In this chapter, we will focus predominantly on memories, but will touch on others as needed.

The focus of this book is on emerging non-volatile memories. Multiferroics and magnetoelectrics are but in the infancy of their investigation and thus there are limited reports of full-scale devices based on these materials. However, as early as 2005, a number of what were referred to as *magnetolectronics* based on magnetoelectric materials were proposed [244]. The idea was a simple one, to use the net magnetic moment created by an electric field in a magnetoelectric thin film to change the magnetization of a neighboring ferromagnetic layer through exchange coupling. The authors went on to propose a number of electrically tunable giant magnetoresistance (GMR) spin valves (Fig. 3.22a) and tunnel magnetoresistance (TMR) (Fig. 3.22b) elements that could be made possible if such structures could be achieved. One additional field that could be greatly affected by this research is the burgeoning field of spintronics. Spin-based electronics, or spintronics, have already found successful application in magnetic read-heads and sensors that take advantage of GMR and TMR effects. The future of spintronics is partially focused on evolving beyond passive magnetolectronic components, like those used today, to devices which combine memory and logic functions in one [245]. There has been

growing interest in studying a direct method for magnetization reversal involving spin-transfer from a spin-polarized current injected into the device. This effect has been theoretically predicted by Slonczewski [246, 247] and Berger [248], and has been experimentally confirmed by several groups [249–252]. And it is at this point that the first major stumbling block is met.

From these initial experiments and theoretical treatments, it was found that significant current densities (larger than 10^7 A/cm²) were required for switching the orientation of even a magnetic nanowire [250]. One option is to further scale down materials so that spin-transfer becomes a more attractive alternative to stray magnetic field techniques. In the end, integration of such effects into actual devices has been limited because there are a number of technical difficulties involved in reliably making such small structures, applying such large currents—while avoiding heating of the samples, and based on the fact that the intrinsic sample resistance (on the order of a few ohms) further limits the practical use for GMR devices. Similar issues are found in TMR devices, which are hindered by the fact that a large current density must pass through a very thin insulator and the few reports on TMR systems to date have been inconclusive [253, 254].

At the heart of what Binek and Doudin [244] were asking in 2005 was whether we should attempt to use currents or some alternative method (i.e., electric field) to create actual devices with new functionalities. Materials discoveries aside, a critical materials physics question emerges from this question that lies at the heart of the last 20 years of research on correlated oxides as well. This has to do with the role of energy scales (as well as time and length scales) of relevance to the ultimate implementation of these materials into actual devices. Let us explore this issue in a bit more detail using the data presented in Fig. 3.23 for the colossal magnetoresistant (CMR) manganites (data shown here is for $\text{La}_{0.7}\text{Ca}_{0.3}\text{MnO}_3$ (LCMO)) as a frame of reference. Over the past 20 years, there has been extensive research conducted on these materials. By far the most interesting aspect of these very intriguing materials is the large (colossal) change in resistance that occurs with the application of a magnetic field of several Tesla ($6T$ in the present example) (shown in the green data in Fig. 3.23a). It has also been demonstrated that a commensurate “colossal electroresistance” can be obtained with electric fields of the order of a few hundred kV (shown in blue in Fig. 3.23a) [255]. Let us now compare these two energy scales and ask the question: how do these two types of fields compare from the perspective of external power requirements?

We can understand this through a simple thought experiment. If one needed to generate the necessary magnetic field of $6T$ at a distance of $1\ \mu\text{m}$ from a metal wire (Fig. 3.23b), a current of ~ 30 A would be required! We note that a $6T$ magnetic field translates to a temperature scale in the material of ~ 8 K [256], which is significantly smaller than the critical temperatures (for example, the magnetic transition temperature or the peak in the resistivity). Regardless, this current is prohibitive both from the point of view of the integrity of the metal wire that would carry the current as well as the power requirements—especially as device sizes are decreased. Let us now examine an alternative pathway to achieve the same effect through the use of an electric field (Fig. 3.23c). If one desires to create the appropriate electric field needed to observe colossal electroresistance in a $100\ \text{nm}$ thick film, a potential of

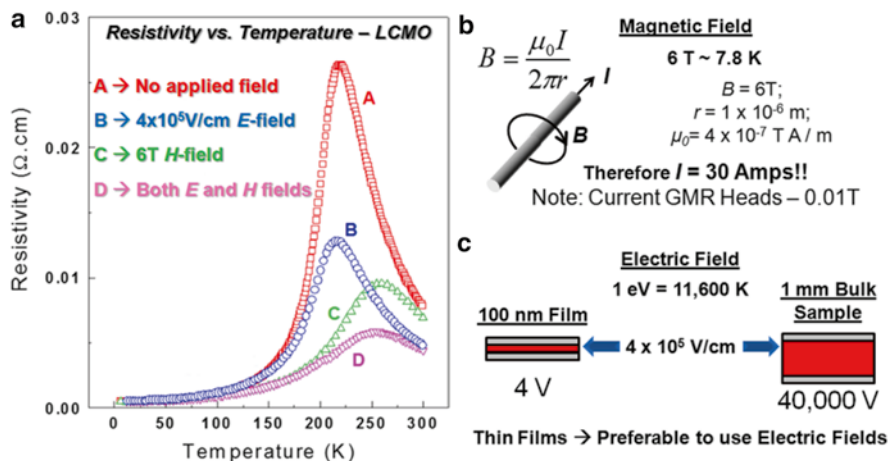


Fig. 3.23 Motivation for electric field control of properties. (a) Resistivity versus temperature for $\text{La}_{0.7}\text{Ca}_{0.3}\text{MnO}_3$ thin films with no applied field (red), applied electric field (blue), applied magnetic field (green), and both applied electric and magnetic fields (pink). Energy scales in materials dictate the eventual incorporation of such materials into device structures. (b) The production of the large magnetic fields ($\sim 6\text{T}$) required for colossal magnetoresistance in CMR materials requires large currents ($\sim 30 \text{ A}$) while (c) production of the appropriate electric fields to produce colossal electroresistance ($\sim 4 \text{ V}$ for a 100 nm thick thin film) are much more reasonable and possible in standard semiconductor electronics circuitry. (Adapted from [255])

only 4 V is required. This is easily generated by standard semiconductor electronics circuitry. However, if the thickness of the material is, say 1 mm, then a potential of 40,000 V is required to generate the same field.

These two scenarios present a number of important considerations. First, if the energy scales for manipulation of these materials (be they CMR or multiferroics) do not become significantly smaller, then the use of magnetic fields to probe and manipulate them becomes technologically prohibitive. Indeed, this can be identified as the most important reason why CMR based systems have not become commercially viable. Second, if these energy scales are indeed maintained, it is clear that using thin film heterostructures and manipulating them with electric fields is a more attractive way to proceed in terms of technological manifestations of these phenomena. These ideas form the technological foundation for the next section of our treatment.

3.5.1 Electric Field Control of Ferromagnetism

The overall motivating question for this section is a simple one: can we deterministically control ferromagnetism at room temperature with an electric field? One possible solution to this question is to utilize heterostructures of existing multiferroic materials, such as BiFeO_3 , to create new pathways to functionalities not

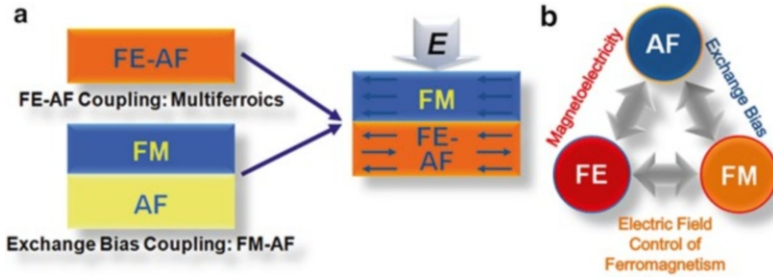


Fig. 3.24 Schematics illustrating the design algorithm for gaining electrical control of ferromagnetism. (a) By combining multiferroics together with traditional ferromagnets, we can create heterostructures that might have new functionalities. (b) These structures rely on two types of coupling—magnetoelectric and exchange bias—to gain electrical control of ferromagnetism. (Adapted from [7])

presented in nature. Such a concept is illustrated in Fig. 3.24. The idea is to take advantage of two different types of coupling in materials—*intrinsic* magnetoelectric coupling like that in multiferroic materials such as BiFeO_3 which will allow for electrical control of antiferromagnetism and the *extrinsic* exchange coupling between ferromagnetic and antiferromagnetic materials—to create new functionalities in materials (Fig. 3.24a). By utilizing these different types of coupling we can then effectively couple ferroelectric and ferromagnetic order at room temperature and create an alternative pathway to electrical control of ferromagnetism (Fig. 3.24b). But what exactly are the opportunities for using multiferroics to gain electrical control over interactions like exchange bias anisotropy? Until recently the materials and the understanding of the appropriate materials did not exist to make this a plausible undertaking. Let us investigate, in detail, the work done in this field of study.

In the time since the proposal of these magnetoelectronics, studies have been done on a number of multiferroic materials. Among the earliest work was a study of heterostructures of the soft ferromagnet permalloy on YMnO_3 [257]. This report found that, indeed, the multiferroic layer could be used as an antiferromagnetic pinning layer that gives rise to exchange bias and enhanced coercivity, but suggested that YMnO_3 would likely be an inappropriate choice for continued study as these values varied greatly with crystal orientation and rendered actual device generation unlikely. Soon after this initial result, Marti et al. [258] reported the observation of exchange bias in all-oxide heterostructure of the ferromagnet SRO and the antiferromagnetic, multiferroic YMnO_3 . In both of these studies, the exchange bias existed only at very low temperatures due to the low magnetic ordering temperature of the YMnO_3 . Around the same time, the first studies using BiFeO_3 as the multiferroic, antiferromagnetic layer were appearing with hopes that these intriguing properties could be extended to high temperatures. As part of this J. Dho et al. [259] showed the existence of exchange bias in spin-valve structures based on permalloy and BiFeO_3 at room temperature and Béa et al. [260] extended this idea to demonstrate how BiFeO_3 films could be used in first generation spintronics devices. This work

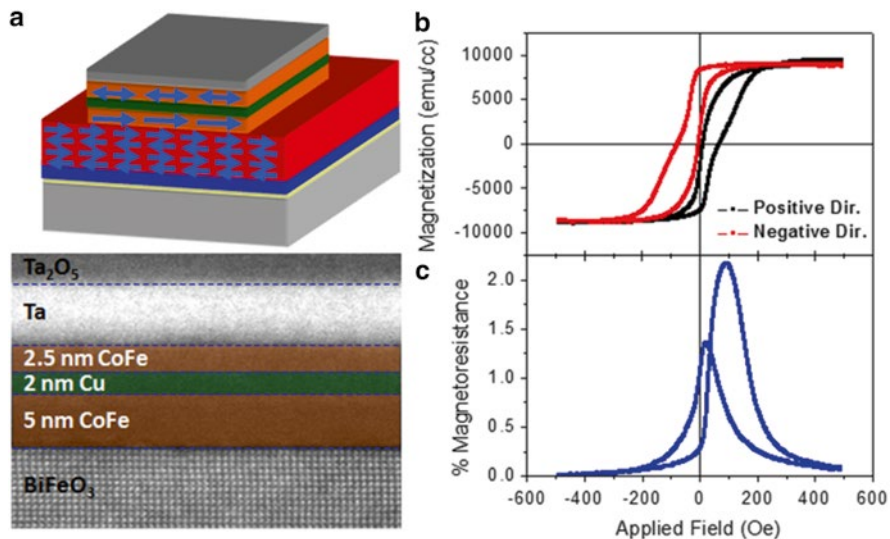


Fig. 3.25 Spin valve structures based on $\text{Co}_{0.9}\text{Fe}_{0.1}/\text{Cu}/\text{Co}_{0.9}\text{Fe}_{0.1}/\text{BiFeO}_3$ heterostructures. (a) Schematic illustration and scanning transmission electron microscopy image of the actual device. (b) Magnetic hysteresis loops of spin valve structures. (c) Current-in-plane magnetoresistance measurements. (Adapted from [261])

included the use of ultrathin BiFeO_3 tunnel barriers in magnetic tunnel junctions with LSMO and Co electrodes where positive TMR up to $\sim 30\%$ was observed at 3 K and also demonstrated that room temperature exchange bias could be generated using $\text{CoFeB}/\text{BiFeO}_3$ heterostructures. Finally, Martin et al. [261] reported the growth and characterization of exchange bias and spin-valve heterostructures based on $\text{Co}_{0.9}\text{Fe}_{0.1}/\text{BiFeO}_3$ heterostructures on Si substrates. In this work large negative exchange bias values (typically 150–200 Oe in magnitude) were observed along with the absence of a training effect—or a systematic decrease in the magnitude of the exchange bias with repeated magnetic cycling (confirming the results of Bea et al. [260])—even with over 14,000 magnetic cycles. This work also demonstrated room temperature magnetoresistance of $\sim 2.25\%$ for spin-valve structures of 2.5 nm $\text{Co}_{0.9}\text{Fe}_{0.1}/2$ nm Cu/5 nm $\text{Co}_{0.9}\text{Fe}_{0.1}/100$ nm BiFeO_3 (Fig. 3.25). What these initial studies established was that exchange bias with antiferromagnetic multiferroics was possible in a static manner, but these studies had not yet demonstrated dynamic control of exchange coupling in these systems.

A first attempt at this concept was done by Borisov et al. [262] who reported that they could affect changes on the exchange bias field in $\text{Cr}_2\text{O}_3(111)/(\text{Co}/\text{Pt})_3$ heterostructures by using the magnetoelectric nature of the substrate (Cr_2O_3) and a series of different cooling treatments with applied electric and magnetic fields. A unique aspect of this work was the ability to change the sign of the exchange bias with different field cooling treatments. Dynamic switching of the exchange bias field with an applied electric field, however, remained elusive until a report by Laukhin et al.

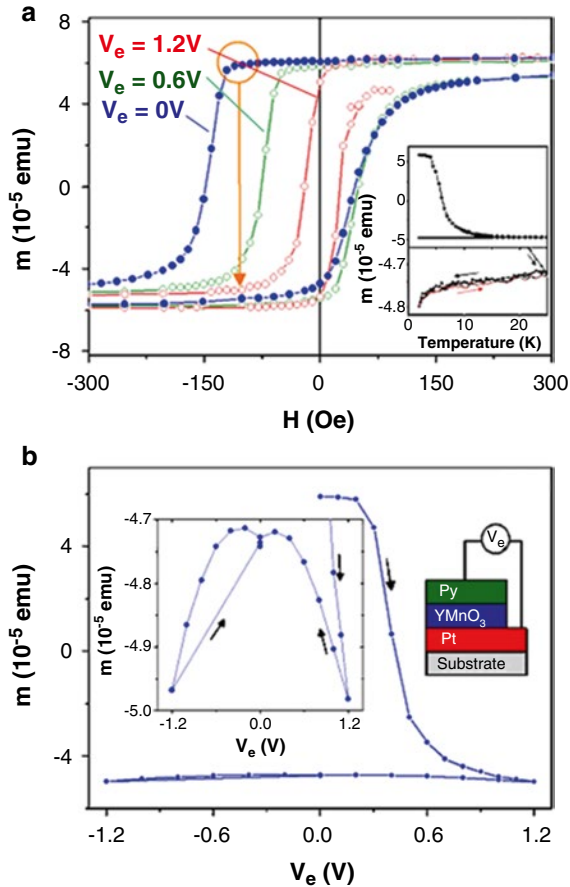


Fig. 3.26 Low temperature electric field control of ferromagnetism. (a) Magnetization loops for permalloy/YMnO₃/Pt, measured at 2 K, after cooling the sample from 300 K in a 3 kOe field, under various biasing-voltage (V_e) values. The circle and arrow illustrate schematically the expected change of magnetization when biasing the sample by an electric field. The *inset* shows the temperature dependence of the magnetization at $H=100$ Oe and $V_e=0$ when heating the sample from 2 K to 25 K (*top panel*) and subsequent cooling-heating-cooling cycles between 25 K and 2 K (*bottom panel*). (b) Dependence of the magnetization on V_e measured at 2 K in $H=100$ Oe field after cooling the sample from 300 K in 3 kOe field. The *inset* shows (*left*) a zoom of the -1.2 to 1.2 V portions of the bias excursion and (*right*) a sketch of the sample structure and electric biasing. (Adapted from [263])

[263] focusing on YMnO₃ at 2 K. Utilizing heterostructures of permalloy and (0001) YMnO₃ films, the authors demonstrated that after cooling samples from 300 to 2 K in an applied field of 3 kOe and at various applied electric field biases, significant changes in the magnitude of magnetization were observed (Fig. 3.26a). Subsequent cycling of the voltage at low temperatures resulted in reversal of the magnetization direction in the heterostructure (Fig. 3.26b).

In the last few years, significant advances in the understanding of the interactions present in such heterostructures have been presented. Initial reports noted an inverse relationship between domain size in BiFeO₃ film and the exchange bias measured in CoFeB/BiFeO₃ heterostructures [264]. This initial report offered little detail on how the domain structures were controlled and the nature of the domain walls present in the films. A study that soon followed found a correlation not only to the density of domain walls but also to the density of certain types of domain walls [140]. What was observed was the presence of two distinctly different types of magnetic properties for Co_{0.9}Fe_{0.1}/BiFeO₃ heterostructures. Through careful control of the growth process—specifically controlling the growth rate of the BiFeO₃ films—the authors were able to create two starkly different types of domain structures: so-called stripe- and mosaic-like domain structures. These different structures were found to possess vastly different fractions of the different domain walls that can exist in BiFeO₃. It was observed that not only was there an inverse relationship between domain size and the magnitude of the exchange bias measured, but that it was directly related to the density and total length of 109° domain walls present in the sample. In addition to identifying the importance of 109° domain walls in creating exchange bias (and in turn suggesting the relationship with enhanced magnetism in BiFeO₃ thin films), this report outlined the idea that two distinctly different types of exchange interactions are occurring in these exchange bias heterostructures. The first interaction was called an *exchange bias* interaction and takes place between pinned, uncompensated spin occurring at 109° domain walls in BiFeO₃ and spins in the Co_{0.9}Fe_{0.1} layer. This interaction results in a shift of the magnetic hysteresis loop for the ferromagnetic layer. The second interaction has been called an *exchange enhancement* interaction and it arises from an interaction of the spins in the ferromagnet and the fully compensated (001) surface of the G-type antiferromagnetic surface of BiFeO₃. This interaction results in an enhancement of the coercive field of the ferromagnetic layer.

Utilizing these findings, researchers have moved to create the first room temperature devices designed to enable control of ferromagnetism with an electric field. Initial results point to the ability to utilize the above *exchange enhancement* interaction to deterministically change the direction of ferromagnetic domains by 90° upon application of an applied electric field (Fig. 3.27) [265]. By creating very high quality Co_{0.9}Fe_{0.1}/BiFeO₃/SrRuO₃/SrTiO₃ (001) heterostructures, the authors were able to demonstrate the first example of a room temperature device structure that utilizes a multiferroic material to access new functionalities in materials. This work also outlined the complexity of such an undertaking. It has become apparent that in order to achieve significant advances with such systems one will need to understand and be able to control (at least at some level) the coupling between the two (in this case dissimilar) materials. This requires that one will have a perfunctory understanding of the various energies-scales at play (including shape anisotropy effects, how processing effects the interfacial coupling strength, magnetostriction effects, and more). This initial work also demonstrated the importance of length scales in this work as the observed ferromagnetic domain structures were typically much more

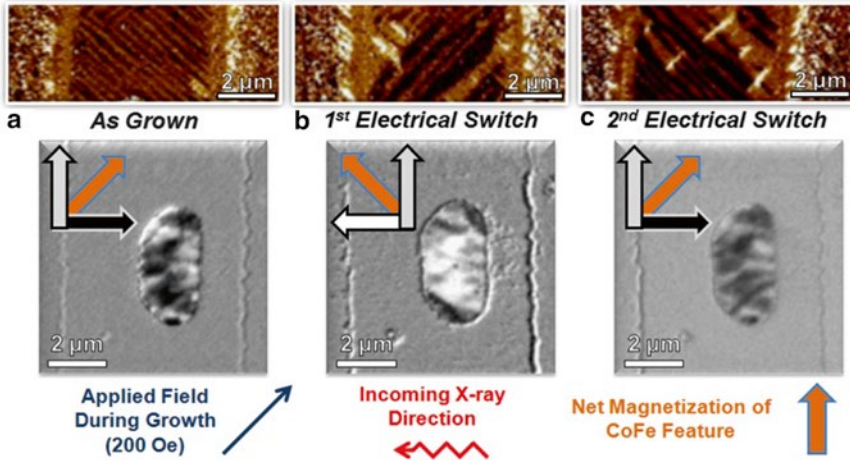


Fig. 3.27 Electric field control of ferromagnetic domain structures at room temperature. In-plane piezoresponse force microscopy images of ferroelectric domain structure (*top*) and corresponding photoemission electron microscopy image of ferromagnetic domain structure (*bottom*) of $\text{Co}_{0.9}\text{Fe}_{0.1}$ features on BiFeO_3 as a function of applied electric field in the (a) as-grown state, (b) after application of an electric field, and (c) following application of the opposite electric field. This represents the first demonstration of reversible electric field control of ferromagnetic domain structures at room temperature. (Adapted from [265])

complex than the underlying ferroelectric domain structures suggesting that diminished feature sizes could give rise to single magnetic domain configurations and therefore a more robust and simple device. In this spirit, current work is focused on making the coupling in such heterostructures more robust in hopes of extending this coupling to high temperatures and producing more deterministic control of electric field switching.

More recently, He et al. [266] have reported the exciting possibility of obtaining deterministic, 180° switching control of ferromagnetic structures using one of the oldest known multiferroics— Cr_2O_3 . The elegance of this finding lies in the discovery of new phenomena on the (0001) surface of Cr_2O_3 . Specifically, through the use of a combination of magnetometry, spin-polarized photoemission spectroscopy, symmetry arguments, and first-principles calculations researchers have demonstrated that there is an electrically switchable magnetization at this surface in Cr_2O_3 . By coupling the Cr_2O_3 to an out-of-plane magnetized ferromagnetic Pd/Co multilayer, they have demonstrated isothermal switching of exchange bias between positive and negative values (Fig. 3.28). By applying combination electric- and magnetic-fields the researchers were able to demonstrate the ability to change the direction of exchange bias without changing the direction of the applied magnetic field. This represents a strong step forward in the understanding of multiferroic materials and further proof of the power of these materials for next generation applications.

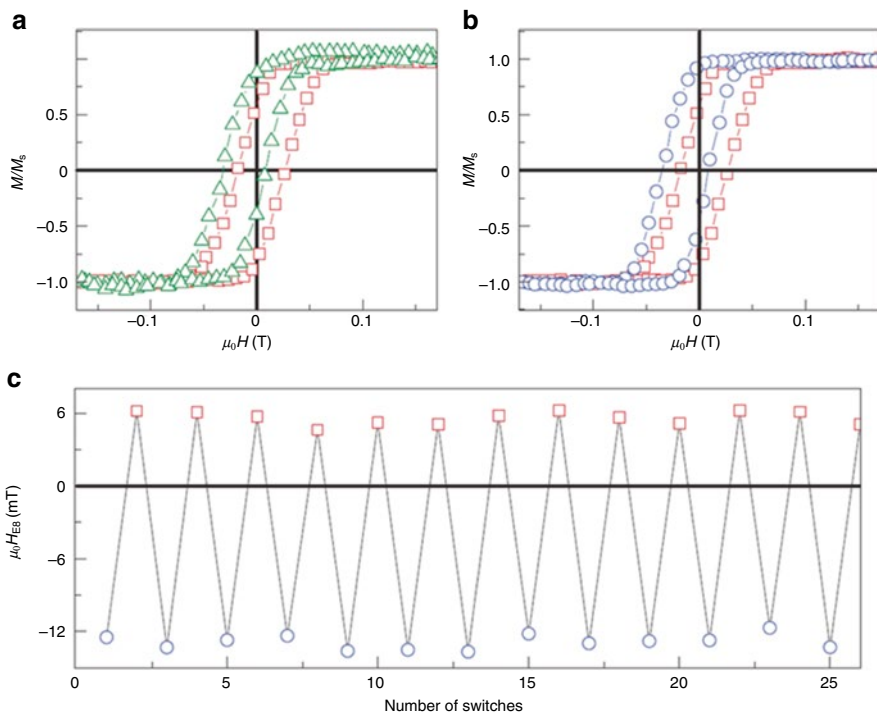


Fig. 3.28 (a) Exchange-biased hysteresis loops of Cr_2O_3 (0001)/Pd 0.5 nm/(Co 0.6 nm, Pd 1.0 nm)₃ at $T=303$ K after initial magnetoelectric annealing in $E=0.1$ kV/mm and $\mu_0H=77.8$ mT. Hysteresis loops are measured by polar Kerr magnetometry in $E=0$, respectively. The *squares* show the virgin curve with a positive exchange-bias field of $\mu_0H_{\text{EB}}=+6$ mT. Isothermal-field exposure in $E=-2.6$ kV/mm and $\mu_0H=+154$ mT gives rise to a loop with a negative exchange-bias field of $\mu_0H_{\text{EB}}=-13$ mT (*triangles*). (b) The *squares* show the same virgin reference loop. The *circles* show the hysteresis loop after isothermal-field exposure in $E=+2.6$ kV/mm and of $\mu_0H=-154$ mT, giving rise to the same negative exchange bias of $\mu_0H_{\text{EB}}=-13$ mT. (c) μ_0H_{EB} versus number of repeated isothermal switching through exposure to $E=+2.6$ kV/mm (*circles*) and $E=2.0$ kV/mm (*squares*) at constant $\mu_0H=-154$ mT, respectively (adapted from [266])

3.5.2 Multiferroic-Based Devices

In 2007, Scott offered a brief, but elegant summary of where multiferroic-based devices, especially memory applications, might make an impact [267]. It is important to note that although ferroelectric random access memories (FeRAMs) have achieved fast access speeds (5 ns) and high densities (64 Mb) in a number of different materials, they remain limited by the need for a destructive read and reset operation. By comparison, magnetic random access memories (MRAMs) have been lagging far behind, although Freescale Corporation reported commercial production in 2006 of a smaller MRAM for testing. The appeal of multiferroics is that they offer the possibility of combining the best qualities of FeRAMs and MRAMs: fast

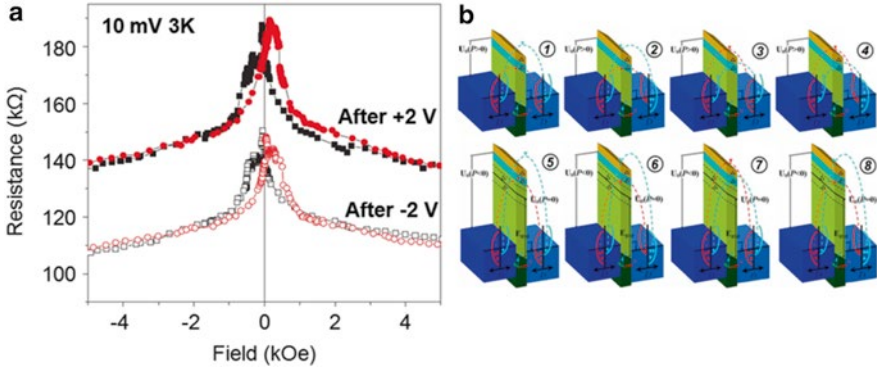


Fig. 3.29 Multiferroic-based devices. (a) Tunnel magnetoresistance curves at 4 K at $V_{dc} = 10$ mV in an $\text{La}_{2/3}\text{Sr}_{1/3}\text{MnO}_3/\text{La}_{0.1}\text{Bi}_{0.9}\text{MnO}_3$ (2 nm)/Au junction, after applying a voltage of +2 V (filled symbols) and -2 V (open symbols). The combination of the electroresistance effect and the tunnel magnetoresistance produces a four-resistance-state system. (Adapted from [96]) (b) The sketch of the potential profiles for each of the eight configurations of a multiferroic-based tunnel junction. Here, the arrows denote majority- and minority-spin carriers, D displays the electronic density of states. (Adapted from [270])

low-power electrical write operation, and non-destructive magnetic read operation. At the 256 Mbit level, such memory devices [268] would be a “disruptive technology” and could eliminate competition such as EEPROMs (electrically erasable programmable read-only memories) for applications including megapixel photomemories for digital cameras or audio memories in devices such as mp3 players.

With this in mind, over the last few years, a number of new devices based on multiferroic materials and heterostructures have been demonstrated and proposed. In early 2007, Ju et al. [269] presented a theoretical investigation of an electrically controllable spin filter based on a multiferroic tunnel junction that could be switched between multiple resistance states. Soon after this, Gajek et al. [96] demonstrated the production of four logic states based on ultrathin multiferroic films used as barriers in spin-filter-type tunnel junctions. The junctions were made of $\text{La}_{0.1}\text{Bi}_{0.9}\text{MnO}_3$ which was proven to be both ferroelectric and magnetic down to film thickness of only 2 nm and the devices exploited the magnetic and ferroelectric degrees of freedom of that layer. The ferromagnetism permitted read operations reminiscent of MRAM and the electrical switching evoked FeRAM write operations without the need for destructive ferroelectric readout. The results (Fig. 3.29a) suggest that it is possible to encode quaternary information by both ferromagnetic and ferroelectric order parameters, and to read it non-destructively by a resistance measurement. This work represented the starting point for future studies on the interplay between ferroelectricity and spin-dependent tunneling using multiferroic barrier layers and, in a wider perspective, suggested a new pathway toward novel reconfigurable logic spintronic architectures.

Yang et al. [270] proposed that eight different logic states could be achieved by combining spin-filter effects and the screening of polarization charges between two

electrodes through a multiferroic tunnel barrier (Fig. 3.29b). In this work, the conductance ratio was found to be dependent on the magnitude of the ferroelectric polarization, exchange splitting, barrier width, and bias voltage. In 2009, Jia and Berakdar [271] proposed a modified spin-field-effect transistor fabricated in a two-dimensional electron gas (2DEG) formed at the surface of multiferroic oxides with a transverse helical magnetic order. The local magnetic moments in the oxide are said to induce a resonant momentum-dependent effective spin-orbit interaction acting on the 2DEG and thus the carrier spin precession is dependent on the magnetic spin helicity that can be electrically controlled in the multiferroic. Such a device could, in turn, be used as a nanometer-scale, decoherence-suppressed spin field-effect transistor and as a nanometer flash-memory device.

As a final note, there are other possible applications for multiferroics and magnetoelectrics that might make impact in the coming year. The first is in sensors. By far, the quickest implementation of multiferroics and magnetoelectrics, especially bi-layered systems (consisting of a piezoelectric/magnetostrictive composite) is in magnetic field sensing elements. The work of Srinivasan, Viehland, and co-workers [228, 231] has already shown proof of this concept. These structures sense changes in magnetic field as a voltage signal through the mechanical coupling between the piezoelectric and magnetostrictive layer. The key advantage of this approach is its inherent simplicity, i.e., it does not require sophisticated processing, small dimensions, or expensive peripheral circuitry. Furthermore, there is a current trend to utilize antiferromagnetic resonance in ultrahigh frequency signal processing—opening up a new door for multiferroics to make in-roads into devices. This is an area that has not been well explored to date, but the idea is to take advantage of the possibility of controlling antiferromagnetic resonance with electric fields, thereby utilizing pre-existing multiferroic materials. Previous work (as is illustrated in Fig. 3.15) clearly demonstrated that the antiferromagnetic order of multiferroics such as BiFeO_3 can be manipulated through electric field control of ferroelectricity [156, 158]. The question of interest today is to what frequency can this coupling be pushed? It is well known that as a consequence of the large magnetic anisotropy fields, resonance in antiferromagnets occurs at a frequency much higher than in conventional ferromagnets [272, 273]. In the case of the related orthoferrites (the parent compound to BiFeO_3) antiferromagnetic resonances occur in the few hundred GHz range, thus opening up the frequency range from ~ 100 GHz to 1 THz for future applications in signal processing.

3.6 Challenges for Multiferroic-Based Memories and Devices

The memory market is a highly competitive, as illustrated by the DRAM and Flash product evolution over the past decade or so. Thus, by far the biggest challenge facing new materials systems, such as multiferroic and magnetoelectric systems, is the ability to make a memory product that is competitive with the existing volatile and nonvolatile memories. Within the nonvolatile memory market-space, two fundamental attributes control the market penetration by any given technology. The first is

the density, often quantified in Flash. For SRAM and DRAM products the figure of merit is “ F^2 ” where “ F ” is the minimum feature dimension. In CMOS based memories such as the ones described above, F generally relates to the characteristic CMOS generation, controlled by the gate metal lateral dimensions. Clearly, the smallest dimension could be simply F^2 , i.e., the metal gate sets the storage cell dimension as well. This has not been achieved in *any* memory architecture. As a comparison, state-of-the-art Flash works at $8F^2$, while SRAMS work at $40F^2$. State-of-the-art FeRAM designs project a $16\text{--}20F^2$ cell size, still significantly larger than Flash, while MRAMS are even larger (due to the need for an additional transistor). Multiferroics, can in principle, compete in this space if the multiple functionality (i.e., both the charge and the spin degrees of freedom) is capitalized. Challenges are present at the processing level as well. These challenges are also common to FeRAMs, namely the integration of complex oxides onto a Si-CMOS platform. Very little work has been done to explore the integration of multiferroics on such a platform. Likewise, the effect of polycrystallinity in multiferroic materials on the ultimate properties and performance needs to be explored in greater detail. Additionally, the reliability and robustness of switching processes and logic states have to be carefully studied as well. Finally, on a fundamental level, the limits of coupling behavior need to be fully explored.

3.7 Conclusions: Looking to the Future

We are poised at a very interesting juncture in the evolution of these novel materials. It has been over a decade since the reincarnation of multiferroics and magnetoelectrics. In this time, much progress has been made in synthesis, characterization, and theoretical treatments of such materials. It is, however, clear that the next few years are particularly critical in terms of the evolution of these materials into real applications. Thus, the concerted and collaborative effort of materials scientists, physicists, and device engineers is essential. Particularly, the critical role of device physicists in designing new possible pathways to use the multiferroic behavior is obvious. It may only be through the development of revolutionary new capabilities that the significant energy barrier to system development will be overcome. The onus is on the researchers of today to provide the impetus for this significant investment of time and money.

References

1. R. Ramesh, N.A. Spaldin, Multiferroics: Progress and prospects in thin films. *Nat. Mater.* **6**, 21–29 (2007)
2. S.-W. Cheong, M. Mostovoy, Multiferroics: A magnetic twist for ferroelectricity. *Nat. Mater.* **6**, 13–20 (2007)
3. L.W. Martin, Y.-H. Chu, R. Ramesh, Advances in the growth and characterization of magnetic, ferroelectric, and multiferroic oxide thin films. *Mater. Sci. Eng. R* **68**, 89–133 (2010)
4. H. Schmid, Multi-ferroic magnetoelectrics. *Ferroelectrics* **162**, 317–338 (1994)

5. M. Fiebig, Revival of the magnetoelectric effect. *J. Phys. D* **38**, R123–R152 (2005)
6. W. Prellier, M.P. Singh, P. Murugavel, The single-phase multiferroic oxides: From bulk to thin film. *J. Phys. Condens. Matter.* **17**, R803–R832 (2005)
7. L.W. Martin, S.P. Crane, Y.-H. Chu, M.B. Holcomb, M. Gajek, H. Huijben, C.-H. Yang, N. Balke, R. Ramesh, Multiferroics and magnetoelectrics: Thin films and nanostructures. *J. Phys. Condens. Matter.* **20**, 434220 (2008)
8. W. Eerenstein, N.D. Mathur, J.F. Scott, Multiferroic and magnetoelectric materials. *Nature* **442**, 759–765 (2006)
9. D.I. Khomskii, Multiferroics: Different ways to combine magnetism and ferroelectricity. *J. Magn. Magn. Mater.* **306**, 1–8 (2006)
10. J.B. Goodenough, J.M. Longo, *Landolt-Börnstein, Numerical Data and Functional Relationships in Science and Technology, New Series*, vol. III.4 (Springer, Berlin, 1970), p. 126
11. T. Mitsui, E. Nakamura, Y. Shiozaki, *Landolt-Börnstein, Numerical Data and Functional Relationships in Science and Technology, New Series*, vol. 16(1) (Springer, Berlin, 1981), p. 126
12. N.A. Hill, Why are there so few magnetic ferroelectrics. *J. Phys. Chem. B* **104**, 6694–6709 (2000)
13. N.A. Hill, N. Filippetti, Why are there any magnetic ferroelectrics? *J. Magn. Magn. Mater.* **242**, 976–979 (2002)
14. U. Opik, M.H.L. Pryce, Studies of the Jahn-Teller effect. I. A survey of the static problem. *Proc. Royal Soc. Lond. A* **238**, 425–447 (1957)
15. P.S. Halasyamani, K.R. Poeppelmeier, Noncentrosymmetric oxides. *Chem. Mater.* **10**, 2753–2769 (1998)
16. D. Khomskii, Classifying multiferroics: Mechanisms and effects. *Physics* **2**, 20 (2009)
17. J. Wang, J.B. Neaton, H. Zheng, V. Nagarajan, S.B. Ogale, B. Liu, D. Viehland, V. Vaithyanathan, D.G. Schlom, U.V. Waghmare, N.A. Spaldin, K.M. Rabe, M. Wuttig, R. Ramesh, Epitaxial BiFeO₃ multiferroic thin film heterostructures. *Science* **299**, 1719–1722 (2003)
18. A.M. dos Santos, A. Parashar, A.R. Raju, Y.S. Zhao, A.K. Cheetham, C.N.R. Rao, Evidence for the likely occurrence of magnetoferroelectricity in the simple perovskite, BiMnO₃. *Solid State Commun.* **122**, 49–52 (2002)
19. T. Atou, H. Chiba, K. Ohoyama, Y. Yamaguichi, Y. Syono, Structure determination of ferromagnetic perovskite BiMnO₃. *J. Solid State Chem.* **145**, 639–642 (1999)
20. R.V. Shpanchenko, V.V. Chernaya, A.A. Tsirlin, P.S. Chizhov, D.E. Sklovsky, E.V. Antipov, Synthesis, structure, and properties of new perovskite PbVO₃. *Chem. Mater.* **16**, 3267–3273 (2004)
21. A.A. Belik, M. Azuma, T. Saito, Y. Shimakawa, M. Takano, Crystallographic features and tetragonal phase stability of PbVO₃, a new member of the PbTiO₃ family. *Chem. Mater.* **17**, 269–273 (2005)
22. L.W. Martin, Q. Zhan, Y. Suzuki, R. Ramesh, M. Chi, N. Browning, T. Mizoguchi, J. Kreisel, Growth and structure of PbVO₃ thin films. *Appl. Phys. Lett.* **90**, 062903 (2007)
23. A. Kumar, L.W. Martin, S. Denev, J.B. Kortright, Y. Suzuki, R. Ramesh, V. Gopalan, Polar and magnetic properties of PbVO₃ thin films. *Phys. Rev. B* **75**, 060101(R) (2007)
24. R. Seshadri, N.A. Hill, Visualizing the role of Bi 6s “lone pairs” in the off-centering distortion in ferromagnetic BiMnO₃. *Chem. Mater.* **13**, 2892–2899 (2001)
25. A.P. Levanyuk, D.G. Sannikov, Improper ferroelectrics. *Sov. Phys. Usp.* **17**, 199–214 (1974)
26. J. Kreisel, N. Kenselmann, Multiferroics—The challenge of coupling magnetism and ferroelectricity. *Europhys. News* **40**, 17–20 (2009)
27. B.B. van Aken, T.T.M. Palstra, A. Filippetti, N.A. Spaldin, The origin of ferroelectricity in magnetoelectric YMnO₃. *Nat. Mater.* **3**, 164–170 (2004)
28. N. Ikeda, H. Ohsumi, K. Ohwada, K. Ishii, T. Inami, K. Kakurai, Y. Murakami, K. Yoshii, S. Mori, Y. Horibe, H. Kito, Ferroelectricity from iron valence ordering in the charge-frustrated system LuFe₂O₄. *Nature* **436**, 1136–1138 (2005)
29. E.J. Verwey, Electronic conduction of magnetite (Fe₃O₄) and its transition point at low temperatures. *Nature* **144**, 327–328 (1939)

30. E.J. Verwey, P.W. Haayman, Electronic conductivity and transition point of magnetite ("Fe₃O₄"). *Physica* **8**, 979–987 (1941)
31. D.V. Efremov, J. van den Brink, D.I. Khomskii, Bond- versus site-centered ordering possible ferroelectricity in manganites. *Nat. Mater.* **3**, 853–856 (2004)
32. T. Kimura, T. Goto, H. Shintani, K. Ishizaka, T. Arima, Y. Tokura, Magnetic control of ferroelectric polarization. *Nature* **426**, 55–58 (2003)
33. N. Hur, S. Park, P.A. Sharma, J.S. Ahn, S. Guha, S.-W. Cheong, Electric polarization reversal and memory in a multiferroic material induced by magnetic fields. *Nature* **429**, 392–395 (2004)
34. M. Kenzelmann, A.B. Harris, S. Jonas, C. Broholm, J. Schefer, S.B. Kim, C.L. Zhang, S.-W. Cheong, O.P. Vajk, J.W. Lynn, Magnetic inversion symmetry breaking and ferroelectricity in TbMnO₃. *Phys. Rev. Lett.* **95**, 087206 (2005)
35. I.E. Dzyaloshinskii, Thermodynamic theory of weak ferromagnetism in antiferromagnetic substances. *Sov. Phys. JETP* **5**, 1259–1272 (1957)
36. T. Moriya, Anisotropic superexchange interaction and weak ferromagnetism. *Phys. Rev.* **120**, 91–98 (1960)
37. G. Lawes, A.B. Harris, T. Kimura, N. Rogado, R.J. Cava, A. Aharony, O. Entin-Wohlman, T. Yildirim, M. Kenzelmann, A.P. Ramirez, Magnetically driven ferroelectric order in Ni₃V₂O₈. *Phys. Rev. Lett.* **95**, 087205 (2005)
38. P. Curie, Sur la symétrie dans les phénomènes physiques. Symétrie d'un champ électrique d'un champ magnétique. *J. Phys.* **3**, 393–416 (1894)
39. D.N. Astrov, The magnetoelectric effect in antiferromagnetics. *Sov. Phys. JETP* **11**, 708–709 (1960)
40. D.N. Astrov, Magnetoelectric effect in chromium oxide. *Sov. Phys. JETP* **13**, 729–733 (1961)
41. G.T. Rado, V.J. Folen, Observation of the magnetically induced magnetoelectric effect and evidence for antiferromagnetic domains. *Phys. Rev. Lett.* **7**, 310–311 (1961)
42. V.J. Folen, G.T. Rado, E.W. Stalder, Anisotropy of the magnetoelectric effect in Cr₂O₃. *Phys. Rev. Lett.* **6**, 607–608 (1961)
43. V.W. Wood, A.E. Austin, Possible applications for magnetoelectric materials. *Int. J. Magn.* **5**, 303–315 (1974)
44. L.D. Landau, E.M. Lifshitz, *Electrodynamics of Continuous Media* (Pergamon, Oxford, 1960)
45. T.H. O'Dell, *Electrodynamics of Magneto-Electric Media* (North-Holland, Amsterdam, 1970)
46. R.R. Birss, *Symmetry and Magnetism* (North-Holland, Amsterdam, 1966)
47. J.P. Rivera, On definitions, units, measurements, tensor forms of the linear magnetoelectric effect and on a new dynamic method applied to Cr-Cl boracite. *Ferroelectrics* **161**, 165–180 (1994)
48. G.A. Smolensky, V.A. Ioffe, Commun. No. 71, Colloque International du Magnetisme, Grenoble (1958)
49. G.A. Smolensky, A.I. Agranovskaya, V.A. Isupov, New ferroelectrics of complex compound. *Sov. Phys. Solid State* **1**, 149–150 (1959)
50. N.A. Spaldin, M. Fiebig, The renaissance of magnetoelectric multiferroics. *Science* **309**, 391–392 (2005)
51. M. Eibschütz, H.J. Guggenheim, Antiferromagnetic-piezoelectric crystals: BaMe₄ (M=Mn, Fe, Co, and Ni). *Solid State Commun.* **6**, 737–739 (1968)
52. J.F. Scott, Spectroscopy of incommensurate ferroelectrics. *Ferroelectrics* **24**, 127–134 (1980)
53. Y.N. Venevtsev, V.V. Gagulin, I.D. Zhitomirsky, Materials science aspects of seignette-magnetism problem. *Ferroelectrics* **73**, 221–248 (1987)
54. Y.Y. Tomashpol'ski, Y.N. Venevtsev, V.N. Beznodrev, *Fiz. Tverd. Tela.* **7**, 2763 (1965)
55. E. Ascher, H. Schmid, D. Tar, Dielectric properties of boracites and evidence for ferroelectricity. *Solid State Commun.* **2**, 45–49 (1964)
56. H. Schmid, H. Rieder, E. Ascher, Magnetic susceptibilities of some 3d transition metal boracites. *Solid State Commun.* **3**, 327330 (1965)
57. A.V. Kovalev, G.T. Andreeva, *C. R. Acad. Sci.* **256**, 1958 (1963)

58. P. Coeuré, F. Guinet, J.C. Peuzin, G. Buisson, E.F. Bertaut, in *Proceedings of International Meeting on Ferroelectricity*, ed. by V. Dvůřák, A. Fousková, P. Glogar, vol. 1 (Institute of Physics, Czechoslovak Academy of Sciences, Prague 1966), p. 332–340
59. E.F. Bertaut, M. Mercier, Structure magnetique de MnYO_3 . *Phys. Lett.* **5**, 27–29 (1963)
60. H. Sugie, N. Iwata, K. Kohn, Magnetic ordering of rare earth ions and magnetic-electric interaction of hexagonal RMnO_3 ($\text{R}=\text{Ho}$, Er , Yb or Lu). *J. Phys. Soc. Jpn.* **71**, 1558–1564 (2002)
61. D.G. Schlom, J.H. Haeni, J. Lettieri, C.D. Theis, W. Tian, J.C. Jiang, X.Q. Pan, Oxide nano-engineering using MBE. *Mater. Sci. Eng. B* **87**, 282–291 (2001)
62. D.G. Schlom, L.-Q. Chen, C.-B. Eom, K.M. Rabe, S.K. Streiffer, J.-M. Triscone, Strain tuning of ferroelectric thin films. *Annu. Rev. Mater. Res.* **37**, 589626 (2007)
63. H.L. Yakel, W.D. Koehler, E.F. Bertaut, E.F. Forrat, On the crystal structure of the manganese (III) trioxides of the heavy lanthanides and yttrium. *Acta Crystallogr.* **16**, 957–962 (1963)
64. T. Lottermoser, T. Lonkai, U. Amann, D. Hohlwein, J. Ihringer, M. Fiebig, Magnetic phase control by an electric field. *Nature* **430**, 541–544 (2004)
65. T. Kimura, G. Lawes, T. Goto, Y. Tokura, A.P. Ramirez, Magnetolectric phase diagrams of orthorhombic RMnO_3 ($\text{R}=\text{Gd}$, Tb , and Dy). *Phys. Rev. B* **71**, 224425 (2005)
66. D. Ito, N. Fujimura, T. Yoshimura, T. Ito, Ferroelectric properties of YMnO_3 epitaxial films for ferroelectric-gate field-effect transistors. *J. Appl. Phys.* **93**, 5563 (2003)
67. N. Fujimura, T. Ishida, T. Yoshimura, T. Ito, Epitaxially grown YMnO_3 film: New candidate for nonvolatile memory devices. *Appl. Phys. Lett.* **69**, 1011 (1996)
68. P. Salvador, T.-D. Doan, B. Mercey, B. Raveau, Stabilization of YMnO_3 in a perovskite structure as a thin film. *Chem. Mater.* **10**, 2592–2595 (1998)
69. D.C. Yoo, J.Y. Lee, I.S. Kim, Y.T. Kim, Microstructure control of YMnO_3 thin films on Si (100) substrates. *Thin Solid Films* **416**, 62–65 (2002)
70. K. Suzuki, D. Fu, K. Nishizawa, T. Miki, K. Kato, Ferroelectric properties of alkoxy-derived YMnO_3 films crystallized in argon. *Jpn. J. Appl. Phys.* **42**, 5692–5695 (2003)
71. J. Dho, C.W. Leung, J.L. MacManus-Driscoll, M.G. Blamire, Epitaxial control and oriented YMnO_3 film growth by pulsed laser deposition. *J. Cryst. Growth* **267**, 548–553 (2004)
72. A. Posadas, J.-B. Yau, C.H. Ahn, J. Han, S. Gariglio, K. Johnston, K.M. Rabe, J.B. Neaton, Epitaxial growth of multiferroic YMnO_3 on GaN. *Appl. Phys. Lett.* **87**, 171915 (2005)
73. Y. Chye, T. Liu, D. Li, K. Lee, D. Lederman, T.H. Myers, Molecular beam epitaxy of YMnO_3 on c-plane GaN. *Appl. Phys. Lett.* **88**, 132903 (2006)
74. K.T. Kim, C.L. Kim, The effects of drying temperature on the crystallization of YMnO_3 thin films prepared by sol-gel method using alkoxides. *J. Eur. Ceram. Soc.* **24**, 2613–2617 (2004)
75. L. Zhou, Y.P. Wang, Z.G. Liu, W.Q. Zou, Y.W. Du, Structure and ferroelectric properties of ferroelectromagnetic YMnO_3 thin films prepared by pulsed laser deposition. *Phys. Status Solidi A* **201**, 497–501 (2004)
76. N. Shigemitsu, H. Sakata, D. Ito, T. Yoshimura, T. Ashida, N. Fujimura, Pulsed-laser-deposited YMnO_3 epitaxial films with square polarization-electric field hysteresis loop and low-temperature growth. *Jpn. J. Appl. Phys.* **43**, 6613–6616 (2004)
77. D. Kim, D. Klingensmith, D. Dalton, V. Olariu, F. Gnadinger, M. Rahman, A. Mahmud, T.S. Kalkur, C-axis oriented MOCVD YMnO_3 thin film and its electrical characteristics in MFIS FeTRAM. *Integr. Ferroelectr.* **68**, 75–84 (2004)
78. N. Fujimura, H. Sakata, D. Ito, T. Yoshimura, T. Yokota, T. Ito, Ferromagnetic and ferroelectric behaviors of A-site substituted YMnO_3 -based epitaxial thin films. *J. Appl. Phys.* **93**, 6990 (2003)
79. T. Choi, J. Lee, Bi modification for low-temperature processing of YMnO_3 thin films. *Appl. Phys. Lett.* **84**, 5043 (2004)
80. A. Sundaresan, A. Maignan, B. Raveau, Effect of A-site cation size mismatch on charge ordering and colossal magnetoresistance properties of perovskite manganites. *Phys. Rev. B* **56**, 5092–5095 (1997)
81. A.A. Nugroho, N. Bellido, U. Adem, G. Nénert, C. Simon, M.O. Tjia, M. Mostovoy, T.T.M. Palstra, Enhancing the magnetoelectric coupling in YMnO_3 by Ga doping. *Phys. Rev. B* **75**, 174435 (2007)

82. A.A. Bosak, A.A. Kamenev, I.E. Graboy, S.V. Antonov, O.Y. Gorbenko, A.R. Kaul, C. Dubourdieu, J.P. Senateur, V.L. Svechnikov, H.W. Zandbergen, B. Holländer, Epitaxial phase stabilization phenomena in rare earth manganites. *Thin Solid Films* **400**, 149–153 (2001)
83. K. Suzuki, K. Nishizawa, T. Miki, K. Kato, Preparation and orientation control of RMnO_3 ($\text{R}=\text{Y}, \text{Yb}$) thin film by chemical solution deposition. *J. Cryst. Growth* **237**, 482–486 (2002)
84. J.H. Lee, P. Murugavel, H. Ryu, D. Lee, J.Y. Jo, J.W. Kim, H.J. Kim, K.H. Kim, Y. Jo, M.-H. Jung, Y.H. Oh, Y.-W. Kim, J.-G. Yoon, J.-S. Chung, T.W. Noh, Epitaxial stabilization of a new multiferroic hexagonal phase of TbMnO_3 thin films. *Adv. Mater.* **18**, 3125–3129 (2006)
85. K.R. Balasubramaniam, S. Havelia, P.A. Salvador, H. Zheng, J.F. Mitchell, Epitaxial stabilization and structural properties of REMnO_3 ($\text{RE}=\text{Dy}, \text{Gd}, \text{Sm}$) compounds in a layered, hexagonal ABO_3 structure. *Appl. Phys. Lett.* **91**, 232901 (2007)
86. Y. Cui, C. Wang, B. Cao, TbMnO_3 epitaxial thin films by pulsed-laser deposition. *Solid State Commun.* **133**, 641–645 (2005)
87. D. Rubi, C. de Graaf, C.J.M. Daumont, D. Mannix, R. Broer, B. Noheda, Ferromagnetism and increased ionicity in epitaxially grown TbMnO_3 films. *Phys. Rev. B* **79**, 014416 (2009)
88. B.J. Kirby, D. Kan, A. Luykx, M. Murakami, D. Kundaliya, I. Takeuchi, Anomalous ferromagnetism in TbMnO_3 thin films. *J. Appl. Phys.* **105**, 07D917 (2009)
89. C.J.M. Daumont, D. Mannix, S. Venkatesan, G. Catalan, D. Rubi, B.J. Kooi, J.T.M. De Hosson, B. Noheda, Epitaxial TbMnO_3 thin films on SrTiO_3 substrates: a structural study. *J. Phys. Condens. Matter* **21**, 182001 (2009)
90. D.K. Shukla, R. Kumar, S.K. Sharma, P. Thakur, R.J. Choudhary, S. Mollah, N.B. Brookes, M. Knobel, K.H. Chae, W.K. Choi, Thin film growth of multiferroic BiMn_2O_5 using pulsed laser ablation and its characterization. *J. Phys. D* **42**, 125304 (2009)
91. M. Azuma, N. Seiji, A. Belik, I. Shintaro, S. Takashi, T. Kazuhide, Y. Ikuya, S. Yuichi, T. Mikio, Magnetic ferroelectrics Bi, Pb-3d transition metal perovskites. *Trans. Mater. Res. Soc. Jpn.* **31**
92. A.M. dos Santos, A.K. Cheetham, W. Tian, X. Pan, Y. Jia, N.J. Murphy, J. Lettieri, D.G. Schlom, Epitaxial growth and properties of metastable BiMnO_3 thin films. *Appl. Phys. Lett.* **84**, 91 (2004)
93. A. Sharan, J. Lettieri, Y. Jia, W. Tian, X. Pan, D.G. Schlom, V. Gopalan, Bismuth manganite: a multiferroic with large nonlinear optical response. *Phys. Rev. B* **69**, 214109 (2004)
94. J.Y. Son, B.G. Kim, C.H. Kim, J.H. Cho, Writing polarization bits on multiferroic BiMnO_3 thin film using Kelvin probe force microscope. *Appl. Phys. Lett.* **84**, 4971 (2004)
95. M. Gajek, M. Bibes, A. Barthélémy, K. Bouzehouane, S. Fusil, M. Varela, J. Fontcuberta, A. Fert, Spin filtering through ferromagnetic BiMnO_3 tunnel barriers. *Phys. Rev. B* **72**, 020406(R) (2005)
96. M. Gajek, M. Bibes, S. Fusil, K. Bouzehouane, J. Fontcuberta, A. Barthélémy, A. Fert, Tunnel junctions with multiferroic barriers. *Nat. Mater.* **6**, 296–302 (2007)
97. C.-H. Yang, S.H. Lee, T.Y. Koo, Y.H. Jeong, Dynamically enhanced magnetodielectric effect and magnetic-field-controlled electric relaxations in La-doped BiMnO_3 . *Phys. Rev. B* **75**, 140104 (2007)
98. A.A. Belik, S. Iikubo, K. Kodama, N. Igawa, S. Shamoto, M. Maie, T. Nagai, Y. Matsui, S.Y. Stefanovich, B.I. Lazoryak, E. Takayama-Muromachi, BiScO_3 : Centrosymmetric BiMnO_3 -type oxide. *J. Am. Chem. Soc.* **128**, 706–707 (2006)
99. P. Baettig, R. Seshadri, N.A. Spaldin, Anti-polarity in ideal BiMnO_3 . *J. Am. Chem. Soc.* **129**, 9854–9855 (2007)
100. T. Shishidou, N. Mikamo, Y. Uratani, F. Ishii, T. Oguchi, First-principles study of the electronic structure of bismuth transition-metal oxides. *J. Phys. Condens. Matter* **16**, S5677–S5683 (2004)
101. R. Schmidt, W. Eerenstein, P.A. Midgley, Large dielectric response to the paramagnetic-ferromagnetic transition ($T_C \sim 100$ K) in multiferroic BiMnO_3 epitaxial thin films. *Phys. Rev. B* **79**, 214107 (2009)
102. P. Royen, K. Swars, Das system wismutoxyd-eisenoxyd im bereich von 0 bis 55mol% eisenoxyd. *Angew. Chem.* **24**, 779 (1957)

103. F. Kubel, H. Schmid, Structure of a ferroelectric and ferroelastic monodomain crystal of the perovskite BiFeO_3 . *Acta. Crystallogr.* **B46**, 698–702 (1990)
104. S.V. Kiselev, R.P. Ozerov, G.S. Zhdanov, Detection of magnetic order in ferroelectric BiFeO_3 by neutron diffraction. *Sov. Phys. Dokl.* **7**, 742–744 (1963)
105. J.R. Teague, R. Gerson, W.J. James, Dielectric hysteresis in single crystal BiFeO_3 . *Solid State Commun.* **8**, 1073–1074 (1970)
106. C. Michel, J.M. Moreau, G.D. Achenbach, R. Gerson, W.J. James, The atomic structure of BiFeO_3 . *Solid State Commun.* **7**, 701–703 (1969)
107. J.M. Moreau, C. Michel, R. Gerson, W.J. James, Ferroelectric BiFeO_3 x-ray and neutron diffraction study. *J. Phys. Chem. Solids* **32**, 1315–1320 (1971)
108. C. Tabares-Muñoz, J.P. Rivera, A. Bezinge, A. Monnier, H. Schmid, Measurement of the quadratic magnetoelectric effect on single crystalline BiFeO_3 . *Jpn. J. Appl. Phys.* **24**, 1051–1053 (1985)
109. D. Lebeugle, D. Colson, A. Forget, M. Viret, P. Bonville, J.F. Marucco, S. Fusil, Room-temperature coexistence of large electric polarization and magnetic order in BiFeO_3 single crystals. *Phys. Rev. B* **76**, 024116 (2007)
110. J.B. Neaton, C. Ederer, U.V. Waghmare, N.A. Spaldin, K.M. Rabe, First-principles study of spontaneous polarization in BiFeO_3 . *Phys. Rev. B* **71**, 014113 (2005)
111. F. Zavaliche, S.-Y. Yang, T. Zhao, Y.-H. Chu, M.P. Cruz, C.-B. Eom, R. Ramesh, Multiferroic BiFeO_3 films: Domain structure and polarization dynamics. *Phase Transit.* **79**, 991–1017 (2006)
112. P. Fischer, M. Polomska, I. Sosnowska, M. Szymanski, Temperature dependence of the crystal and magnetic structures of BiFeO_3 . *J. Phys. C* **13**, 1931–1940 (1980)
113. I. Sosnowska, T. Peterlin-Neumaier, E. Steichele, Spiral magnetic ordering in bismuth ferrite. *J. Phys. C* **15**, 4835–4846 (1982)
114. G.W. Pabst, L.W. Martin, Y.-H. Chu, R. Ramesh, Leakage mechanisms in BiFeO_3 . *Appl. Phys. Lett.* **90**, 072902 (2007)
115. J. Kabelac, S. Ghosh, P. Dobal, R. Katiyar, rf oxygen plasma assisted molecular beam epitaxy growth of BiFeO_3 thin films on SrTiO_3 (001). *J. Vac. Sci. Technol.* **25**, 1049–1052 (2007)
116. J.F. Ihlefeld, A. Kumar, V. Gopalan, D.G. Schlom, Y.B. Chen, X.Q. Pan, T. Heeg, J. Schubert, X. Ke, P. Schiffer, J. Orenstein, L.W. Martin, Y.-H. Chu, R. Ramesh, Adsorption-controlled molecular-beam epitaxial growth of BiFeO_3 . *Appl. Phys. Lett.* **91**, 071922 (2007)
117. V.R. Palkar, J. John, R. Pinto, Observation of saturated polarization and dielectric anomaly in magnetoelectric BiFeO_3 thin films. *Appl. Phys. Lett.* **80**, 1628 (2002)
118. Y.H. Lee, C.S. Liang, J.M. Wu, Crystal growth and characterization of highly oriented BiFeO_3 thin films. *Electrochem. Solid-State Lett.* **8**, F55–F57 (2005)
119. R.R. Das, D.M. Kim, S.H. Baek, C.B. Eom, F. Zavaliche, S.-Y. Yang, R. Ramesh, Y.B. Chen, X.Q. Pan, X. Ke, M.S. Rzchowski, S.K. Streiffer, Synthesis and ferroelectric properties of epitaxial BiFeO_3 thin films grown by sputtering. *Appl. Phys. Lett.* **88**, 242904 (2006)
120. S.-Y. Yang, F. Zavaliche, L. Mohaddes-Ardabili, V. Vaithyanathan, D.G. Schlom, Y.J. Lee, Y.-H. Chu, M.P. Cruz, T. Zhao, R. Ramesh, Metalorganic chemical vapor deposition of lead-free ferroelectric BiFeO_3 films for memory applications. *Appl. Phys. Lett.* **87**, 102903 (2005)
121. R. Ueno, S. Okamura, H. Funakubo, K. Saito, Crystal structure and electrical properties of epitaxial BiFeO_3 thin films grown by metal organic chemical vapor deposition. *Jpn. J. Appl. Phys.* **44**, L1231–L1233 (2005)
122. S.K. Singh, Y.K. Kim, H. Funakubo, H. Ishiura, Epitaxial BiFeO_3 thin films fabricated by chemical solution deposition. *Appl. Phys. Lett.* **88**, 162904 (2006)
123. J. Wang, H. Zheng, Z. Ma, S. Prasertchoung, M. Wuttig, R. Droopad, J. Yu, K. Eisenbeiser, R. Ramesh, Epitaxial BiFeO_3 films on Si. *Appl. Phys. Lett.* **85**, 2574 (2004)
124. W. Tian, V. Vaithyanathan, D.G. Schlom, Q. Zhan, S.-Y. Yang, Y.-H. Chu, R. Ramesh, Epitaxial integration of (0001) BiFeO_3 with (0001) GaN. *Appl. Phys. Lett.* **90**, 172908 (2007)
125. Y.-H. Chu, T. Zhao, M.P. Cruz, Q. Zhan, P.-L. Yang, L.W. Martin, M. Huijben, C.-H. Yang, F. Zavaliche, H. Zheng, R. Ramesh, Ferroelectric size effects in multiferroic BiFeO_3 thin films. *Appl. Phys. Lett.* **90**, 252906 (2007)

126. S.K. Streiffer, C.B. Parker, A.E. Romanov, M.J. Lefevre, L. Zhao, J.S. Speck, W. Pompe, C.M. Foster, G.R. Bai, Domain patterns in epitaxial rhombohedral ferroelectric films. I. Geometry and experiments. *J. Appl. Phys.* **83**(2742) (1998)
127. J.X. Zhang, Y.L. Li, S. Choudhury, L.Q. Chen, Y.-H. Chu, F. Zavaliche, M.P. Cruz, R. Ramesh, Q.X. Jia, Computer simulation of ferroelectric domain structures in epitaxial BiFeO₃ thin films. *J. Appl. Phys.* **103**, 094111 (2008)
128. Y.-H. Chu, Q. Zhan, L.W. Martin, M.P. Cruz, P.-L. Yang, G.W. Pabst, F. Zavaliche, S.-Y. Yang, J.-X. Zhang, L.-Q. Chen, D.G. Schlom, I.-N. Lin, T.-B. Wu, R. Ramesh, Nanoscale domain control in multiferroic BiFeO₃ thin films. *Adv. Mater.* **18**, 2307–2311 (2006)
129. Y.-H. Chu, M.P. Cruz, C.-H. Yang, L.W. Martin, P.-L. Yang, J.-X. Zhang, K. Lee, P. Yu, L.-Q. Chen, R. Ramesh, Domain control in multiferroic BiFeO₃ through substrate vicinality. *Adv. Mater.* **19**, 2662–2666 (2007)
130. Y.-H. Chu, Q. He, C.-H. Yang, P. Yu, L.W. Martin, P. Shafer, R. Ramesh, Nanoscale control of domain architectures in BiFeO₃ thin films. *Nano Lett.* **9**, 1726–1730 (2009)
131. C.M. Folkman, S.H. Baek, H.W. Jang, C.B. Eom, C.T. Nelson, X.Q. Pan, Y.L. Li, L.-Q. Chen, A. Kumar, V. Gopalan, S.K. Streiffer, Stripe domain structure in epitaxial (001) BiFeO₃ thin films on orthorhombic TbScO₃ substrate. *Appl. Phys. Lett.* **94**, 251911 (2009)
132. M.P. Cruz, Y.-H. Chu, J.X. Zhang, P.-L. Yang, F. Zavaliche, Q. He, P. Shafer, L.Q. Chen, R. Ramesh, Strain control of domain-wall stability in epitaxial BiFeO₃ (110) films. *Phys. Rev. Lett.* **99**, 217601 (2007)
133. P. Shafer, F. Zavaliche, Y.-H. Chu, P.-L. Yang, M.P. Cruz, R. Ramesh, Planar electrode piezoelectric force microscopy to study electric polarization switching in BiFeO₃. *Appl. Phys. Lett.* **90**, 202909 (2007)
134. C. Ederer, N.A. Spaldin, Weak ferromagnetism and magnetoelectric coupling in bismuth ferrite. *Phys. Rev. B* **71**, 060401(R) (2005)
135. W. Eerenstein, F.D. Morrison, J. Dho, M.G. Blamire, J.F. Scott, N.D. Mathur, Comment on “epitaxial BiFeO₃ multiferroic thin film heterostructures”. *Science* **307**(1203a) (2005)
136. H. Béa, M. Bibes, S. Fusil, K. Bouzehouane, E. Jacquet, K. Rode, P. Bencok, A. Barthélémy, Investigation on the origin of the magnetic moment of BiFeO₃ thin films by advanced x-ray characterizations. *Phys. Rev. B* **74**, 020101 (2006)
137. J. Wang, A. Scholl, H. Zheng, S.B. Ogale, D. Viehland, D.G. Schlom, N.A. Spaldin, K.M. Rabe, M. Wuttig, L. Mohaddes, J. Neaton, U. Waghmare, T. Zhao, R. Ramesh, Response to comment on “epitaxial BiFeO₃ multiferroic thin film heterostructures”. *Science* **307**(1203b) (2005)
138. F. Gao, X. Chen, K. Yin, S. Dong, Z. Ren, F. Yuan, T. Yu, Z. Zou, J.M. Liu, Visible-light photocatalytic properties of weak magnetic BiFeO₃ nanoparticles. *Adv. Mater.* **19**, 2889–2892 (2007)
139. M.B. Holcomb, L.W. Martin, A. Scholl, Q. He, P. Yu, C.-H. Yang, S.-Y. Yang, P.-A. Glans, M. Valvidares, M. Huijben, J.B. Kortright, J. Guo, Y.-H. Chu, R. Ramesh, Probing the evolution of antiferromagnetism in multiferroics. *Phys. Rev. B* **81**, 134406 (2010)
140. L.W. Martin, Y.-H. Chu, M.B. Holcomb, M. Huijben, S.J. Han, D. Lee, E. Arenholz, S.X. Wang, R. Ramesh, Nanoscale control of exchange bias with BiFeO₃ thin films. *Nano Lett.* **8**, 2050–2055 (2008)
141. J. Přívratská, V. Janovec, Pyromagnetic domain walls connecting antiferromagnetic non-ferroelastic magnetoelectric domains. *Ferroelectrics* **204**, 321–331 (1997)
142. J. Přívratská, V. Janovec, Spontaneous polarization and/or magnetization in non-ferroelastic domain walls: symmetry predictions. *Ferroelectrics* **222**, 23–32 (1999)
143. L. Thomas, M. Hayashi, X. Jiang, R. Moriya, C. Rettner, S. Parkin, Resonant amplification of magnetic domain-wall motion by a train of current pulses. *Science* **315**, 1553–1556 (2007)
144. V. Goltsev, R.V. Pisarev, T. Lottermoser, M. Fiebig, Structure and interaction of antiferromagnetic domain walls in hexagonal YMnO₃. *Phys. Rev. Lett.* **90**, 177204 (2003)
145. M. Mostovoy, Ferroelectricity in spiral magnets. *Phys. Rev. Lett.* **96**, 067601 (2006)
146. A. Aird, E.K.H. Salje, Sheet superconductivity in twin walls: experimental evidence of WO_{3-x}. *J. Phys. Condens. Matter.* **10**, L377–L380 (1998)

147. M. Bartels, V. Hagen, M. Burianek, M. Getzlaff, U. Bismayer, R. Wiesendanger, Impurity-induced resistivity of ferroelastic domain walls in doped lead phosphate. *J. Phys. Condens. Matter*. **15**, 957–962 (2003)
148. P. Zubko, G. Catalan, A. Buckley, P.R.L. Welche, J.F. Scott, Strain-gradient-induced polarization in SrTiO₃ single crystals. *Phys. Rev. Lett.* **99**, 167601 (2007)
149. M. Daraktchiev, G. Catalan, J.F. Scott, Landau theory of ferroelectric domain walls in magnetoelectrics. *Ferroelectrics* **375**, 122–131 (2008)
150. G. Catalan, J.F. Scott, Physics and applications of bismuth ferrite. *Adv. Mater.* **21**, 2463–2485 (2009)
151. Q. He, C.-H. Yeh, J.-C. Yang, G. Singh-Bhalla, C.-W. Liang, P.-W. Chiu, G. Catalan, L.W. Martin, Y.-H. Chu, J.F. Scott, R. Ramesh, Magnetotransport at domain walls in BiFeO₃. *Phys. Rev. Lett.* **108**, 067203 (2012)
152. J. Seidel, L.W. Martin, Q. He, Q. Zhan, Y.-H. Chu, A. Rother, M.E. Hawkrige, P. Maksymovych, P. Yu, M. Gajek, N. Balke, S.V. Kalinin, S. Gemming, F. Wang, G. Catalan, J.F. Scott, N.A. Spaldin, J. Orenstein, R. Ramesh, Conduction at domain walls in oxide multiferroics. *Nat. Mater.* **8**, 229–324 (2009)
153. S.S.P. Parkin, M. Hayashi, L. Thomas, Magnetic domain-wall racetrack memory. *Science* **320**, 190–194 (2008)
154. D.A. Allwood, G. Xiong, C.C. Faulkner, D. Atkinson, D. Petit, R.P. Cowburn, *Science* **309**, 1688–1692 (2005)
155. E.K.H. Salje, Multiferroic domain boundaries as active memory devices: trajectories towards domain boundary engineering. *Chem. Phys. Chem.* **11**, 940–950 (2010)
156. T. Zhao, A. Scholl, F. Zavaliche, K. Lee, M. Barry, A. Doran, M.P. Cruz, Y.-H. Chu, C. Ederer, N.A. Spaldin, R.R. Das, D.M. Kim, S.H. Baek, C.B. Eom, R. Ramesh, Electrical control of antiferromagnetic domain in multiferroic BiFeO₃ films at room temperature. *Nat. Mater.* **5**, 823–829 (2006)
157. D. Lebeugle, D. Colson, A. Forget, M. Viret, A.M. Bataille, A. Gukasov, Electric-field-induced spin flop in BiFeO₃ single crystals at room temperature. *Phys. Rev. Lett.* **100**, 227602 (2008)
158. S. Lee, W. Ratcliff, S.-W. Cheong, V. Kiryukhin, Electric field control of the magnetic state of BiFeO₃ single crystals. *Appl. Phys. Lett.* **92**, 192906 (2008)
159. Y.-H. Lee, J.-M. Wu, C.-H. Lai, Influence of La doping in multiferroic properties of BiFeO₃ thin films. *Appl. Phys. Lett.* **88**, 042903 (2006)
160. X. Qi, J. Dho, R. Tomov, M.G. Blamire, J.L. MacManus-Driscoll, Greatly reduced leakage current and conduction mechanism in aliovalent-ion-doped BiFeO₃. *Appl. Phys. Lett.* **86**, 062903 (2005)
161. G.L. Yuan, S.W. Or, Enhanced piezoelectric and pyroelectric effects in single-phase Bi_{1-x}Nd_xFeO₃ (x=0–0.15) ceramics. *Appl. Phys. Lett.* **88**, 062905 (2006)
162. C.F. Chung, J.P. Lin, J.M. Wu, Influence of Mn and Nb dopants on electric properties of chemical-solution-deposited BiFeO₃ films. *Appl. Phys. Lett.* **88**, 242909 (2006)
163. J.K. Kim, S.S. Kim, W.J. Kim, A.S. Bhalla, R. Guo, Enhanced ferroelectric properties of Cr-doped BiFeO₃ thin films grown by chemical solution deposition. *Appl. Phys. Lett.* **88**, 132901 (2006)
164. Z.V. Gabbasova, M.D. Kuz'min, A.K. Zvezdin, I.S. Dubenko, V.A. Murashov, D.N. Rakov, I.B. Krynetsky, Bi_{1-x}R_xFeO₃ (R=rare earth): a family of novel magnetoelectrics. *Phys. Lett. A* **158**, 491–498 (1991)
165. A.V. Zaleskii, A.A. Frolov, T.A. Khimich, A.A. Bush, Composition-induced transition of spin-modulated structure into a uniform antiferromagnetic state in Bi_{1-x}La_xFeO₃ system studied using ⁵⁷Fe NMR. *Phys. Solid State* **45**, 141–145 (2006)
166. D. Lee, M.G. Kim, S. Ryu, H.M. Jang, S.G. Lee, Epitaxially grown La-modified BiFeO₃ magnetoferroelectric thin films. *Appl. Phys. Lett.* **86**, 222903 (2005)
167. Y.-H. Chu, Q. Zhan, M.P. Cruz, L.W. Martin, T. Zhao, P. Yu, R. Ramesh, P.T. Joseph, I.N. Lin, W. Tian, D.G. Schlom, Low voltage performance of epitaxial BiFeO₃ films on Si substrates through lanthanum substitution. *Appl. Phys. Lett.* **92**, 102909 (2008)

168. D.H. Wang, W.C. Goh, M. Ning, C.K. Ong, Effect of Ba doping on magnetic, ferroelectric, and magnetoelectric properties in multiferroic BiFeO₃ at room temperature. *Appl. Phys. Lett.* **88**, 212907 (2006)
169. V.A. Chomchenko, D.A. Kiselev, J.M. Vieira, A.L. Kholkin, M.A. Sa, Y.G. Pogorelov, Synthesis and multiferroic properties of Bi_{0.8}A_{0.2}FeO₃ (A=Ca, Sr, Pb) ceramics. *Appl. Phys. Lett.* **90**, 242901 (2007)
170. S. Fujino, M. Murakami, V. Anbusathaiah, S.-H. Lim, V. Nagarajan, C.J. Fennie, M. Wuttig, L. Salamanca-Riba, I. Takeuchi, Combinatorial discovery of a lead-free morphotropic phase boundary in a thin-film piezoelectric perovskite. *Appl. Phys. Lett.* **92**, 202904 (2008)
171. C.-J. Cheng, D. Kan, S.-H. Lim, W.R. McKenzie, P.R. Munroe, L.G. Salamanca-Riba, R.L. Withers, I. Takeuchi, V. Nagarajan, Structural transitions and complex domain structures across a ferroelectric-to-antiferroelectric phase boundary in epitaxially Sm-doped BiFeO₃ thin films. *Phys. Rev. B* **80**, 014109 (2009)
172. C.-J. Cheng, A.Y. Borisevich, D. Kan, I. Takeuchi, V. Nagarajan, Nanoscale structural and chemical properties of antipolar clusters in Sm-doped BiFeO₃ ferroelectric epitaxial thin films. *Chem. Mater.* **22**, 2588–2596 (2010)
173. D. Kan, L. Pálová, V. Anbusathaiah, C.-J. Cheng, S. Fujino, V. Nagarajan, K.M. Rabe, I. Takeuchi, Universal behavior and electric-field-induced structural transition in rare-earth substituted BiFeO₃. *Adv. Funct. Mater.* **20**, 1108–1115 (2010)
174. C.H. Yang, J. Seidel, S.Y. Kim, P.B. Rossen, P. Yu, M. Gajek, Y.-H. Chu, L.W. Martin, M.B. Holcomb, Q. He, P. Maksymovych, N. Balke, S.V. Kalinin, A.P. Baddorf, S.R. Basu, M.L. Scullin, R. Ramesh, Electric modulation of conduction in multiferroic Ca-doped BiFeO₃ films. *Nat. Mater.* **8**, 485–493 (2009)
175. D.C. Tsui, H.L. Stormer, A.C. Gossard, Two-dimensional magnetotransport in extreme quantum limit. *Phys. Rev. Lett.* **48**, 1559–1562 (1982)
176. C. Michel, J.M. Moreau, G.D. Achenbach, R. Gerson, W.J. James, Atomic structures of two rhombohedral ferroelectric phases in the Pb(Zr, Ti)O₃ solid solution series. *Solid State Commun.* **7**, 865–868 (1969)
177. C. Ederer, N.A. Spaldin, Effect of epitaxial strain on the spontaneous polarization of thin film ferroelectrics. *Phys. Rev. Lett.* **95**, 257601 (2005)
178. P. Ravindran, R. Vidyaa, A. Kjekshus, H. Fjellvåg, Theoretical investigation of magnetoelectric behavior in BiFeO₃. *Phys. Rev. B* **74**, 224412 (2006)
179. H. Béa, B. Dupé, S. Fusil, R. Mattana, E. Jacquet, B. Warot-Fonrose, F. Wilhelm, A. Rogalev, S. Petit, V. Cros, A. Anane, F. Petroff, K. Bouzouane, G. Geneste, B. Dkhil, S. Lisenkov, I. Ponomareva, L. Bellaiche, M. Bibes, A. Barthélémy, Evidence for room-temperature multiferroicity in a compound with giant axial ratio. *Phys. Rev. Lett.* **102**, 217603 (2009)
180. D. Ricinchi, K.Y. Yun, M. Okuyama, A mechanism for the 150 μC cm⁻² polarization of BiFeO₃ films based on first-principles calculations and new structural data. *J. Phys. Condens. Matter* **18**, L97–L105 (2006)
181. R.J. Zeches, M.D. Rossell, J.X. Zhang, A.J. Hatt, Q. He, C.H. Yang, A. Kumar, C.H. Wang, A. Melville, C. Adamo, G. Sheng, Y.H. Chu, J.F. Ihlefeld, R. Erni, C. Ederer, V. Gopalan, L.Q. Chen, D.G. Schlom, N.A. Spaldin, L.W. Martin, R. Ramesh, A strain-driven morphotropic phase boundary in BiFeO₃. *Science* **326**, 977–980 (2009)
182. Z. Chen, Z. Luo, C. Huang, Y. Qi, P. Yang, L. You, C. Hu, T. Wu, J. Wang, C. Gao, T. Sritharan, Low-symmetry monoclinic phases and polarization rotation path mediated by epitaxial strain in multiferroic BiFeO₃ thin films. *Adv. Funct. Mater.* **21**, 133–138 (2011)
183. H. Christen, J.H. Nam, H.S. Kim, A.J. Hatt, N.A. Spaldin, Stress-induced R-M_A-M_C-T symmetry changes in BiFeO₃ films. *Phys. Rev. B* **83**, 144107 (2011)
184. B. Dupé, I.C. Infante, G. Geneste, P.E. Janolin, M. Bibes, A. Barthélémy, S. Lisenkov, L. Bellaiche, S. Ravy, B. Dkhil, Competing phases in BiFeO₃ thin films under compressive epitaxial strain. *Phys. Rev. B* **81**, 144128 (2010)
185. D. Mazumdar, V. Shelke, M. Iliiev, S. Jesse, A. Kumar, S.V. Kalinin, A.P. Baddorf, A. Gupta, Nanoscale switching characteristics of nearly tetragonal BiFeO₃ thin films. *Nano Lett.* **10**, 2555–2561 (2010)

186. A. Kumar, S. Denev, R.J. Zeches, E. Vlahos, N.J. Podraza, A. Melville, D.G. Schlom, R. Ramesh, V. Gopalan, Probing mixed tetragonal/rhombohedral-like monoclinic phases in strained bismuth ferrite films by optical second harmonic generation. *Appl. Phys. Lett.* **97**, 112903 (2010)
187. A.R. Damodaran, S. Lee, J. Karthik, S. MacClaren, L.W. Martin, Temperature and thickness evolution and epitaxial breakdown in highly-strained BiFeO₃ thin films. *Phys. Rev. B* **85**, 024113 (2012)
188. A.R. Damodaran, E. Breckenfeld, A.R. Choquette, L.W. Martin, Stabilization of mixed-phase structures in highly strained BiFeO₃ thin films via chemical-alloying. *Appl. Phys. Lett.* **100**, 082904 (2012)
189. J.X. Zhang, B. Xiang, Q. He, J. Seidel, R.J. Zeches, P. Yu, S.Y. Yang, C.H. Wang, Y.H. Chu, L.W. Martin, A.M. Minor, R. Ramesh, Large field-induced strains in a lead-free piezoelectric material. *Nat. Nanotechnol.* **6**, 98–102 (2011)
190. J.F. Scott, Iso-structural phase transitions in BiFeO₃. *Adv. Mater.* **22**, 2106–2107 (2010)
191. J. Ouyang, W. Zhang, X. Huang, A.L. Roytburd, Thermodynamics of formation of tetragonal and rhombohedral heterophase polydomains in epitaxial ferroelectric thin films. *Acta. Mater.* **59**, 3779–3791 (2011)
192. A.R. Damodaran, C.W. Liang, Q. He, C.Y. Peng, L. Chang, Y.H. Chu, L.W. Martin, Nanoscale structure and mechanism for enhanced electromechanical response of highly strained BiFeO₃ thin films. *Adv. Mater.* **23**, 3170–3175 (2011)
193. R.K. Vasudevan, Y. Liu, J. Li, W.I. Liang, A. Kumar, S. Jesse, Y.C. Chen, Y.H. Chu, V. Nagarajan, S.V. Kalinin, Nanoscale control of phase variants in strain-engineered BiFeO₃. *Nano Lett.* **11**, 3346–3354 (2011)
194. Q. He, Y.H. Chu, J.T. Heron, S.Y. Yang, W.I. Liang, C.Y. Kuo, H.J. Lin, P. Yu, C.W. Liang, R.J. Zeches, W.C. Kuo, J.Y. Juang, C.T. Chen, E. Arenholz, A. Scholl, R. Ramesh, Electrically controllable spontaneous magnetism in nanoscale mixed phase multiferroics. *Nat. Commun.* **2**, 225 (2011)
195. K.T. Ko, M.H. Jung, Q. He, J.H. Lee, C.S. Woo, K. Chu, J. Seidel, B.G. Jeon, Y.S. Oh, K.H. Kim, W.I. Liang, H.J. Chen, Y.H. Chu, Y.H. Jeong, R. Ramesh, J.H. Park, C.H. Yang, Concurrent transition of ferroelectric and magnetic ordering near room temperature. *Nat. Commun.* **2**, 567 (2011)
196. G.W. MacDougall, H.M. Christen, W. Siemons, M.D. Biegalski, J.L. Zarestky, S. Liang, E. Dagotto, S.E. Nagler, Antiferromagnetic transitions in “T-like” BiFeO₃. *Phys. Rev. B* **85**, 100406(R) (2012)
197. J. Kreisel, P. Jadhav, O. Chaix-Pluchery, M. Varela, N. Dix, F. Sanchez, J. Fontcuberta, A phase transition close to room temperature in BiFeO₃ thin films. *J. Phys. Condens. Matter* **23**, 342202 (2011)
198. W. Siemons, M.D. Biegalski, J.H. Nam, H.M. Christen, Temperature-driven structural phase transition in tetragonal-like BiFeO₃. *Appl. Phys. Express* **4**, 095801 (2011)
199. K.Y. Choi, S.H. Do, P. Lemmens, D. Wulferding, C.S. Woo, J.H. Lee, K. Chu, C.H. Yang, Anomalous low-energy phonons in nearly tetragonal BiFeO₃ thin films. *Phys. Rev.* **84**, 132408 (2011)
200. J.C. Wojdel, J. Íñiguez, *Ab initio* indications for giant magnetoelectric effects driven by structural softness. *Phys. Rev. Lett.* **105**, 037208 (2010)
201. H.J. Mamin, B.D. Terris, L.S. Fan, S. Hoen, R.C. Barrett, D. Rugar, High-density data storage using proximal probe techniques. *IBM J. Res. Dev.* **39**, 681–700 (1995)
202. N.A. Hill, P. Battig, C. Daul, First principles search for multiferroism in BiCrO₃. *J. Phys. Chem. B* **106**, 3383–3388 (2002)
203. M. Murakami, S. Fujino, S.-H. Lim, C.J. Long, L.G. Salamanca-Riba, M. Wuttig, I. Takeuchi, V. Nagarajan, A. Varatharajan, Fabrication of multiferroic epitaxial BiCrO₃ thin films. *Appl. Phys. Lett.* **88**, 152902 (2006)
204. D.H. Kim, H.N. Lee, M. Varela, H.M. Christen, Antiferroelectricity in multiferroic BiCrO₃ epitaxial films. *Appl. Phys. Lett.* **89**, 162904 (2006)

205. A.A. Belik, S. Iikubo, K. Kodama, N. Igawa, S. Shamota, S. Niitaka, M. Azuma, Y. Shimakawa, M. Takano, F. Izumi, E. Takayama-Muromachi, Neutron powder diffraction study on the crystal and magnetic structures of BiCoO_3 . *Chem. Mater.* **18**, 798–803 (2006)
206. Y. Uratani, T. Shishidou, F. Ishii, T. Oguchi, First-principles predictions of giant electric polarization. *Jpn. J. Appl. Phys.* **44**, 7130–7133 (2005)
207. S. Yasui, K. Nishida, H. Naganuma, S. Okamura, T. Iijima, H. Funakubo, Crystal structure analysis of epitaxial BiFeO_3 - BiCoO_3 solid solution films grown by metalorganic chemical vapor deposition. *Jpn. J. Appl. Phys.* **46**, 6948–6951 (2007)
208. M. Sakai, A. Msauno, D. Kan, M. Hashisaka, K. Takata, M. Azume, M. Takano, Y. Shimakawa, Multiferroic thin films of $\text{Bi}_2\text{NiMnO}_6$ with ordered double-perovskite structure. *Appl. Phys. Lett.* **90**, 072903 (2007)
209. N.A. Hill, Density functional studies of multiferroic magnetoelectrics. *Annu. Rev. Mater. Res.* **32**, 1–37 (2002)
210. C. Ederer, N.A. Spaldin, Recent progress in first-principles studies of magnetoelectric multiferroics. *Curr. Opin. Solid State Mater. Sci.* **9**, 128–139 (2005)
211. S. Picozzi, C. Ederer, First principles studies of multiferroic materials. *J. Phys. Condens. Matter* **21**, 303201 (2009)
212. C.J. Fennie, K.M. Rabe, Magnetic and electric phase control in epitaxial EuTiO_3 from first principles. *Phys. Rev. Lett.* **97**, 267602 (2006)
213. C.J. Fennie, Ferroelectrically induced weak ferromagnetism by design. *Phys. Rev. Lett.* **100**, 167203 (2008)
214. T. Varga, A. Kumar, E. Vlahos, S. Denev, M. Park, S. Hong, T. Sanehira, Y. Wang, C.J. Fennie, S.K. Streiffer, X. Ke, P. Schiffer, V. Gopalan, J.F. Mitchell, Coexistence of weak ferromagnetism and ferroelectricity in high pressure LiNbO_3 -phase of FeTiO_3 . *Phys. Rev. Lett.* **103**, 047601 (2009)
215. J.H. Lee, K.M. Rabe, Epitaxial-strain-induced multiferroicity in SrMnO_3 from first principles. *Phys. Rev. Lett.* **104**, 207204 (2010)
216. J. van den Boogaard, D.R. Terrell, R.A.J. Born, An in-situ grown eutectic magnetoelectric composite material. *J. Mater. Sci.* **9**, 1705–1709 (1974)
217. M. Avellaneda, G. Harshe, Magnetoelectric effect in piezoelectric/magnetostrictive multilayer (2-2) composites. *J. Intell. Mater. Syst. Struct.* **5**, 501–513 (1994)
218. J. Ryu, S. Priya, A.V. Carazo, K. Uchino, H. Kim, Effect of the magnetostrictive layer on magnetoelectric properties in PZT/Terfenol-D laminate composites. *J. Am. Ceram. Soc.* **84**, 2905–2908 (2001)
219. S. Ryu, J.H. Park, H.M. Jang, Magnetoelectric coupling of [001]-oriented $\text{Pb}(\text{Zr}_{0.4}\text{Ti}_{0.6})\text{O}_3$ - $\text{Ni}_{0.8}\text{Zn}_{0.2}\text{Fe}_2\text{O}_4$ multilayered thin films. *Appl. Phys. Lett.* **91**, 142910 (2007)
220. J. Ryu, A.V. Carazo, K. Uchino, H. Kim, Piezoelectric and magnetoelectric properties of lead zirconate titanate/Ni-ferrite particulate composites. *J. Electroceram.* **7**, 17–24 (2001)
221. G. Srinivasan, E.T. Rasmussen, J. Gallegos, R. Srinivasan, Y.I. Bokhan, V.M. Laletin, Magnetoelectric bilayer and multilayer structures of magnetostrictive and piezoelectric oxides. *Phys. Rev. B* **64**, 214408 (2001)
222. G. Srinivasan, E.T. Rasmussen, B.J. Levin, R. Hayes, Magnetoelectric effects in bilayers and multilayers of magnetostrictive and piezoelectric perovskite oxides. *Phys. Rev. B* **65**, 134402 (2002)
223. G. Srinivasan, E.T. Rasmussen, A.A. Bush, K.E. Kamentsev, Structural and magnetoelectric properties of MFe_2O_4 -PZT (M=Ni, Co) and $\text{La}_x(\text{Ca}, \text{Sr})_{1-x}\text{MnO}_3$ -PZT multilayer composites. *Appl. Phys. A* **78**, 721–728 (2004)
224. J. Ryu, S. Priya, K. Uchino, H.E. Kim, Magnetoelectric laminate composites of piezoelectric and magnetostrictive materials. *J. Electroceram.* **8**, 107–119 (2002)
225. P. Murugavel, M.P. Singh, W. Prellier, B. Mercey, C. Simon, B. Raveau, The role of ferroelectric-ferromagnetic layers on the properties of superlattice-based multiferroics. *J. Appl. Phys.* **97**, 103914 (2005)

226. S. Stein, M. Wuttig, D. Viehland, E. Quandt, Magnetoelectric effect in sputtered composites. *J. Appl. Phys.* **97**, 10Q301 (2005)
227. M.I. Bichurin, V.M. Petrov, G. Srinivasan, Theory of low-frequency magnetoelectric coupling in magnetostrictive-piezoelectric bilayers. *Phys. Rev. B* **68**, 054402 (2003)
228. C.-W. Nan, M.I. Bichurin, S. Dong, D. Viehland, G. Srinivasan, Multiferroic magnetoelectric composites: historical perspective, status, and directions. *J. Appl. Phys.* **103**, 031101 (2008)
229. J. Zhai, Z. Xing, S. Dong, J. Li, D. Viehland, Magnetoelectric laminate composites: an overview. *J. Am. Ceram. Soc.* **91**, 351–358 (2008)
230. L. Yan, Y. Yang, Z. Wang, Z. Xing, J. Li, D. Viehland, Review of magnetoelectric perovskite-spinel self-assembled nano-composite thin films. *J. Mater. Sci.* **44**, 5080–5094 (2009)
231. G. Srinivasan, Magnetoelectric composites. *Ann. Rev. Mater. Sci.* **40**, 153–178 (2010)
232. H. Zheng, J. Wang, S.E. Lofland, Z. Ma, L. Mohaddes-Ardabili, T. Zhao, L. Salamanca-Riba, S.R. Shinde, S.B. Ogale, F. Bai, D. Viehland, Y. Jia, D.G. Schlom, M. Wuttig, A. Roytburg, R. Ramesh, Multiferroic BaTiO₃-CoFe₂O₄ nanostructures. *Science* **303**, 661–663 (2004)
233. F. Zavaliche, T. Zhao, H. Zheng, F. Straub, M.P. Cruz, P.-L. Yang, D. Hao, R. Ramesh, Electrically assisted magnetic recording in multiferroic nanostructures. *Nano Lett.* **7**, 1586–1590 (2007)
234. H. Zheng, Q. Zhan, F. Zavaliche, M. Sherburne, F. Straub, M.P. Cruz, L.-Q. Chen, U. Dahmen, R. Ramesh, Controlling self-assembled perovskite-spinel nanostructures. *Nano Lett.* **7**, 1401–1407 (2006)
235. J. Li, I. Levin, J. Slutsker, V. Provenzano, P.K. Schenck, R. Ramesh, J. Ouyang, A.L. Roytburd, Self-assembled multiferroic nanostructures in the CoFe₂O₄-PbTiO₃ system. *Appl. Phys. Lett.* **87**, 072909 (2005)
236. J.G. Wan, X.W. Wang, Y.J. Wu, M. Zeng, Y. Wang, H. Jiang, W.Q. Zhou, G.H. Wang, J.M. Liu, Magnetoelectric CoFe₂O₄-Pb(Zr, Ti)O₃ composite thin films derived by a sol-gel process. *Appl. Phys. Lett.* **86**, 122501 (2005)
237. S. Ren, M. Wuttig, Spinodally synthesized magnetoelectric. *Appl. Phys. Lett.* **91**, 083501 (2007)
238. Q. Zhan, R. Yu, S.P. Crane, H. Zheng, C. Kisielowski, R. Ramesh, Structure and interface chemistry of perovskite-spinel nanocomposite thin films. *Appl. Phys. Lett.* **89**, 172902 (2006)
239. M. Murakami, S. Fujino, S.-H. Lim, L.G. Salamanca-Riba, M. Wuttig, I. Takeuchi, B. Varughese, H. Sugaya, T. Hasegawa, S.E. Lofland, Microstructure and phase control in Bi-Fe-O multiferroic nanocomposite thin films. *Appl. Phys. Lett.* **88**, 112505 (2006)
240. H. Ryu, P. Murugavel, J.H. Lee, S.C. Chae, T.W. Noh, Y.S. Oh, H.J. Kim, K.H. Kim, J.H. Jang, M. Kim, C. Bae, J.-G. Park, Magnetoelectric effects in nanoparticulate Pb(Zr_{0.52}Ti_{0.48})O₃-NiFe₂O₄ composite films. *Appl. Phys. Lett.* **89**, 102907 (2006)
241. J.-G. Wan, Y. Weng, Y. Wu, Z. Li, J.-M. Liu, G. Wang, Controllable phase connectivity and magnetoelectric coupling behavior in CoFe₂O₄-Pb(Zr, Ti)O₃ nanostructured films. *Nanotechnology* **18**, 465708 (2007)
242. F. Zavaliche, H. Zheng, L. Mohaddes-Ardabili, S.-Y. Yang, Q. Zhan, P. Shafer, E. Reilly, R. Chopdekar, Y. Jia, P. Wright, D.G. Schlom, Y. Suzuki, R. Ramesh, Electric field-induced magnetization switching in epitaxial columnar nanostructures. *Nano Lett.* **5**, 1793–1796 (2005)
243. M. Liu, X. Li, H. Imrane, Y. Chen, T. Goodrich, Z. Cai, K.S. Ziemer, J.Y. Huang, N.X. Sun, Synthesis of ordered arrays of multiferroic NiFe₂O₄-Pb(Zr_{0.52}Ti_{0.48})O₃ core-shell nanowires. *Appl. Phys. Lett.* **90**, 152501 (2007)
244. C. Binek, B. Doudin, Magnetoelectronics with magnetoelectrics. *J. Phys. Condens. Matter* **17**, L39–L44 (2005)
245. A. Ney, C. Pampuch, R. Koch, K.H. Ploog, Programmable computing with single magneto-resistive element. *Nature* **425**, 485–487 (2003)
246. J.C. Slonczewski, Current-driven excitation of magnetic multilayers. *J. Magn. Magn. Mater.* **159**, L1–L7 (1996)
247. J.C. Slonczewski, Excitation of spin waves by an electric current. *J. Magn. Magn. Mater.* **195**, 261–268 (1999)

248. L. Berger, Emission of spin waves by a magnetic multilayer traversed by a current. *Phys. Rev. B* **54**, 9353–9358 (1996)
249. M. Tsoi, A.G.M. Jansen, W.-C. Chiang, M. Seck, V. Tsoi, P. Wyder, Excitation of a magnetic multilayer by an electric current. *Phys. Rev. Lett.* **80**, 4281–4284 (1998)
250. J.E. Wegrowe, D. Kelly, Y. Jaccard, P. Guittienne, J.-P. Ansermet, Current-induced magnetization reversal in magnetic nanowires. *Europhys. Lett.* **45**, 626–632 (1999)
251. E.B. Myers, D.C. Ralph, J.A. Katine, R.N. Louie, R.A. Buhrman, Current-induced switching of domains in magnetic multilayer devices. *Science* **285**, 867–870 (1999)
252. S. Urazhdin, N.O. Birge, W.P. Pratt Jr., J. Bass, Current-driven magnetic excitations in permalloy-based multilayer nanopillars. *Phys. Rev. Lett.* **91**, 146803 (2003)
253. Y. Liu, Z. Zhang, P.P. Freitas, J.L. Martins, Current-induced magnetization switching in magnetic tunnel junctions. *Appl. Phys. Lett.* **82**, 2871 (2003)
254. Y. Huai, F. Albert, P. Nguyen, M. Pakala, T. Valet, Observation of spin-transfer switching in deep submicron-sized and low-resistance magnetic tunnel junctions. *Appl. Phys. Lett.* **84**, 3118 (2004)
255. T. Wu, S.B. Ogale, J.E. Garrison, B. Nagaraj, A. Biswas, Z. Chen, R.L. Greene, R. Ramesh, T. Venkatesan, *Phys. Rev. Lett.* **86**, 5998–6001 (2001)
256. E. Dagotto, *Nanoscale Phase Separation and Colossal Magnetoresistance* (Springer, New York, 2003)
257. J. Dho, M.G. Blamire, Competing functionality in multiferroic YMnO_3 . *Appl. Phys. Lett.* **87**, 252504 (2005)
258. X. Martí, F. Sánchez, J. Fontcuberta, M.V. García-Cuenca, C. Ferrater, M. Varela, Exchange bias between magnetoelectric YMnO_3 and ferromagnetic SrRuO_3 epitaxial films. *J. Appl. Phys.* **99**, 08P302 (2006)
259. J. Dho, X. Qi, H. Kim, J.L. MacManus-Driscoll, M.G. Blamire, Large electric polarization and exchange bias in multiferroic BiFeO_3 . *Adv. Mater.* **18**, 1445–1448 (2006)
260. H. Béa, M. Bibes, S. Cherifi, F. Nolting, B. Warot-Fonrose, S. Fusil, G. Herranz, C. Dernalot, E. Jacquet, K. Bouzehouane, A. Barthélémy, Tunnel magnetoresistance and robust room temperature exchange bias with multiferroic BiFeO_3 epitaxial thin films. *Appl. Phys. Lett.* **89**, 242114 (2006)
261. L.W. Martin, Y.-H. Chu, Q. Zhan, R. Ramesh, S.J. Han, S.X. Wang, M. Warusawithana, D.G. Schlom, Room temperature exchange bias and spin valves based on $\text{BiFeO}_3/\text{SrRuO}_3/\text{SrTiO}_3/\text{Si}$ (001) heterostructures. *Appl. Phys. Lett.* **91**, 172513 (2007)
262. P. Borisov, A. Hochstrat, X. Chen, W. Kleeman, C. Binek, Magnetoelectric switching of exchange bias. *Phys. Rev. Lett.* **94**, 117203 (2005)
263. V. Laukhin, V. Skumryev, X. Martí, D. Hrabovsky, F. Sánchez, M.V. García-Cuenca, C. Ferrater, M. Varela, U. Lünder, J. Fontcuberta, Electric-field control of exchange bias in multiferroic epitaxial heterostructures. *Phys. Rev. Lett.* **97**, 227201 (2006)
264. H. Béa, M. Bibes, F. Ott, B. Dupé, X.H. Zhu, S. Petit, S. Fusil, C. Deranlot, K. Bouehouane, A. Barthélémy, Mechanisms of exchange bias with multiferroic BiFeO_3 epitaxial thin films. *Phys. Rev. Lett.* **100**, 017204 (2008)
265. Y.-H. Chu, L.W. Martin, M.B. Holcomb, M. Gajek, S.J. Han, N. Balke, C.-H. Yang, D. Lee, W. Hu, Q. Zhan, P.-L. Yang, A. Fraile-Rodriguez, A. Scholl, S.X. Wang, R. Ramesh, Electric-field control of local ferromagnetism using a magnetoelectric multiferroic. *Nat. Mater.* **7**, 478–482 (2008)
266. X. He, N. Wu, A.N. Caruso, E. Vescovo, K.D. Belaschenko, P.A. Dowben, C. Binek, Robust isothermal electric control of exchange bias at room temperature. *Nat. Mater.* **9**, 579–585 (2010)
267. J.F. Scott, Data storage: multiferroic memories. *Nat. Mater.* **6**, 256–257 (2007)
268. C.M. Cristensen, *The Innovator's Dilemma* (Harvard Business School Press, Boston, MA, 1997)
269. S. Ju, T.-Y. Cai, G.-Y. Guo, Z.-Y. Li, Electrically controllable spin filtering and switching in multiferroic tunneling junctions. *Phys. Rev. B* **75**, 064419 (2007)

270. F. Yang, M.H. Tang, Z. Ye, Y.C. Zhou, X.J. Zheng, J.X. Tang, J.J. Zhang, J. He, Eight logic states of tunneling magnetoelectroresistance in multiferroic tunnel junctions. *J. Appl. Phys.* **102**, 044504 (2007)
271. C. Jia, J. Berakdar, Multiferroic oxides-based flash memory and spin-field-effect transistor. *Appl. Phys. Lett.* **95**, 012105 (2009)
272. K. Abraha, D.R. Tilley, Theory of far infrared properties of magnetic surfaces, films, and superlattices. *Surf. Sci. Rep.* **24**, 125–222 (1996)
273. G.A. Smolenskii, I.E. Chupis, Ferroelectromagnets. *Sov. Phys. Usp.* **25**, 475–493 (1982)